Mathematical Modeling as a Tool to Elucidate HCV Infection Kinetics and Treatment Response

BY

NATASHA D SANSONE
B.A., University of Chicago, 2010

THESIS

Submitted as partial fulfillment of the requirements
for the degree of Doctor of Philosophy in Microbiology and Immunology
in the Graduate College of the University of Illinois at Chicago, 2017

Chicago, Illinois

Defense committee
Susan L. Uprichard, advisor
Alan McLachlan, chair
Howard Lipton
Karl Volz
Bin He
Harel Dahari, Medicine

This thesis is dedicated to all of my teachers, coaches, classmates, labmates, family, and friends. Especially Ms. Collins, Ms. Fagan, Mr. Osbourne, Ms. Wallmuth, Dr. Dosch, and Dr. Wilcox Yang. Thank you for challenging me and showing me how to give my best. Grandpa, thank you for the abacus, practice arithmetic problems, and tours of your work space in Fermilab.

ACKNOWLEDGMENTS

I would like to thank all of my past and present committee members, as well as mentors during my laboratory rotations –Drs. Deepak Shukla, Arnon Lavie, Michael Federle, Bin He, Howard Lipton, Karl Volz, Alan McLachlan, Harel Dahari, and Susan L. Uprichard– for their guidance and encouragement. They have always emphasized how much more there is to learn about our world, and for that I am grateful.

NDS

TABLE OF CONTENTS

TABLE OF CONTENTS (CONTINUED)

TABLE OF CONTENTS (CONTINUED)

CHAPTER PAGE

LIST OF TABLES

LIST OF FIGURES

FIGURE PAGE

LIST OF FIGURES (CONTINUED)

LIST OF ABBREVIATIONS

CD81	Cluster of Differentiation 81
CLDN1	Claudin-1
DAA	Direct Acting Antiviral
DCV	Daclatasvir
EGFR	Epidermal Growth Factor Receptor
EOT	End of Treatment
HCC	Hepatocellular Carcinoma
HCV	Hepatitis C Virus
HCVcc	Cell Culture-Derived HCV
HIV	Human Immunodeficiency Virus
IFN	Interferon-α
JFH-1	Japanese Fulminant Hepatitis-1
LDLR	Low-Density Lipoprotein Receptor
MOA	Mechanism of Action
NAFLD	Non-Alcoholic Fatty Liver Disease
NANBH	Non-A Non-B Hepatitis
NASH	Non-Alcoholic Steatohepatitis
NPC1L1	Niemann-Pick C1-Like 1
NS	Non-Structural Protein
OCLN	Occludin
RNA	Ribonucleic Acid
RT-qPCR	Real-Time Quantitative Polymerase Chain Reaction
SR-B1	Scavenger Receptor Class B Member 1
SVR	Sustained Virologic Response
TFR1	Transferrin Receptor Protein 1

SUMMARY

Hepatitis C Virus (HCV) chronically infects 170 million people around the globe, leading to steatosis, fibrosis, cirrhosis, and hepatocellular carcinoma (HCC). Despite this enormous public health burden, current treatments are too costly and no preventative therapy or vaccine exists. In order to facilitate the development of effective and affordable HCV therapeutics, we have utilized mathematical modeling as an analytical tool to advance our understanding of the dynamics of HCV infection and treatment response.

In Chapter Three, we used our published HCV replicon mathematical model to analyze HCV RNA synthesis and degradation in the context of antiviral treatment. Using the model to analyze HCV replicon treatment response data allowed us to estimate the intrinsic rate of RNA degradation as well as the efficacies and mechanisms of action of HCV antivirals.

In Chapter Four, we describe the creation of the first data-driven mathematical model of the HCV cell culture (HCVcc) infection system. Through the process of testing the model against experimental HCV inhibition data, we identified a gap in our knowledge about HCV steady-state dynamics. Specifically, this initial model revealed that our empirically measured half-life of extracellular HCV particles was not fast enough to account for the inhibition kinetics observed empirically during DAA treatment, leading us to investigate the mechanism(s) of extracellular HCV clearance through *in vitro* and *in vivo* experimentation. Based on these data, we revised our HCVcc mathematical model to include non-productive entry of not only infectious, but also non-infectious HCV particles into cells.

In Chapter Five and Appendix A Manuscript 1, we used mathematical modeling to

investigate the MOA of the HCV NS5a inhibitor daclatasvir (DCV). First, we found that a multiscale model was needed to explain DCV inhibition kinetics in patients. Although only serum HCV RNA levels were measured, this model was able to make predictions about intracellular mechanisms of DCV –that it blocked both HCV RNA synthesis and assembly/secretion.

We confirmed this hypothesis via *in vitro* experimentation, however, our *in vitro* HCVcc mathematical model could not simulate non-parallel reduction kinetics of extracellular infectious versus non-infectious HCV particles. We incorporated two alternative strategies that could allow the model to simulate non-parallel extracellular viral kinetics and tested these two hypotheses by fitting these alternative models to data and found that the most likely hypothesis was that DCV was altering specific infectivity. While this prediction needs to be tested experimentally, we have already utilized this concept to create new *in vivo* mathematical models that can successfully simulate the new, DAA-associated phenomenon of patients testing positive for HCV RNA at the conclusion of treatment, but going on to achieving sustained virologic response (SVR) or cure (Appendix B).

In Chapter Six, we give an overview of the cyclical process of experimentation and mathematical modeling, illustrated throughout this thesis, and how it drives experimental design and hypothesis generation. We also discuss the key findings our combined experimental/theoretical modeling approach has revealed and the future directions we feel would continue to advance the HCV field.

1. INTRODUCTION

1.1 Importance of Studying Hepatitis C Virus

Hepatitis C virus (HCV) treatment options have advanced significantly during the course of this thesis work, however, currently there are approximately 170 million people chronically infected with HCV and our understanding of infection dynamics and treatment response is still limited. Of the patients acutely infected with HCV, only 20% experience symptoms such as fever, fatigue, vomiting, or jaundice, however, only ~20% will clear the infection naturally depending to varying extents on the degree of liver health, ethnicity, gender, and genetic composition of the host[1,2]. Unfortunately, the majority of those infected fail to clear the virus and their infections become chronic, gradually leading to steatosis, fibrosis, cirrhosis, non-alcoholic fatty liver disease (NAFLD), non-alcoholic steatohepatitis (NASH), and hepatocellular carcinoma (HCC)[3]. This chronic liver damage results in 700,000 deaths per year around the world with total costs related to HCV projected to increase to $16.16 billion per year by 2019[4,5]. In 2015 in the United States, each patient with HCC incurred an average of $6,279 in medical bills per month of observation. For patients requiring liver transplants, that average cost increased to $7,492 per month.[6] These statistics do not mention the cost to the economy when the employee must take leaves of absence, to the patient who loses their quality of life, or to the family that often loses a relative. Because of this global health burden, HCV is a focus of intense scientific research with the goal of discovering better methods of treating and preventing HCV infection.

1.2 Hepatitis C Virus Epidemiology

HCV is transmitted by blood. Before HCV was isolated and identified, most infections occurred via contaminated blood products because it was not possible to screen for HCV[7]. Today HCV is spread most frequently through injected drug use. Infected mothers can also pass the virus on to their children, which is the case for 5% of HCV-positive mothers and 19.4% of HIV-positive, HCV-positive mothers. Though less common, it can also be transmitted by other breaches of the skin such as occupational exposure to blood, tattooing/body piercing, or sexual activity.

Without a vaccine to protect against HCV[8] and after decades of ineffective therapeutics, the prevalence of HCV-infected patients in a given nation typically ranges between <1% and >10%[7], with certain populations such as prison inmates reaching 38%[9]. Hence, although the acute infection rate has fallen since the 1980's, approximately 2-3% of the global population are still chronically infected with HCV- 4 times more than are infected with human immunodeficiency virus (HIV). In the United States, about 2% of the population is infected with HCV, but for military veterans that rate is estimated at 10%. Nations with the most notably high rates of HCV-infected individuals include Egypt (>30%) and other African or East Asian nations.

To date, seven HCV genotypes have been identified, each of which exhibit distinct disease manifestations and treatment response characteristics. Globally, the most frequent genotype is HCV genotype 1, causing 83.4 million or 46.2% of infections. Because HCV genotype 1 is most prevalent in developed countries like the USA, most drug and vaccine development has been

focused on combating genotype 1, even though it only causes about half of HCV infection cases worldwide. The next most prevalent HCV genotype is 3 (54.3 million or 30.1% of cases). In combination, genotypes 2, 4, and 6 cause 22.6% of HCV infections and genotype 5 causes less than 1% of cases[10].

1.3 Hepatitis C Virus Discovery and Experimental Systems

Historically, it took decades to isolate HCV and establish it as a cause of transfusion-associated hepatitis. During the mid-1970's physicians noted that there were patients with chronic, transfusion-associated hepatitis that were testing negative for hepatitis B virus. It was also apparent that this chronic hepatitis was not caused by hepatitis A virus, which was known to cause acute, easily-transferrable hepatitis. Because of this, the symptoms of HCV were known as non-A non-B hepatitis (NANBH) until the virus was isolated in 1988.[11] After this, a diagnostic test for HCV was developed and the virus was demonstrated to be the cause of the majority of non-A, non-B Hepatitis in patients that had received blood transfusions.

Initially the only available experimental model for HCV research was chimpanzees. After the virus was isolated in 1988, it would take another decade for researchers to establish an *in vitro* HCV replication system.[12] Cells stably supporting autonomous replication of HCV were made by transfecting modified HCV "replicon" RNA – in which the viral structural genes were replaced by an antibiotic selection marker (Fig. 1A) – into hepatoma cells. Replicons are useful for studying the replication of viral RNA and the function of the viral protease and polymerase.

However, it was not until 2005 that three laboratories, including my thesis laboratory, would discover that a particular clinical isolate of HCV could productively infect Huh7 hepatoma cells *in vitro* (complete HCV genome shown in Fig. 1B).[13–15] This advance has allowed researchers to investigate the full viral lifecycle at the molecular level and develop strategies for targeting the virus at each of these steps. While we still await an affordable small animal model to study the liver pathology caused by chronic HCV infections, the new *in vitro* infection system has been fundamental in the understanding of HCV infection and the development of effective HCV antivirals.

Developing a small animal infection model has been a goal since the early days of HCV research, but in light of the NIH's mandate on chimpanzee research it is even more urgent. Currently, immunocompromised mouse models with humanized livers exist for studying HCV infection, but researchers are still striving for a model that will allow a robust HCV infection in the context of an intact immune system.[16] As another way to address that goal, preliminary work has been done to develop a macaque model[8] and there are also a few recently identified viruses closely related to HCV that can infect small primates[17] or non-primates.[16,18,19]

1.4 Hepatitis C Virus Molecular Virology

HCV is an RNA virus, classified in the hepacivirus genus of the flaviviridae family. HCV virions are 55-65 nm in diameter[14] and consist of positive-strand RNA protected by an icosahedral capsid made of multiple copies of a viral protein called Core[20], which is surrounded by an envelope derived from the host cell. The viral envelope is decorated with viral glycoproteins

E1 and E2[21] and associates with host apolipoproteins[22], a combination that allows it to enter human and chimpanzee hepatocytes. As such, HCV particles have a broad density profile (1.03 – 1.18 g/mL), with most infectious particles being in the lower buoyant density range.[23]

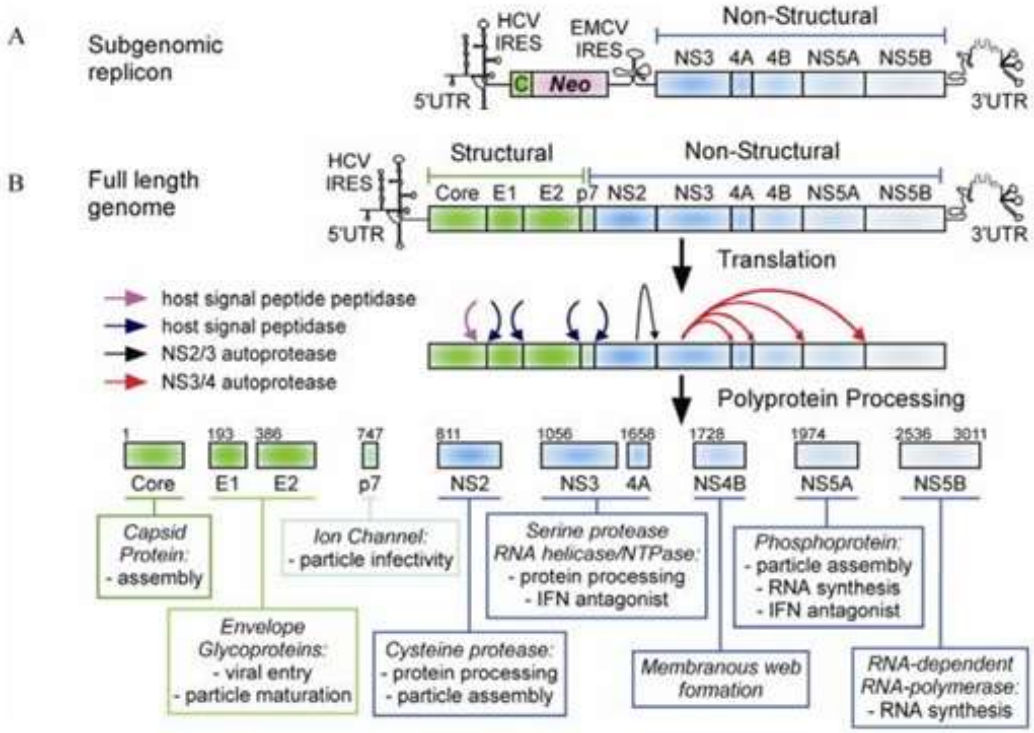

Figure 1. Hepatitis C Virus Constructs. **(A)** Schematic of HCV subgenomic replicon. **(B)** Schematic of HCV genome as well as cleavage sites and known functions of proteins. Structural proteins are highlighted green and non-structural proteins are highlighted blue. (Modified from [24])

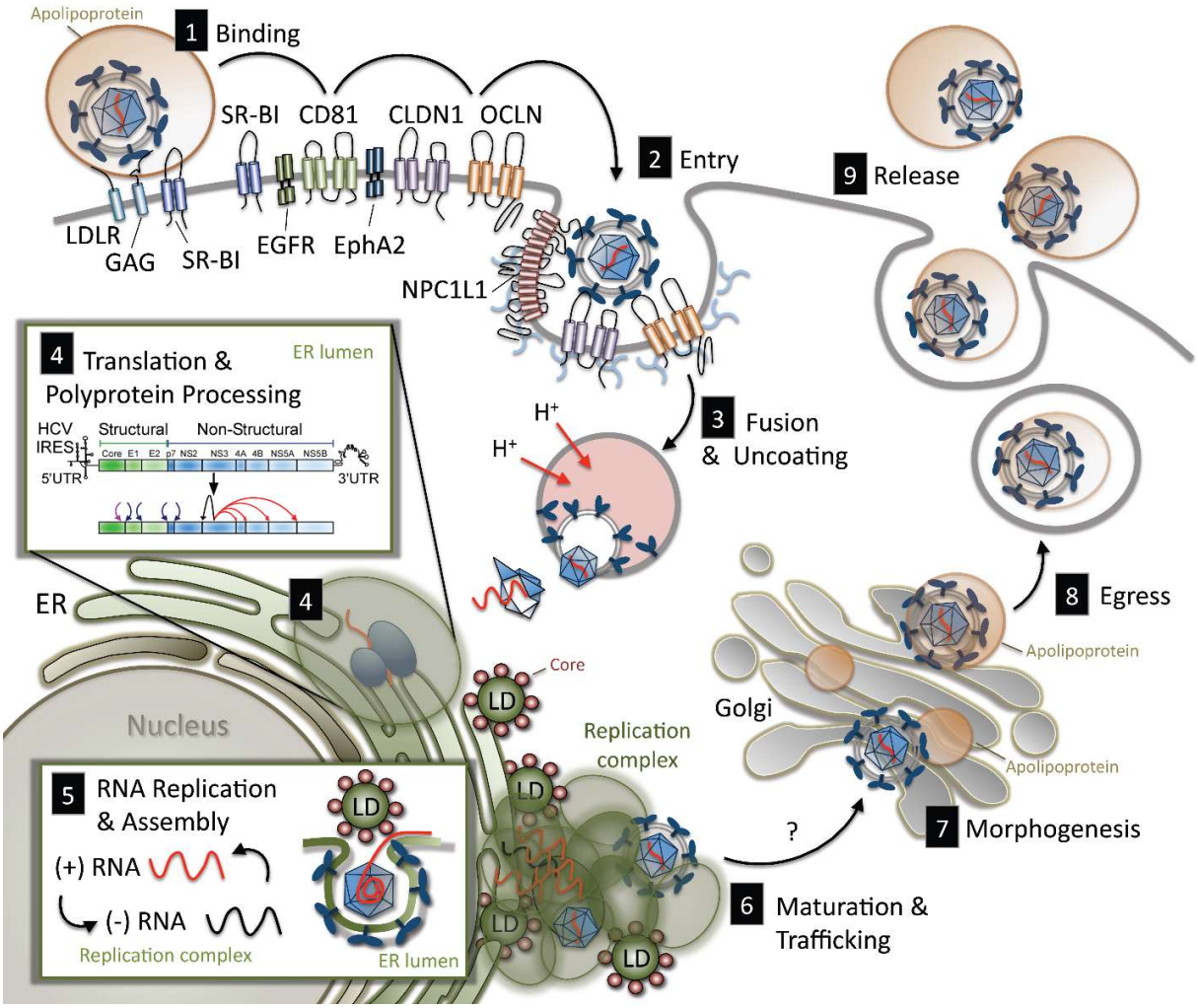

Figure 2. Schematic of the Hepatitis C Virus Lifecycle.

Unlike many viruses that require only one receptor to enter a cell, HCV uses multiple cellular entry factors to bind and enter hepatocytes in a series of events that are still not completely understood (Fig. 2, #1-2). This long list of entry factors includes cluster of differentiation 81 (CD81)[25,26], low-density lipoprotein receptor (LDLR)[27,28], scavenger receptor class B member 1 (SR-B1)[29,30], claudin-1 (CLDN1)[31], occludin (OCLN)[32], Niemann-Pick C1-like 1 (NPC1L1)[33], transferrin receptor protein 1 (TFR1)[34], and epidermal growth factor receptor (EGFR)[35]. After entering the cell, HCV's 9600 nucleotide positive-sense RNA genome (Fig. 1B) is released into the cytosol (Fig. 2, #3). It has no cap to initiate translation; instead, the internal ribosome entry site (IRES) in HCV's 5' un-translated region guides the cellular 40S ribosomal subunit to the correct position to translate a polyprotein with about 3,000 amino acids.[36] During translation, this polyprotein is cleaved by a combination of viral and host proteases into at least ten functional proteins (Fig. 1B; Fig. 2, #4).[37]

At the N-terminus of this polyprotein are the structural proteins needed to form the viral particle: the capsid and the envelope glycoproteins E1 and E2 (Fig. 1B, green). Moving toward the C-terminus, next is a hydrophobic peptide called p7, which is an ion channel that is important for particle infectivity (Fig. 1B, green) and then the non-structural proteins (NS) 2-5 (Fig. 1B, blue).[38] NS2 is not required for the replication of HCV RNA in the replicon system[12], but is required for particle assembly; furthermore, it is a proteinase that cleaves its own C-terminus from the viral polyprotein.[39-41] NS3 is a helicase/NTPase and serine protease, which complexes with NS4A to cleave HCV's polyprotein at four sites (Fig. 1B). NS3/4A also cleaves the host cell's mitochondrial antiviral signaling (MAVS) protein to block the retinoic acid-inducible gene 1 (RIG-

I) pathway to interrupt innate immune signaling[42]. NS4B is a co-factor that can integrate into membranes and causes the morphology of the endoplasmic reticulum to change into a conducive environment for the production of HCV RNA[43] This modified organelle is referred to as the membranous web.

NS5A is a phosphoprotein with no known enzymatic activity that is involved in both RNA replication and virion assembly, as demonstrated by mutation studies[44]. The protein has a site for binding HCV RNA, and microscopic analyses during normal infection have shown that it is located both at the membranous web replication complex and at the lipid droplet sites of virion assembly.[45–49] The protein relies on cellular kinases to be phosphorylated and is observed in two major forms, hyper-phosphorylated (p58) and basal-phosphorylated (p56). It can activate the viral polymerase regardless of its phosphorylation status, possibly through direct interaction or by binding RNA. It also recruits VAPA and VAPB to the membranous web, which in turn interacts with oxysterol-binding protein (OSBP) to recruit cholesterol to the membranous web, promoting both RNA replication and virion production.[50] In its hyper-phosphorylated form, NS5A appears more likely to co-localize with lipid droplets and HCV core protein, facilitating the assembly step of the viral lifecycle (Fig. 1, #8).[51] NS5A is also important for subverting Interferon signaling.[52] During my thesis work, DAA's that target NS5A appeared to reduce patient serum HCV RNA very rapidly during clinical trials[53], so NS5A inhibitors became a focus of my research. Since then, NS5A inhibitors have since been incorporated into what have become the most effective FDA-approved HCV antivirals.

Finally, the protein closest to the C-terminus of the polyprotein is NS5B, the viral RNA-dependent RNA polymerase (RdRp) responsible for replicating HCV RNA (Fig. 1B, blue). This enzyme has a catalytic site that can bind two nucleotides to initiate HCV RNA synthesis. A modified nucleoside known as guanosine triphosphate (GTP) also binds to NS5B at an allosteric site, which changes the conformation of NS5B to make space for dsRNA. At the 3' end of the template higher concentrations of GTP are required for RNA elongation.[50]

As the necessary viral proteins accumulate in the infected cell, the virus proceeds to modify the membrane of the endoplasmic reticulum into an environment known as the membranous web (Fig. 2, #5). Many viral and cellular factors work together, but the key viral factors appear to be NS4B and NS5A. In order to create the membranous web, HCV also increases lipid production and membrane biosynthesis through both the sterol regulatory element-binding protein (SREBP) and DEAD box polypeptide 3 X-linked (DDX3X) pathways. Cells infected with HCV have higher levels of lipogenic transcripts like fatty acid synthase and HMG-CoA, as well as high levels of cleaved, activated SREBPs. The membranous web minimizes the distance between factors required for HCV RNA replication and subsequent steps of the viral lifecycle, and it is the site of HCV RNA replication; the web may also function to block innate immune recognition of viral RNA.[54] Within the membranous web, viral replicase complexes (comprising at least NS3-NS5B) create a negative-strand RNA from the initial positive-strand and then many positive-strand copies from each negative-strand template. Positive-strands outnumber negative-strands 10:1. Positive-strands can be translated into polyproteins, packaged into virion particles, or used as templates to create more negative-strands (Fig. 2, #5).[50]

After genome synthesis packaging of the viral RNA occurs at lipid droplets (LDs) in the cytosol (Fig. 2, #5-6). Cellular enzymes that affect LD homeostasis such as cytosolic phospholipase A2 and diacylglycerol acyltransferase-1 (DGAT-1) recruit Core protein to LDs. Because hyperphosphorylated NS5A is recruited to LD, can bind to HCV RNA, and is necessary for both replication and assembly, it has been suggested that NS5a may function to traffic the HCV genome from the site of replication to assembly at LDs. NS5A also binds to DGAT-1, which encourages interaction between NS5A and Core, possibly causing interaction between Core and HCV RNA if it is bound to NS5A.

The viral capsid is then secreted non-cytolytically via the host's ER/Golgi secretory pathway, during which the viral glycoproteins E1 and E2 are modified (Fig. 2, #7-8).[55] The virus seems to specifically utilize the vLDL secretion pathway[56], during which it acquires a membrane from the host cell in which its viral glycoproteins are embedded and it associates with host-derived apolipoproteins, especially ApoE (which can interact with NS5A and HCV glycoproteins E1 and E2), A1, C1, and B. Then, ESCRT machinery appears to be necessary for HCV egress in an indirect manner (Fig. 2, #8). After a virion is released from the cell, it is free to find a new cell to infect.[57]

Alternatively, the virus can spread cell-cell without undergoing egress, avoiding antibody neutralization. The mechanism is not completely understood, so this process is the focus of several ongoing studies, including one of the projects in our lab. A better understanding of this process could be applied during treatment of chronic patients or in instances when a patient's

naïve liver is at risk for infection, for instance after a liver transplant or in the case of uninfected individuals that may have been exposed to HCV.[58,59]

1.5 History of Hepatitis C Virus Treatment

There has been a long evolution of drugs developed for the treatment of HCV. For many years, the only option for patients was intravenous treatments of the immunostimulatory molecule Interferon-alpha (IFN). Beginning in 1991, interferon alpha was available for HCV treatment. Interferon-alpha treatments had to be administered intravenously by a medical staff in a hospital setting. Patients had to come in for daily appointments because the low stability interferon alpha molecule levels could not be kept high enough to treat the HCV. SVR rates for each of these treatments were a mere 9% for patients with HCV genotype 1 and 30% for HCV genotype 2 or 3, but also varied depending on the gender, genetics, HCV genotype, ethnicity, insulin resistance, HIV infection status, and relative degree of liver health of the patient.[60]

One year later in 1998, a combination of Intron-A with Ribavirin (RBV) became available and increased the SVR rate of genotype 1 to 29% and the rates of genotype 2 and 3 to 62%. In 2001 interferon alpha 2b was pegylated (marketed as Peg-Intron) to increase its stability in the body and reduced the intravenous appointments to three times per week, which increased patient compliance by making the treatment more convenient. In 2002, interferon alpha 2a was successfully pegylated (marketed as Pegasys); in combination with Ribavirin in 2003 it increased SVR rates in clinical trials up to 51% for genotype 1, 82% for genotypes 2 and 3, and 70% for

genotypes 4-6, and this was still the standard of care in 2010 when the experimental work for this thesis began.

In 2011 the FDA approved the first drugs that could target HCV proteins directly. These DAA's significantly improved SVR rates in patients.[61,62] However, the first two DAA's to be approved, which targeted the viral protease NS3/4a, had to be administered in conjunction with pegylated interferon and ribavirin. During clinical trials, these drugs increased SVR rates from 51% to about 80% for genotype 1, when combined with pegylated interferon alpha and ribavirin. In late 2013, an HCV polymerase inhibitor called Sovaldi (Sofosbuvir) was approved for use in patients and had such high SVR rates in the absence of IFN during clinical trials that it was approved for use with ribavirin in the absence of IFN. This meant that patients would not be subjected to IFN's serious side effects and would not have to visit the hospital to receive injections, increasing patient compliance rates. In 2015 another major improvement in treatment was approved for use in patients- the NS5A inhibitor Daklinza (daclatasvir), a drug that reduced viral loads faster than any previous drug during clinical trials. Over time, additional protease, polymerase, and NS5a inhibitors have been approved and there are currently numerous combination therapies available from different companies[63]. The SVR rates for these new all-oral DAA combination therapies are generally unaffected by a patient's gender, genetics, ethnicity, or metabolic/liver health, which is a great improvement over the IFN-based therapies. The amount of time required for treatment is also much shorter, with most therapies taking only 12 weeks to achieve SVR in the patient, versus the 6-12 months that previous IFN-based treatments required.[64]

With HCV treatment improving so much in the past 5 years, almost every patient who can afford the medication can clear the virus and in theory screenings can catch HCV-positive patients before the virus causes advanced liver disease. However, there are remaining challenges. First, not every patient can afford the medication. Prices are coming down, but as an example, Sovaldi can cost as much as $84,000 for a 12-week regimen, meaning that each pill costs $1,000. This makes treatment particular difficult to justify in high risk populations as treatment does not protect against re-infection. Finally, viral escape also remains a problem in up to 20% of patients depending on compliance. Thus, research is still needed to improve and decrease cost of treatment and design preventative treatments and/or vaccines.

1.6 Mathematical Modeling of Biological Systems

The underlying premise of this thesis is that by combining both experimental and modeling approaches we can achieve a more quantitative understanding of the viral lifecycle and develop mathematical tools to generate hypotheses and facilitate the investigations necessary to further our understanding of the system. Mathematical modeling consists of designing equations that mimic the behavior of data. Similar to the way physics equations describe the behavior of objects in the natural world, these equations describe biological processes in a quantitative way and are based on all of the major hypotheses we have about how a biological system works. When we compare the behavior of the equations to empirical data, we are essentially testing all of those hypotheses simultaneously. Because of this, discrepancies between the equations and the data can indicate where there are holes in our understanding. The changes that have to be made to a

mathematical model in order to simulate empirical data generate theoretical hypotheses which can then be tested experimentally, creating a repeating cycle of theoretical mathematical modeling and physical experimentation, each in response to the other.

Once the model is updated to minimize the discrepancy between the empirical data and a mathematical simulation, the models can be used as data analysis tools. In an experiment where multiple factors had an effect on the output, mathematical models make it easier to rank the factors in terms of which were most influential on the experimental output. The models can also offer quantitative estimates of parameters that are difficult to isolate and measure directly in the context of a complex system, i.e. production and decay rates for objects that are simultaneously being produced and destroyed in the context of a complex system. For example, in this thesis when modeling the viral lifecycle, the model simulations can analyze the kinetic pattern of the change in viral load in response to different treatments and predict which viral lifecycle steps were most affected to create that pattern, what percent inhibition occurred at each step and estimate parameters such as viral RNA rates, which would otherwise be difficult or impossible to measure directly because the system is simultaneously creating and destroying HCV RNA. Identifying the step(s) affected is especially useful if the drug targets a viral protein that is not well-characterized, or if the target is not known.[53,65] Likewise, being able to quantitatively compare the efficacies of different drugs and/or different doses of the same drug in silico provides a much more efficient means of predicting which drugs/drug combination are most effective.

1.7 Historical Use of Mathematical Modeling in the Clinical Setting

In a clinical setting mathematical modeling has historically been used to quantitatively assess the ongoing success of a patient's treatment in real time, throughout the regimen to determine what improvements could be made to the therapy protocol. Mathematical modeling has been employed in this way during the treatment of human immunodeficiency virus (HIV)[65] and hepatitis B virus (HBV)[66], but most prominently for HCV. In the past, when IFN-based therapies required extended treatment times and had low chances of success, mathematical modeling was used to predict whether a patient would fail treatment, allowing the physician to stop this uncomfortable treatment if the patient had no chance of achieving SVR. Often, mathematical models could predict whether treatment would fail after 6-48h of initiation[67-69], and mathematical modeling has been used to assess the value of delivering treatment daily versus 3x/week.[66] These mathematical analyses helped clinicians maximize the success rates of HCV therapies and saved time, money, and frustration if it was demonstrated that the patient was not headed toward achieving SVR. Mathematical modeling has also been used to estimate multiple *in vivo* parameters such as the death rate of HCV-infected cells[70], HCV's mutation rate[71], and the occurrence rate of drug-resistant HCV mutations.[72]

In contrast, mathematically modeling a patient's response to treatment has a much different role now. Because current therapy regimens have higher success rates, monitoring HCV levels during treatment is not used to advise a patient whether he or she should prematurely abandon the treatment, but instead it is used to: investigate the molecular mechanisms that make the most successful drugs so effective, quantitatively determine which therapies are most

effective for which HCV genotypes, and predict what is the *minimum time* a patient needs to be treated to achieve SVR.[73] This type of modeling can inform antiviral development as well as the optimization of HCV treatment regimens so that they are as short as possible, saving thousands of dollars per patient, and millions per nation. Modeling is also now being used to understand the relatively new phenomenon of patients who achieve SVR after the end of treatment even though they are still positive for HCV RNA when treatment stops, an observation that was never seen before the use of DAA's to treat HCV.[72,74]

1.8 Advantages of Mathematically Modeling *in vitro* Data

Mathematical modeling of numerous patient datasets has provided all of these insights listed here and more. However, these *in vivo* datasets are generally limited to infrequent observational extracellular (serum) measures of HCV RNA. Furthermore, there is no assay for measuring the infectious titer of clinical isolates, which makes it impossible to monitor infectious viral levels *in vivo*. In contrast, in this thesis we focus on *in vitro* studies as this allows a much broader range of experimental opportunities and measurement of more viral parameters (e.g. intracellular data and viral infectivity), enabling mathematical modeling predictions to be more specific, especially when used in conjunction with mathematical analyses of patient data to provide hypotheses concerning the molecular mechanisms of viral response to therapy. As such, this thesis will describe hypotheses generated and investigated while developing and using mathematical models to analyze data that we gathered while treating either HCV replicon cells,

cells that were chronically infected with HCV, as well as kinetic data from chronically HCV-infected patients.

1.9 *In vitro* Hepatitis C Virus Mathematical Models

Our group had previously published a simple *in vitro* mathematical model for analyzing the HCV replicon system.[75-78] When starting the work for this thesis, the main goal was to determine the mechanism of action (MOA) by which IFN reduced HCV levels. We wanted to describe this MOA in terms of the viral lifecycle steps that were most affected by the treatment, hoping to inform drug development by determining which lifecycle steps were most important to target during treatment. Subsequently, the focus of this thesis work shifted to studying DAAs and in Chapter 3 we present model predictions of drug efficacy. Because these drugs have well-defined MOA's that would help us estimate additional viral parameters (Chapter 3) and build our HCVcc mathematical model (Chapter 4).

Building from that published replicon model, we developed the first mathematical model for fully infectious, cell culture-derived HCV (HCVcc) infection. This affords a more complete picture of HCV infection than the HCV replicon system and provides more accurate hypotheses about infection dynamics at the molecular level than extracellular patient data alone. In Chapter 4, we present the first iteration of our model, where we discovered that our understanding of chronic HCV infection was incomplete and obtained experimental evidence that supported the model prediction that non-productive HCV entry into infected cells plays a significant role in steady-state HCV dynamics. In chapter 5, subsequent analysis of the novel and multifunctional

NS5a inhibitor, daclatasvir, revealed not only another important gap in our model regarding the specific infectivity of progeny virus produced, but also provided a plausible hypothesis regarding the new unexplained clinical phenomenon of patients who are positive for HCV RNA at the end of treatment, yet eventually achieve sustained virologic response (SVR i.e. HCV cure) without additional treatment.

2. MATERIALS AND METHODS

2.1 Virus

HCV JFH-1. Huh7-1 cells were electroporated with *in vitro*-transcribed full-length infectious HCV JFH-1 RNA generated from pJFH-1 provided by Takaji Wakita (National Institute of Infectious Diseases, Tokyo, Japan) as described previously.[79] Virus in the media was collected, titered, and used to grow large volumes of cell culture-propagated HCV (HCVcc) by infecting naïve Huh7-1 cells at a multiplicity of infection (MOI) of 0.01 focus-forming units (FFU) per cell. Media was collected from these infected cells, aliquoted and stored at -80℃. This stock was titered and used for experiments.

2.2 Cell Culture

Huh7-1 hepatocytes derived from a human hepatoma have been described previously[80]. Cells were thawed at passage 22 and maintained in complete Dulbecco's modified Eagle's medium (DMEM) (HyClone) supplemented with 10% (vol/vol) FBS (HyClone), 100 U/mL penicillin, 100 mg/mL streptomycin, and 2 mM L-glutamine (Gibco Invitrogen) for a maximum of 15 passages before new P22 cells were thawed.

Huh7-Sg2a replicon cells were created by linearizing the pSGR-JFH-1 plasmid containing the sgJFH-1 HCV genotype 2a JFH-1 replicon, provided by Takaji Wakita (National Institute of Infectious Diseases, Tokyo, Japan), and using it as template to transcribe HCV RNA *in vitro*. The resulting RNA was transfected into Huh7 cells and cell clones were selected by G418 treatment as described.[81] Clone B HCV sg1b Huh7 cells were sourced from the NIH AIDS Research and

Reference Reagent Program and have been previously described.[82] Replicon cells were cultured in complete DMEM (as described above) supplemented with 500 µg/mL Geneticin/G418 (Invitrogen) to select for cells expressing the neomycin gene-containing HCV subgenomic RNA.

For experiments, non-growing Huh7-1 and replicon cells cultures were established by seeding cells in collagen-coated BioCoat 96-well plates in cDMEM. When cells reached 90-95% confluence, media was supplemented with 1% DMSO. Media with 1% DMSO was changed every 48-72 hours. Replicon cells were additionally maintained with Geneticin in their media to select for high production of HCV subgenomic RNA. At day 20 of DMSO-treatment when differentiation was complete.[83,84] At this point, the replicon cells would exhibit HCV steady-state and were used for experiments (Fig. 3).

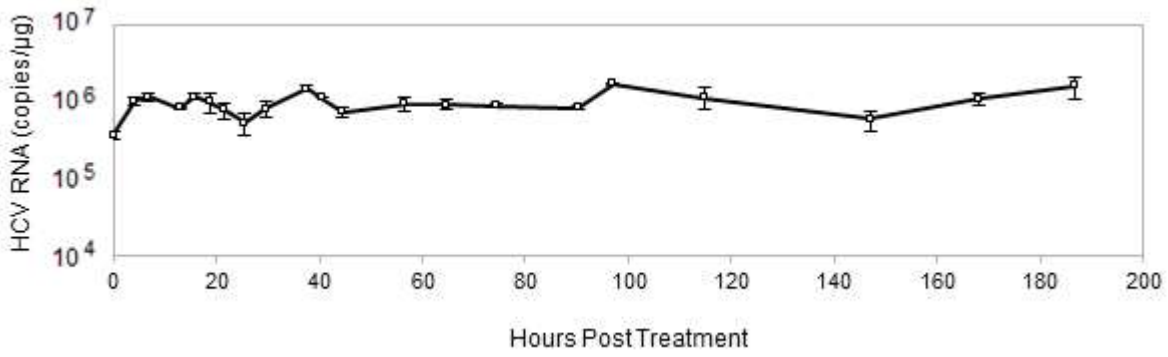

Figure 3. Steady-state HCV Levels in Non-Growing Replicon Cells. We do not observe large fluctuations in the copies of HCV sgRNA (y-axis) in non-growing replicon cells over time (x-axis) (black line).

2.3 Hepatitis C Virus Infections

To establish steady-state HCV infection in non-growing cells, Huh7 cells were infected with JFH-1 at an MOI of 0.02 after 14 days of DMSO cDMEM treatment. Chronic steady-state infection was therefore achieved by day 20 of DMSO treatment (Chapter 3, Fig. 17) and at this point cells were used for HCVcc inhibition kinetics experiments.

2.4 Inhibitors and Reagents

Recombinant human IFN- α-2a (PBL Biomedical Laboratories, New Brunswick, NJ) was resuspended in complete DMEM (as described above) to a stock concentration of 1 U/μl, aliquoted into single-use tubes, and stored at -80°C. Similar resuspension and storage at -80°C was performed with NM107 (Pharmasset, Princeton, NJ), PF254027 (Pfizer, NYC, NY), BILN2061 (Bristol-Myers Squibb, NYC, NY), Naringenin (Sigma, St. Louis, MO), and BMS-790052 (Daclatasvir) (Bristol-Myers Squibb, NYC, NY). Resuspension and storage at 4°C or -20°C was performed according to manufacturer's instructions for the exosome secretion inhibitor GW4869 (Cayman Chemicals, Ann Arbor, MI) and the exosome secretion enhancer A23187 (Sigma, St. Louis, MO). Guanidine Thiocyanate (GTC) (Thermo Fisher Scientific, Waltham, MA) was resuspended to a 5/3 concentration and stored at 4°C.

2.5 Hepatitis C Virus Inhibition Assays

For replicon inhibition experiments, geneticin was removed from all cultures 24h before beginning any antiviral treatment. Media was changed every 48 hours, except in experiments

involving IFN treatments in which fresh vehicle control or IFN-α containing medium was added to the cultures every 12h for the entire duration of the experiment to ensure continuous IFN signaling. Indicated inhibitors or diluent control was added to parallel wells and samples were harvested at the indicated times (see the figures). Culture media was harvested from triplicate wells for cytotoxicity analysis and cells were harvested in 200 µl of 1x Nucleic Acid Purification Lysis Solution (Applied Biosystems, Foster City, CA) for isolation of intracellular RNA.

For HCVcc inhibition experiments, media was changed every 2 days in such a way that avoided changing media on a well within 24 hours of it being harvested, to avoid artificially reducing extracellular HCV levels. At indicated times, medium was harvested from eight replicate wells and pooled for isolation of extracellular HCV RNA, titer analysis, and cytotoxicity analysis. Cellular lysate from 4 individual wells was harvested in 200 µL 1× nucleic acid

2.6 Hepatitis C Virus Infectivity and Particle Decay Assays

Laboratory stock virus was thawed from -80℃, diluted by DMSO cDMEM cell culture medium to $5x10^4$ FFU/mL, aliquoted into 2 mL tubes, and incubated at 37℃. Then we harvested samples at the indicated times and measured the infectious titer by titer assay and total HCV RNA by RT-qPCR in the sample over time to monitor decay. To monitor the effect of spent media on stock virus, virus was thawed and aliquoted into U-bottom 96-deep well plates and an initial sample was harvested. Remaining wells received 25 µl of DMSO cDMEM media that was either fresh, 24-48h old taken from DMSO cell culture that was either naïve, naïve and treated with 100

IU/mL IFN-α, or infected with adenovirus. Every 3 hours, additional samples were harvested for RNA isolation and media was added to remaining wells.

2.7 Intracellular RNA isolation

Cellular lysates were harvested in 1x Nucleic Acid Purification Lysis Solution (Applied Biosystems) and RNA was purified using an ABI Prism 6100 Nucleic Acid PrepStation (Applied Biosystems), per the manufacturer's instructions.

2.8 Extracellular RNA isolation

Manual extracellular RNA isolation. Most extracellular RNA samples were processed manually. For these experiments, 600 µL of supernatant was combined with 1mL 5/3 GTC, mouse liver RNA was added to control for RNA isolation yield variation between samples, and then the sample was divided into two duplicate aliquots and processed independently by phenol chloroform extraction. Each replicate was resuspended in 30 µL.

Semi-automated extracellular RNA isolation. Some extracellular RNA samples were processed using the Kingfisher Duo (Fisher Scientific). Duplicate aliquots were processed according to manufacturer's protocol, each having 150 µL of supernatant, combined with 250 µL of 5/3 GTC and mouse liver RNA. Each replicate was resuspended in 100 µL.

2.9 Reverse Transcription and Real-Time Quantitative Polymerase Chain Reaction

To quantify RNA levels, 3 µL of intracellular RNA (from 30µL total per well) or 9.35 µL of extracellular RNA (from 100µL total per sample) was used for random prime cDNA synthesis using the TaqMan RT reagents (in either a 15 µL or 20 µL reaction, respectively) (Applied Biosystems), followed by SYBR Green RT-qPCR using an Applied Biosystems 7300 real-time thermocycler (Applied Biosystems). Thermal cycling consisted of an initial denaturation step for 10 min at 95°C, followed by 40 cycles of denaturation (15 s at 95°C) and annealing/extension (1 min at 60°C). Primers used are indicated in Table 1. HCV copies were quantified relative to a standard curve comprised of serial dilutions of plasmid containing the pJFH-1 plasmid and normalized to cellular GAPDH.

Gene detected	Forward/sense sequence	Reverse/antisense sequence
HCV (sg1b, sg2a, JFH-1)	5'-CGACACTCCACCATAGATCACT-3'	5'-GAGGCTGCACGACACTCATACT-3'
Human GAPDH	5'-GAAGGTGAAGGTCGGAGTC-3'	5'-GAAGATGGTGATGGGATTTC-3'
Murine GAPDH	5'-GGAGATTGTTGCCATCAACG-3'	5'-CATGGACTGTGGTCATGAGC-3'

Table 1. Real-Time Quantitative Polymerase Chain Reaction Primers

2.10 Hepatitis C Virus Titer Assay

Cell supernatants were serially diluted 10-fold in cDMEM, and 200 µL per well was used to infect quadruplicate Huh7 cultures in 96-well plates. Because antiviral-treated samples contained potentially inhibitory drugs we initially performed dilution and time of inoculation experiments (described in Discussion of Chapter 4) to determine what dilution of the sample and timing of inoculum removal would minimize the effect of the drugs in the these titration assays. However, to control for any residual drug effect, the experimental concentration of each drug was added individually to a mock-treated sample before serial dilution to ensure any effects were similar across all samples. The drug-containing virus/medium sample was then removed at 9 h post inoculation, cells were washed so that the titer assay could proceed in the absence of the antiviral compounds, and monolayers were overlaid with cDMEM containing 0.25% methylcellulose (wt/vol) (Fluka BioChemika). As a control to determine if residual inhibitor effects occurred, mock samples also were titered in the absence of any drug addition. At 72 h post inoculation, medium was removed, cells were fixed with 4% paraformaldehyde (Sigma), and immunohistochemical staining for HCV E2 was performed as described previously[84]. Viral infectivity titers are expressed as FFU per experimental well (200 µL of supernatant), determined by the average number of E2-positive foci detected in quadruplicate samples at the highest HCV-positive dilution.

2.11 Cytotoxicity assay

The presence of lactate dehydrogenase (LDH) in the culture medium indicates that cell membrane integrity is compromised, so cytotoxicity can be determined by measuring the amount

of LDH present in the medium. For that purpose, LDH levels in the medium of antiviral-treated cultures were measured using a CytoTox-ONE Homogeneous Membrane Integrity Assay (Promega, Madison, WI), in accordance with manufacturer's instructions. The fluorescent resorufin product was detected using an excitation wavelength of 560 nm and an emission wavelength of 590 nm (FLUOstar Optima fluorometer; BMGLabtech, Durham, NC). A complete cell lysis sample was run as a positive control, and fresh medium alone was run in the absence of cells as a negative control.

2.12 Isolation and Detection of Exosomes

Non-growing Huh7 cells cultured in T-162 flasks were treated either with exosome secretion enhancer, inhibitor, or vehicle control. After 24h of treatment, 80 mL of supernatant was harvested from each condition. Exosomes were isolated from supernatant via ultracentrifugation, according to Current Protocols in Cell Biology.[85,86] Briefly, supernatants were cleared of live cells and cell debris, then spun at 100,000g for 70 min to pellet exosomes. Pellets were resuspended in 100 µL of PBS for analysis by Bradford protein assay and CD63 ELISA (System Bioscience and Bradford assay) according to manufacturer protocol.

2.13 Normalization of Data for Mathematical Modeling

In order to prepare the data for mathematical modeling, the HCV level in all mock samples was normalized to the average HCV steady-steady level throughout the experiment (i.e. the average mock HCV level) (Fig. 4A versus 4B) This normalization combined with expressing all

experimental conditions relative to mock levels at each time point allows us to see the kinetic profile of the RNA reduction induced by an inhibitor more clearly and negates the need to repeatedly show the control mock treated data, which always is a straight line. Hence in many of the figures throughout this these, the Mock control is not shown in graphs.

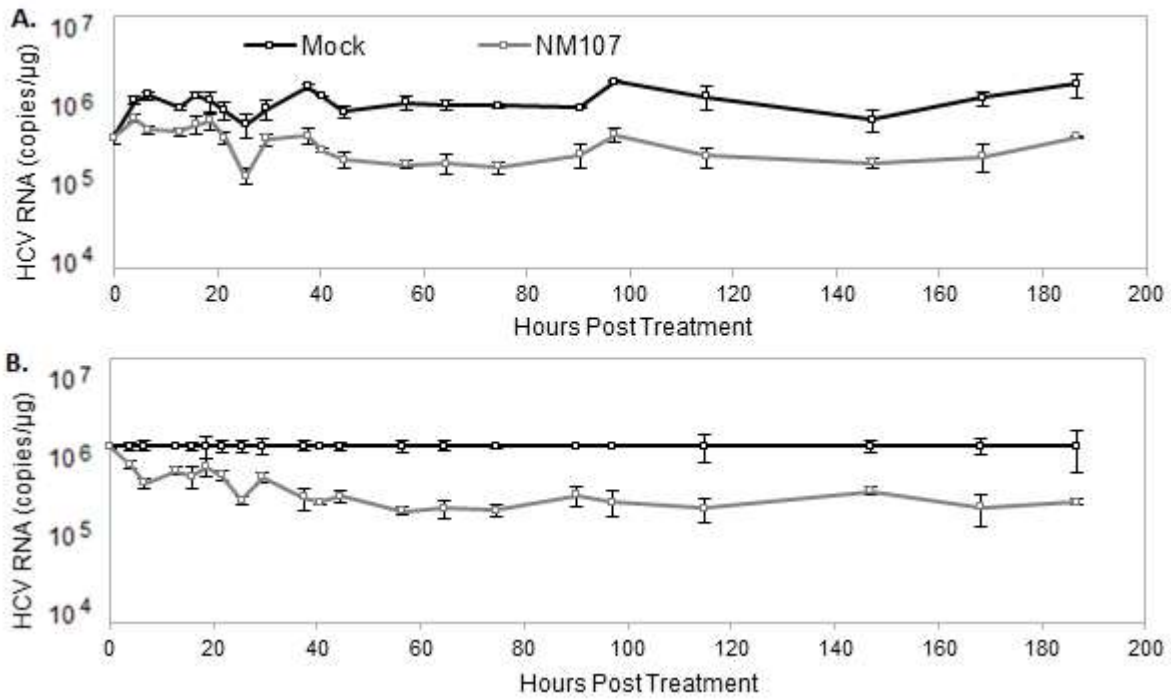

Figure 4. Normalization of Kinetic Inhibition Data. In order to prepare each of our datasets for mathematical modeling, all mock samples were normalized to the average mock HCV level throughout the experiment (1x10^6 in this example) and all other experimental conditions were normalized to mock. (A) Raw data from an example NM107 inhibitor experiment. (B) Normalized data from an example NM107 inhibitor experiment.

2.14 Mathematical Modeling

After developing the initial model based on prior knowledge about the drug MOA and viral life cycle, the first task is to reduce the number of unknown parameters by designing specific experiments to isolate and estimate parameters when possible such as extracellular viral stability and titer infectivity (e.g., parameters c and k_{loss} in chapter 4, Fig. 16). Another example, when calibrating drug-inhibition data we reduce the number of unknown/free parameters in cases that the drug MOA is known: (i) assembly/secretion would not apply in the case of the polymerase inhibitor, and (ii) nor would inhibiting RNA production in the case of the secretion inhibitor (see chapter 4, Table 8).

Next the model steady-state conditions are solved in order to further reduce the number of unknown model parameters (See below, Steady-State Equations). Then the candidate model is simulated to understand the role of each model parameter (called sensitivity analysis and parameter identifiability), which was done in Berkeley Madonna software for this thesis. Thereafter, the unknown parameters are fitted/calibrated against the experimental data and another round of math modeling analysis begins in case the goodness of fit is poor and/or parameter values are not biologically sound.

2.15 Steady-State Equations

At steady-state, differential equations are set to 0 because there are no level changes in the system. Algebraic rearrangement then allows us to link some of the unknown parameters to other model parameters (also see Fig. 15), i.e., to express certain parameters in terms of others

so that the number of unknowns is functionally reduced and the model can be used to simulate steady-state as follows:

; solve d/dt(R)=0
a0=(μ+ks)*Ro-kin*Vio
; solve d/dt(Vni)=0
Vnio=(ks*(1-ρ)*Ro+K_loss*Vio)/c
; d/dt(Vi)=0
ks=(kin+c+K_loss)*Vio/(ρ*Ro)
; plug in ks into Vniod/dt(Vni)=0 and use Vnio=Vtoto-Vio
kin=-c-K_loss/(1-rho)+c*ρ/(1-ρ)*(Vtoto-Vio)/Vio
Equations above are for initial HCVcc model (Fig. 14). Below is the version of equations that includes non-infectious entry for the HCVcc model (Fig. 23):

; solve d/dt(R)=0
a0=(μ+ks)*Ro-kin*Vtoto
; solve d/dt(Vni)=0
Vnio=(ks*(1-ρ)*Ro+K_loss*Vio)/(kin+c)
; d/dt(Vi)=0
ks=(kin+c+K_loss)*Vio/(ρ*Ro)
; plug in ks into Vnio d/dt(Vni)=0 and use Vnio=Vtoto-Vio
kin=(-c*Vtoto+((c+K_loss)*Vio/ρ))/(Vtoto-Vio/ρ)

2.16 Parameter Calibration and Confidence Intervals.

DEDiscover software (http://www.dediscover.org) was used to calculate 95% confidence intervals of estimated parameters.

3. HEPATITIS C VIRUS REPLICON DYNAMICS AND DRUG EFFICACY

3.1 Introduction

In 2010 when the aims in this chapter were conceived, direct-acting antivirals (DAAs) against HCV replication were being developed, but none had been approved by the FDA. At that time, the standard of care for chronic HCV treatment in the clinic was pegylated interferon (pegIFN) plus ribavirin, which subjected patients to serious side effects and up to a 50% fail rate depending on the HCV genotype being treated. In light of the immediate need to understand the antiviral mechanism of action (MOA) of IFN and facilitate drug development, we sought to further understand HCV replication dynamics and drug MOA, by quantitatively characterizing and mathematically modeling HCV RNA replication and treatment response kinetics. The rationale was that mathematical modeling could aid in drug development in several ways: (1) by elucidating the means by which IFN produced its beneficial effects thus enabling the development of compounds that could imitate those mechanisms in a more targeted manner that avoids the serious side effects induced by IFN and (2) by analyzing the treatment response of compounds that were candidates for clinical trials to determine their MOA and predict which drugs (or drug combinations) might be most effective in treating HCV.

When analyzing data with mathematical modeling, reducing the number of unknown parameters in the model makes the results more meaningful. Because the infectious HCV cell culture (HCVcc) system was relatively new at the time with many parameters undefined/unmeasured, we opted to start our analysis using the simpler HCV replicon system to

minimize the number of unknown parameters. Though the HCV replicon model lacks the entry, assembly, and egress steps of the HCV viral lifecycle, it recapitulates the aspect of the HCV life cycle against which all the first HCV DAAs being developed were targeted (i.e. HCV intracellular replication).

Figure 5 contains schematics of the published simple intracellular subgenomic HCV (sgHCV) replicon model from our lab that was the starting point for this thesis.[76] Looking at panel A, the oval represents a cell, and the arrows represent the two main phenomena that can affect the level of intracellular HCV RNA (R). The main contributor to HCV RNA levels is RNA production (α), and the main detractor from HCV RNA levels is RNA degradation (μ).

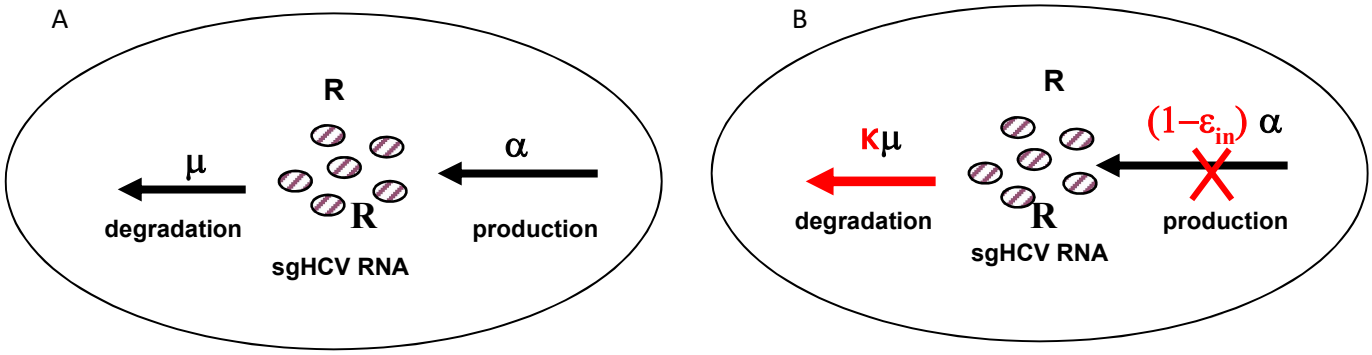

Figure 5. Schematic of the Simple HCV Replicon Mathematical Model and Possible Antiviral Drug Effects. A. HCV subgenomic replicon RNA copies (R) are produced at rate α (copies/day) and degraded at rate μR (copies/day) within a cell. **B.** Possible mechanisms by which antivirals might inhibit HCV subgenomic replicon RNA (R) production (α) and/or enhance degradation (μ) within a cell are shown in red. Inhibition of R is represented by $(1-\epsilon_{in})$ where ϵ_{in} represents percent drug efficacy. Enhancement of R degradation (κ) represents the fold-change in degradation rate caused by the drug.

As shown in Fig. 5B, the model can simulate the effect of a drug that blocks sgRNA production by multiplying the HCV copies per day production rate coefficient α by $1-\epsilon_{in}$ ($0 \leq \epsilon_{in} \leq 1$), which will decrease the production rate. We define ϵ_{in} as the percent efficacy of the drug in blocking RNA production. To simulate the effect of a drug on enhancing sgRNA degradation, the HCV copies per day degradation rate coefficient μ is multiplied by the parameter κ, which is equal to one if the drug has no effect on degradation or $\kappa > 1$ if the drug enhances degradation. These schematics correspond to the following differential equation, which describes the change in sgRNA level (R) over time (t).

$$\frac{dR}{dt} = (1 - \varepsilon_{in})\alpha_0 - \kappa\mu R \qquad \textbf{(Eq. 1)}$$

In order to bring the model (Eq. 1) into steady-state, in which sgRNA level (R_0) remains constant over time (as we discuss in more detail in chapter 2, Fig. 3), dR/dt was set to 0 (i.e., no change in R over time), and we set $\alpha_0 = \mu R_0$.

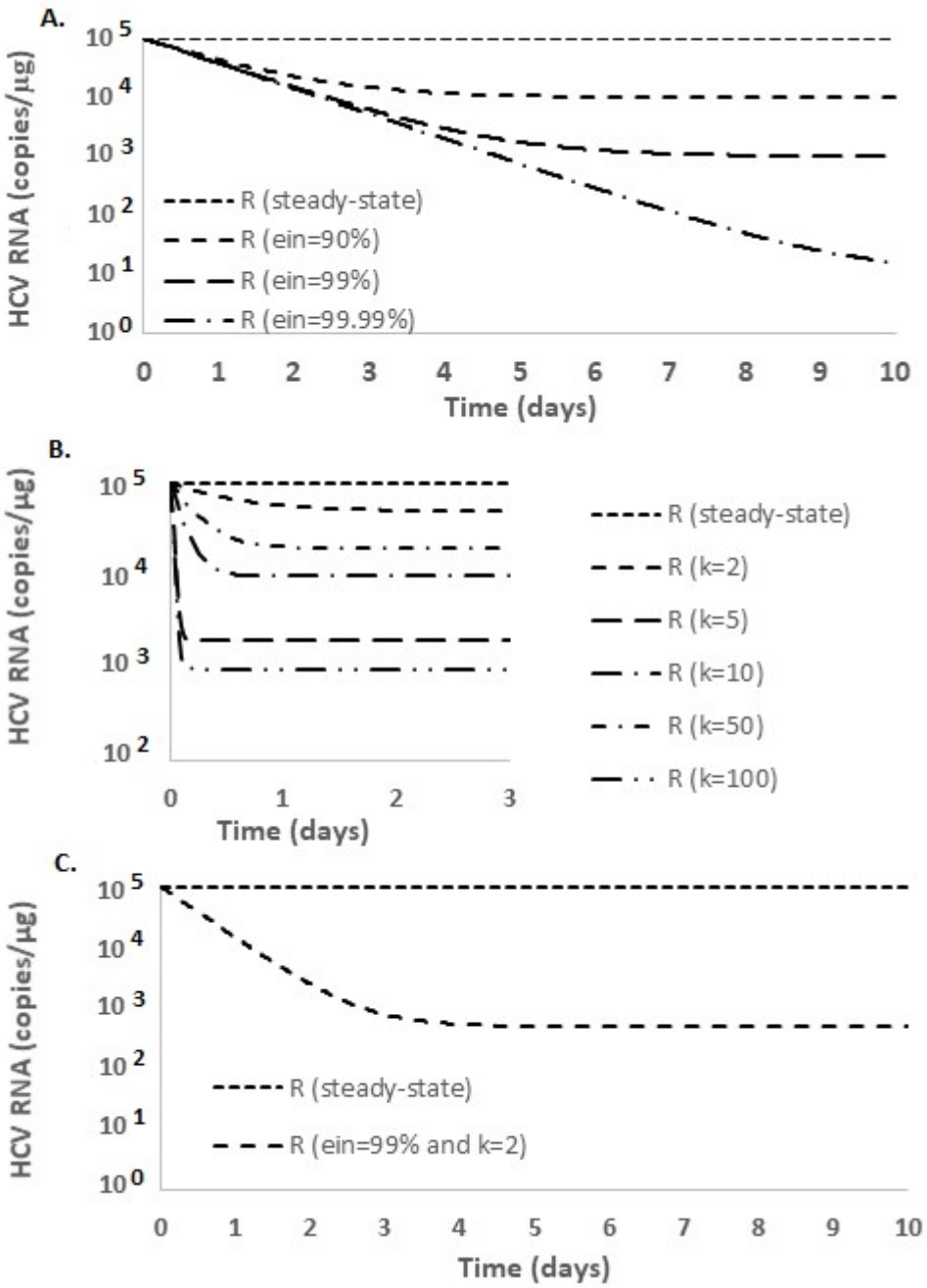

Figure 6. Incomplete Replicon Model Simulations of Antiviral Treatment. Y-axis shows simulated sgRNA level on a logarithmic scale. X-axis shows time in days. **(A)** Model is simulating 0%, 90%, 99%, or 99.99% inhibition of sgRNA synthesis (alpha). **(B)** Model is simulating 1x, 2x, 5x, 10x, 50x, or 100x enhancement of sgRNA degradation. **(C)** Model is simulating steady-state or a combination of both inhibition mechanisms, a 2x enhancement of RNA degradation and a 99% inhibition of RNA synthesis. In all simulations $R0=1x10^5$ log copies/cell, $\mu=0.98$/day

Notably however, it was clear this simple model (Eq. 1) was not sufficient because it can only predict a single exponential sgRNA decline that reaches a new lower set point (Fig. 6), while biphasic declines have been observed *in vitro* [76] (Fig. 4B) and *in vivo* [87]. To allow for this 2nd phase decline in sgRNA levels, a time-dependent term ($\exp^{-gt}$) was added to the model (multiplied by $(1-\epsilon_{in})\alpha_0$) where parameter g accounts for the interruption of sgRNA production to increase over time, representing any non-immediate events that further slow the production of HCV subgenomic RNA, such as the gradual breakdown of RNA replication complexes. Hence, any events that decrease the rate of sgRNA production with an effect that increases with time can be represented by setting parameter g to a value greater than zero. With the addition of this parameter, the model is able to simulate the observed biphasic sgRNA decline[76] (Fig. 7). Hence, the more detailed model equation is

$$\frac{dR}{dt} = (1-\varepsilon_{in})\alpha_0 \exp(-gt) - \kappa\mu R \qquad \textbf{(Eq. 2)}$$

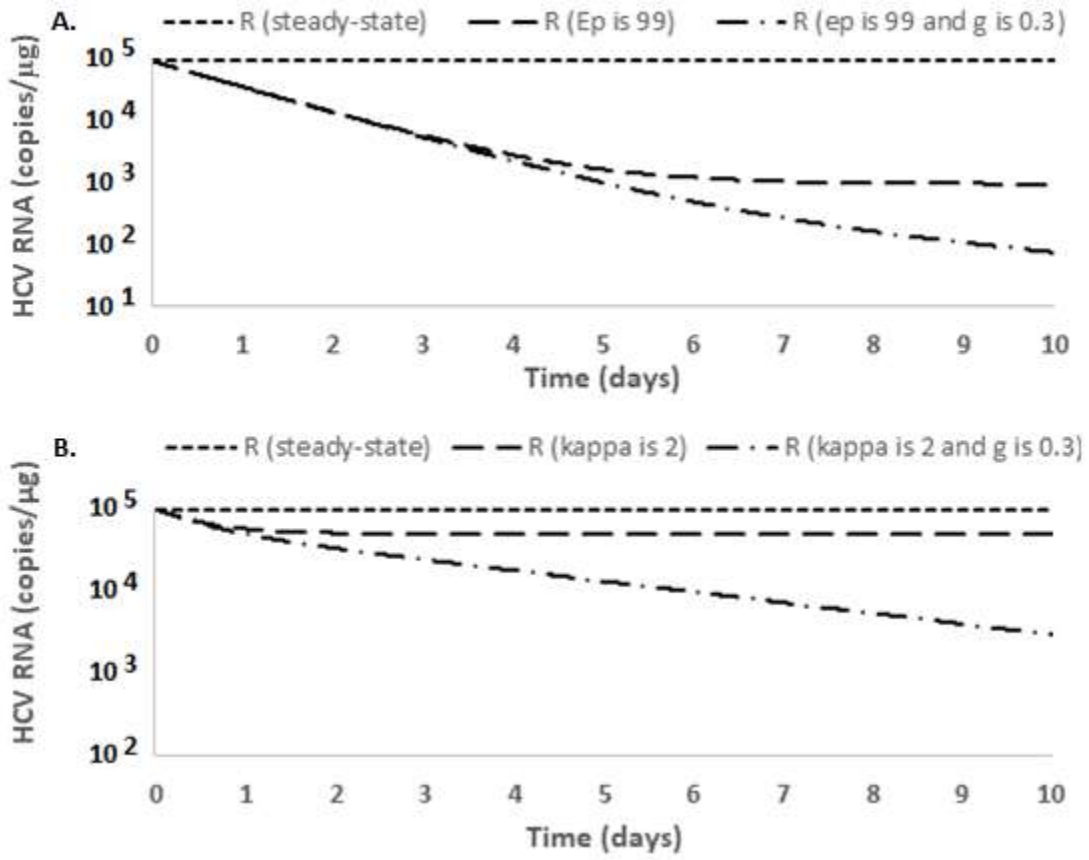

Figure 7. Replicon Model Simulations of Biphasic Antiviral Decline. The final published Replicon Model (Eq. 2) can simulate a biphasic decline when g parameter is greater than 0. **(A)** RNA synthesis inhibition is set at 98% and g is set to either 0 or 0.3. **(B)** RNA degradation is enhanced by 100% and g is set to either 0 or 0.3. Y-axis shows simulated RNA level on a logarithmic scale. X-axis shows time in days. Other model parameters values are as described in Fig. 6.

Anything that increases the amount of HCV RNA will be a positive expression in the equation. Specifically, the production of RNA will be positive, and it is expressed as the production rate α_0 multiplied by $(1-\epsilon_{in})$, multiplied by the term that describes whether any secondary events such as the breakdown of replication complexes occur that would further slow the production of HCV RNA as time increases (exp(-gt)). Anything that reduces the amount of HCV RNA will be a negative expression in the equation. For example, RNA degradation reduces the amount of HCV RNA and is represented by a negative product of the degradation rate coefficient, μ, the effect of the drug in enhancing HCV RNA degradation, κ, and the amount of RNA available to be degraded, R.

Use of the simple intracellular HCV replicon model above to assess the kinetics of IFN inhibition of an HCV subgenomic genotype 1b (sg1b) replicon under the standard growing Huh7 cell culture condition had suggested that IFN mainly blocks HCV RNA replication, but that at higher doses it might also enhance HCV RNA degradation and cause delayed events that further reduce HCV RNA replication (such as break-down of replication complexes)[76] However, there were some limitations inherent in the initial experimental approach utilized. The work described herein overcomes these technical challenges in two significant ways. The first difference is the conversion to the non-growing DMSO Huh7 system. This was a critical change as the non-growing culture system allows for a true HCV steady-state to be achieved,[83,84] enables longer experiments by avoiding issues of cells reaching confluence and requiring splitting, reduces well-to-well variability,[79,84] and reduces changes in intracellular HCV and drug concentration that may result from cell division. Hence, these non-growing DMSO Huh7 features are fundamental for a

more reliable drug-perturbation mathematical modeling. The non-growing DMSO Huh7 cells further exhibit increased liver-specific gene expression[83] and drug metabolism activity more similar to differentiated hepatocytes[88], which is also consistent with an infection environment that is more biologically relevant. Second, we broadened the scope of our inhibition studies to include the use of direct-acting antivirals of known MOA, such as protease and polymerase inhibitors, to help further characterize treatment response kinetics and demonstrate the usefulness of the model in analyzing the response kinetics observed with more defined inhibitors and more effectively estimate unknown parameters such as the intrinsic HCV RNA degradation rate, which would otherwise be difficult to measure empirically.

3.2 Results

3.2.1 Modeling Hepatitis C Virus Replicon Inhibition Kinetics in Non-Growing Huh7 Cells

Our first goal in adapting our mathematical modeling experiments to the non-growing DMSO Huh7 cells[89] was to explore whether the non-growing system would yield similar results as the growing cells by repeating analogous IFN experiments and mathematical analysis and comparing the results between systems. Using the same doses of IFN in the same HCV subgenomic genotype 1b (sg1b) replicon Huh7 cells, we quantified HCV RNA levels across a similar time scale in non-growing DMSO cells. Other than the non-growing status of the cells, the other main difference from the published experimental method was more frequent harvesting of RNA with more replicates at each time point, something that is manageable in the non-growing

cell culture system as it eliminates the need for splitting the cells during the experiment allowing for increased numbers of wells and a smaller 96-well format.

Specifically, non-growing sg1b replicon Huh7 cells (see Materials and Methods2.2) were treated with IFN at doses of 0, 100 or 250, International Units (IU) per mL. Media was replenished every 12 hours to maintain consistent IFN signaling[76] and cells were harvested from triplicate wells for intracellular RNA isolation every 2-4 hours for the first 24h after the initiation of IFN treatment and every 4-8 hours in subsequent days of IFN treatment as indicated across the x-axis (Fig. 8). As was observed in the growing Huh7 cell culture experiments, both 100 IU/mL (Fig. 8A) and 250 IU/mL (Fig. 8B) of IFN in the non-growing Huh7 cell system resulted in a biphasic decline. The 100 IU/mL dose caused a rapid, 1-log reduction in HCV RNA level between 0 and 2 days. Between the second and fifth day there was an additional, slower, ½-log reduction, and then the HCV RNA level plateaued (Fig. 8A). The 250 IU/mL dose showed a rapid, 1.5-log reduction between days 0 and 1.75, then an additional, slower, 1-log reduction beginning at day 1.75 (Fig. 8B).

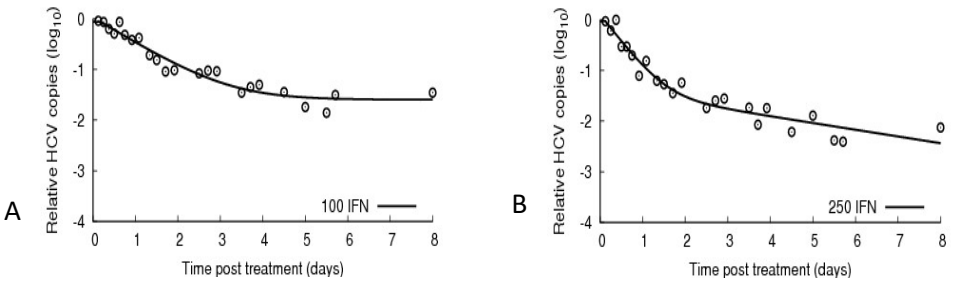

Figure 8. Inhibition Kinetics of HCV sg1b RNA under IFN Treatment in Non-Growing Huh7 Cells. DMSO growth-arrested HCV replicon cells with steady-state HCV RNA levels were treated with (**A)** 100 IU/mL or (**B)** 250 IU/mL doses of IFN or diluent control (not shown, see Materials and Methods). Open circles represent the average of triplicate samples graphed as the difference in HCV RNA copies per μg relative to the diluent treated control cultures at the corresponding time point. The solid line represents the best fit simulation created by the mathematical model (Eq. 2).

Fitting Eq. 2 (Fig. 8, solid line) to the observed inhibition kinetics (Fig. 8, open circles), generated predictions about the MOA of IFN and drug efficacy (Table 2). Specifically, the model suggests that the lower dose of IFN (100 IU/mL) reduced sg1b RNA primarily by reducing HCV RNA production by 97% without significantly enhancing its degradation (κ=1.16 [95% CI =0.89-1.45]). In contrast, while the inhibition kinetics observed during higher doses of IFN (250 IU/mL) treatment exhibited a similar reduction in HCV RNA production (i.e. 96%), the model also predicted an enhancement of HCV RNA degradation (κ=2.54 [95% CI =1.35-3.73]) as well as

time-delayed events that further reduce HCV RNA production over time (i.e. g is greater than 0). Importantly, these MOAs and drug efficacy estimations are consistent with the predictions from our previously published results from growing cell experiments (Table 2). Based on 95% confidence intervals, the model estimates for the delays (t_0) were not significantly different.

IFN Dose (IU/mL)	Cells	Delay t_0 (h) [CI 95%]	Drug efficacy ε_{in} [CI 95%]	Degradation rate coefficient μ (per day) [CI 95%]	g (per day) [CI 95%]
100	DMSO	2.96 [2.95-2.98]	0.97 [0.96-0.98]	1.16 [0.89-1.45]	0
100*	dividing	9.5 [3.6-15.4]	0.97 [0.96-0.98]	0.98 [0.85-1.11]	0 [0-0.001]
250	DMSO	3.00 [0-15]	0.96 [0.91-1.0]	2.54 [1.35-3.73]	0.30 [0.10-0.51]
250*	dividing	7.8 [3.1-12.4]	0.93 [0.88-0.97]	2.32 [1.57-3.07]	0.33 [0.22-0.45]

Table 2. Replicon Model Predictions of IFN Efficacy and Mechanism of Action.
t_0 = delay; ε_{in} = percent inhibition of HCV RNA production; μ = degradation rate coefficient of HCV RNA; g = time-delayed events that further reduced HCV RNA production. *results from published growing cell experiments[76]

Importantly, these results demonstrate that the state of Huh7 cell growth does not inherently alter HCV treatment response kinetics and thus allowed us to transition into this more experimentally amenable system, which offers several advantages. First and foremost, it allows for a true HCV steady-state, which is extremely beneficial for mathematical modeling. Equally valuable, it has technical advantages such as not requiring cell splitting, which reduces variation in HCV RNA levels, allows us to grow these cultures in 96-well plates, and take more frequent samples, enhancing our ability to monitor HCV treatment response kinetics and predict drug mode of action through mathematical modeling.

3.2.2 Quantitative Estimate of the Intrinsic Degradation Rate of Hepatitis C Virus RNA

It can be difficult to directly measure parameters such as intracellular HCV RNA degradation. A major utility of mathematical modeling is the ability to estimate parameters like this, without isolating and measuring them empirically. However, when the non-growing HCV replicon system (and mathematical model) is in steady-state, the RNA production and degradation rates are equal and thus impossible to estimate without altering one individually. In order to estimate the intrinsic degradation rate of the viral RNA, we chose to perturb steady-state of the HCV sg1b replicon system by specifically blocking HCV RNA production with a well-characterized, nucleoside analog inhibitor of the viral NS5b polymerase called NM107. As such, the RNA degradation rate that is observed during treatment with NM107 can be considered the intrinsic degradation rate of the viral RNA. Briefly, non-growing HCV replicon cells with steady levels of HCV RNA were treated with polymerase inhibitor NM107 (open circles) or diluent control

(not shown) and triplicate samples were harvested at indicated time points to determine HCV RNA levels (Fig. 9). After six days of treatment, HCV RNA levels were reduced by 2 logs. Beyond 6 days of treatment, there is only one data point at day 8 of treatment which is difficult to interpret as it may indicate a new steady-state for the HCV RNA levels or the data point may be an outlier.

The simple HCV replicon mathematical model (Eq. 2) is able to fit the NM107 polymerase inhibitor data through day 6 well (Fig. 9, solid line), enabling estimates of intracellular HCV RNA degradation rate and NM107 efficacy in blocking HCV RNA production (Table 2). However, the data were not sufficient to confidently fit the model with the later inhibition kinetics due to a lack of data points taken in that time frame post-treatment. Specifically, the data post day 6 consisted of a single time point taken 8 days after the beginning of drug treatment. Based on this one data point, the model would predict that drug efficacy is 98% and that HCV levels would achieve a new steady-state two logs lower than the starting level (Fig. 9, dashed line), but if that one isolated time point were excluded from the analysis the drug efficacy increased to 99.6% and the new predicted steady-state would be ten-fold lower (Fig. 9, solid line).

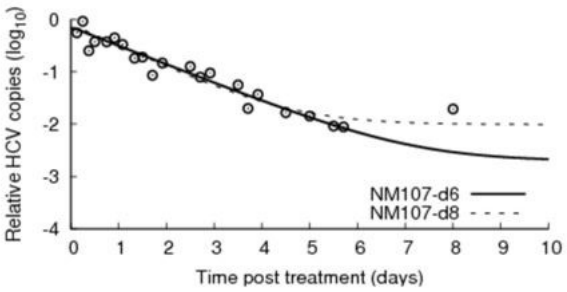

Figure 9. Inhibition Kinetics of HCV sg1b RNA under NM107 Treatment. Non-growing DMSO-Huh7 sg1b replicon cells were treated with 18μM NM107 or diluent control (not shown). Triplicate wells were harvested at indicated times post-treatment and HCV RNA was quantified by RT-qPCR, normalized to cellular GAPDH levels. Open circles represent the average of triplicate samples graphed as the difference in HCV RNA copies per μg relative to the diluent treated control cultures at the corresponding time point. The solid line shows the mathematical model (Eq. 2) simulation fitting data from days 1-6. The dotted line shows the mathematical model simulation fitting all data points.

3.2.3 Increased Sampling Frequency to Resolve Model Fit Ambiguity.

Having converted to the non-growing Huh7 cell culture system we were readily able to design experiments with more frequent sampling to more thoroughly document HCV inhibition kinetics beyond 6 days of treatment. We treated non-growing HCVsg1b replicon cells with 0 or 18μM of HCV polymerase inhibitor NM107 and took frequent samples (every 6 hours or more frequent) during 16 days of treatment to measure intracellular HCV RNA levels (Fig. 10, open circles). The RNA levels were reduced quickly by ¾ log between 0 and 24 hours of treatment, they plateaued until 48h of treatment, then declined quickly by 2 additional logs until day 8 when a new plateau was achieved.

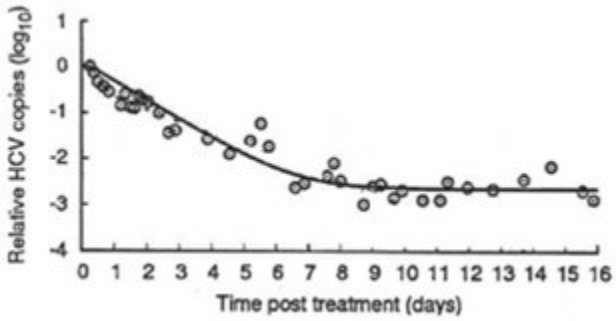

Figure 10. Extended Inhibition Kinetics of HCV sg1b RNA under NM107 Treatment. Non-growing DMSO-Huh7 sg1b replicon cells were treated with 18μM NM107 or diluent control (not shown). Triplicate wells were harvested at indicated times post-treatment and HCV RNA was quantified by RT-qPCR and normalized to cellular GAPDH levels. Open circles represent the average of triplicate samples graphed as the difference in HCV RNA copies per μg relative to the diluent treated control cultures at the corresponding time point. Solid line shows mathematical model simulation fit. The dotted line shows the mathematical model simulation fitting based on experimental data until day 8.

Experiment	Data analyzed	Delay t_0 (hrs)	Drug efficacy ε_{in}	RNA degradation rate constant μ (per day)	g (d^{-1})
Fig. 5	6 days	6 [0-31]	0.996 [0.98-1.0]	0.83 [0.60-1]	0
Fig. 5	8 days	6 [0-36]	0.98 [0.965-1.0]	0.96 [0.70-1.22]	0
Fig. 6	16 days	6 (fixed)	0.998 [0.997-0.999]	0.89 [0.841-0.939]	0

Table 3. Replicon Model Parameter Estimates Based on Extended NM107 Inhibition Kinetics. t_0 = delay; ε_{in} = percent inhibition of HCV RNA production; μ = intrinsic degradation rate constant of HCV RNA; g = time-delayed events that further reduced sg1b RNA production. Due to NM107 known MOA in terminating sg1b RNA synthesis it is not biological plausible that sg1b degradation was enhanced, hence κ=1 under NM107 treatment.

Looking at the model parameter estimates and taking into account the 95% confidence intervals the 18 μM dose of NM107 from the 8 day experiment (excluding the single day 8 outlier)(Fig. 9) and the 16 day experiment (Fig. 10), estimates for efficacy in blocking HCV RNA production, RNA degradation rates, and g decay rates were the same. Because the final plateau observed for sg1b HCV RNA levels is 3 logs lower than the initial HCV RNA viral RNA levels (Fig. 10), these results indicate that the day 8 data point in the first experiment (Fig. 9) was an outlier and confirm the need for samples to be taken frequently especially near the end of a time course.

3.2.4 Polymerase Inhibitors with Distinct Mechanism of Inhibition Yield Similar Treatment Response Kinetics

Intrinsic in this simple model is the expectation that all HCV NS5b polymerase inhibitors (i.e. drugs that specifically/solely block HCV RNA synthesis) would create similar kinetic patterns of HCV decline when dosed to the same efficacy. In order to test that hypothesis, we performed inhibition experiments with two different HCV polymerase inhibitors. Because NM107 is a nucleoside analog, we compare its HCV inhibition kinetics with PF254027, which is a non-nucleoside analog that sterically blocks the HCV polymerase without interacting with its active site. After performing an initial dosing of both polymerase inhibitors to determine which doses gave comparable inhibition of HCV (data not shown), cultures of non-growing HCV sg1b replicon cells with steady levels of HCV RNA were treated with 150 μM PF254027, 18 μM NM107, or control diluent. As expected, when dosed to the same efficacy both polymerase inhibitors exhibited overlapping biphasic inhibition kinetic patterns, reducing HCV sg1b steady-state replicon RNA

levels by 1.25 logs by 8 hours of treatment before achieving new plateaus (Fig. 11). The model parameter estimates and confidence intervals in Table 4 also confirm that at these doses, these two distinct polymerase inhibitors have identical efficacy in blocking HCV RNA production with no enhancement of HCV RNA degradation. Notably, due to large confidence intervals the model estimates for the delay showed no difference between the nucleoside analog (0-36 hours) and the non-nucleoside analog inhibitor (0 hours).

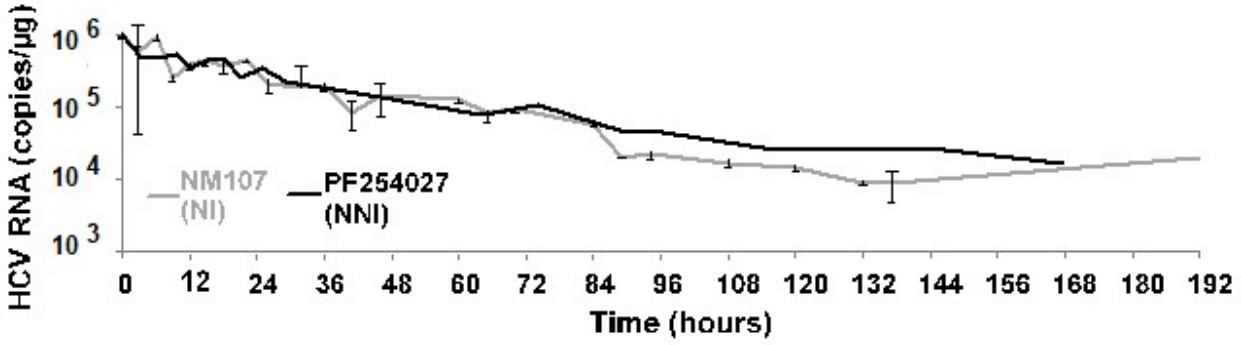

Figure 11. Inhibition Kinetics of Hepatitis C Virus sg1b RNA under NM107 and PF254027 Treatment. Non-growing DMSO-Huh7 sg1b replicon cells were treated with 18 μM NM107 (gray line), 150 μM PF254027 (black line), or diluent control (not shown). Triplicate wells were harvested at indicated times post-treatment and HCV RNA was quantified by RT-qPCR and expressed as HCV copies/μg RNA graphed relative to the HCV RNA levels in the diluent control.

Drug (dose)	Delay t_0 (hrs)	Drug Efficacy ε_{in} [95% CI]	RNA degradation rate constant μ (d^{-1})
PF254027 (150μM)	0	0.98 [0.97–0.99]	1.07 [0.92–1.22]
NM107 (18μM)	6 [0–36]*	0.98 [0.965–1.0]	0.96 [0.70–1.22]

Table 4. Replicon Model Estimates based on Polymerase Inhibition Kinetics. t_0 = delay; ε_{in} = percent inhibition of HCV RNA production; μ = degradation rate constant of sg1b HCV RNA; g = time-delayed events that further reduced HCV RNA production. *Not statistically different from 0 hours because of large confidence interval

3.2.5 Estimating Drug Efficacy and Mechanism of Action of a Viral Protease Inhibitor

At the time, HCV NS3 protease inhibitors were also a focus of drug development, so we investigated the response kinetics of the HCV sg1b replicon under treatment with the protease inhibitor BILN2061. While our simple HCV replicon mathematical model does not in theory distinguish protease and polymerase inhibitors because inhibition of either viral protein interrupts the same HCV RNA production rate (α) in the model, the multiple possible roles of the viral NS3 protein in the viral life cycle (producing functional protein subunits as well as cleaving innate signaling molecules to render them non-functional for HCV detection by the host cell) meant that the protease inhibitor may have multiple MOAs, compared to the inhibitor of the viral

NS5b polymerase, a protein that is presumed to have only one function in the viral lifecycle.

Non-growing HCV sg1b replicon cells with steady levels of HCV RNA were treated with either BILN2061 protease inhibitor or control diluent and triplicate samples were harvested at indicated time points to monitor HCV RNA levels. We saw a much more dramatic 4 log reduction in sg1b RNA by both the 10 nM and 80 nM doses after 7 days of treatment (Fig. 12 A-B). Both doses were equally effective, suggesting that 10nM is significantly above the EC_{90}. Because the protease inhibitor was able to reduce HCV RNA much more than the 98% efficacy doses of polymerase inhibitors (4 logs versus 2), this suggests that the protease inhibitor does indeed have an additional MOA that reduces HCV RNA levels faster than can be achieved simply by blocking HCV RNA production; this is supported by the BILN treatment being able to reduce sgRNA levels by 4 logs in 7 days, while model simulations require 10 days of treatment to reduce sgRNA levels by 4 logs even with 99.99% efficacy in blocking sgRNA synthesis (Fig. 6A).

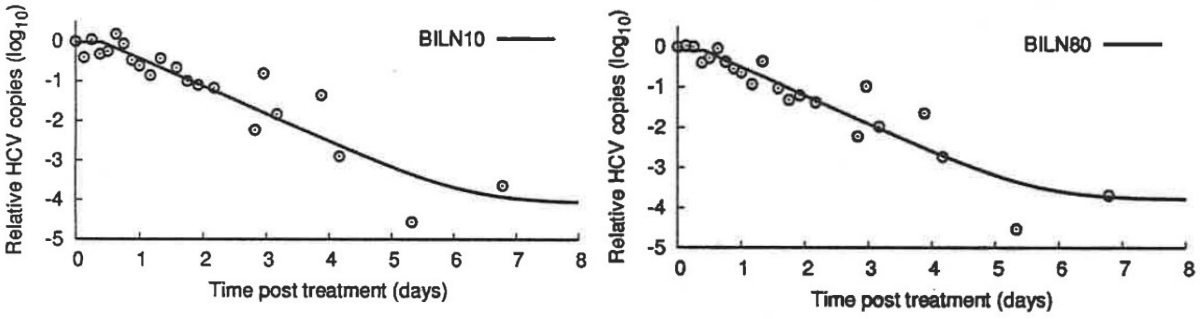

A B

Figure 12. Inhibition Kinetics of Hepatitis C Virus sg1b RNA under BILN2061 Treatment. Non-growing DMSO-Huh7 sg1b replicon cells were treated with 10nM BILN (panel A), 80 nM BILN (panel B), or diluent control (not shown). Triplicate wells were harvested at indicated times post-treatment and HCV RNA was quantified by RT-qPCR and normalized to cellular GAPDH levels. Open circles represent the average of triplicate samples graphed as the difference in HCV RNA copies per µg relative to the diluent treated control cultures at the corresponding time point. Solid line shows mathematical model simulation fit.

Experiment	BILN2061 Dose	Delay t_0 (hrs)	Drug Efficacy ε_{in} [95% CI]	RNA degradation rate constant µ(d^{-1})[95% CI]	Enhancement of RNA degradation κ	g (d^{-1}) [95% CI]
Fig. 6A	10 nM	10 [0-33]	0.999 [0.99-1.0]	1.60 [1.14-2.06]	1.93	0
Fig. 6B	80 nM	9.9 [0-30]	0.999 [0.99-1.0]	1.62 [1.20-2.04]	1.95	0
16-day*	10 nM	6 (fixed)	0.98 [0.97-0.99]	1.79 [1.58-2.00]	2.01	0.10 [0-0.4]

Table 5. Replicon Model Estimates Based on Protease Inhibition Kinetics. t_0 = delay; ε_{in} = percent inhibition of HCV RNA production; μ = degradation rate constant of sg1b HCV RNA; κ = fold-change of RNA degradation rate constant over intrinsic RNA degradation rate constant (estimated during treatment with polymerase inhibitor NM107); g = time-delayed events that further reduced HCV RNA production. *experiment (not shown)

After fitting the mathematical model to the data (solid line, fig. 12 A-B), we estimated that both 10 and 80 nM doses of BILN2061 showed a delay of 10 hours, at least 99% efficacy in blocking HCV RNA production and a 2-fold enhancement of the HCV RNA degradation rate (Table 5). When this experiment was repeated in a 16-day format, we saw similar results.

3.2.6. Direct Acting Antivirals Exhibit Different Efficacy against Different Hepatitis C Virus Genotypes

We began our modeling efforts using the HCV sg1b system, however the *in vitro* JFH-1 HCVcc infection system available for modeling the entire viral life cycle (Chapters 4 and 5) is based on HCV genotype 2. Therefore, before moving to the HCVcc infection system, we tested whether the differences in drug efficacy between HCV genotypes observed in the clinic are recapitulated in our *in vitro* systems. Using both the sg1b and sg2a (JFH-1) subgenomic constructs allowed us to compare results between two HCV genotypes.

Non-growing Huh7 HCV replicon cells (sg1b or sg2a) were treated with direct acting antivirals or diluent controls and intracellular HCV RNA levels were monitored during 8 days of treatment. NM107 (18 μM) was able to reduce sg1b RNA levels by 2 logs after 6 days of treatment (Fig. 13 panel a) with 98% efficacy in blocking HCV RNA production (Table 6). However, a higher dose of NM107 (25 μM), was only able to reduce sg2a RNA levels by 0.75 logs, plateauing after 2 days of treatment (Fig. 13 panel b) with only 70% efficacy in blocking HCV RNA production (Table 7).

PF254027 elicited a dose-dependent response (data not shown) with the highest dose tested (i.e. 150 μM) reducing HCV sg1b and HCV sg2a steady-state replicon RNA levels by 1 log after 1 day of treatment (Fig. 13, panels c and d respectively). However, while the HCV sg2a RNA response plateaued, the HCV sg1b RNA was further reduced by 1 additional log after 4 days of treatment and the drug exhibited 98% efficacy in blocking HCV RNA production (table 6). In sg2a cells, the drug only exhibited 88% efficacy in blocking HCV RNA production (table 6).

BILN2061 (10 nM) was able to reduce sg1b RNA levels by 4 logs after 7 days of treatment (Fig. 13 panel e) with 99.9% efficacy in blocking HCV RNA production (Table 6). However, a higher dose of BILN2061 (80 nM), was only able to reduce sg2a RNA levels by 3 logs after 7 days of treatment (Fig. 13 panel f) with only 93% efficacy in blocking HCV RNA production (table 6).

This shows that these drugs were more effective for sg1b than sg2a, which is consistent with *in vivo* results and the fact that the drugs were designed against HCV genotype 1.

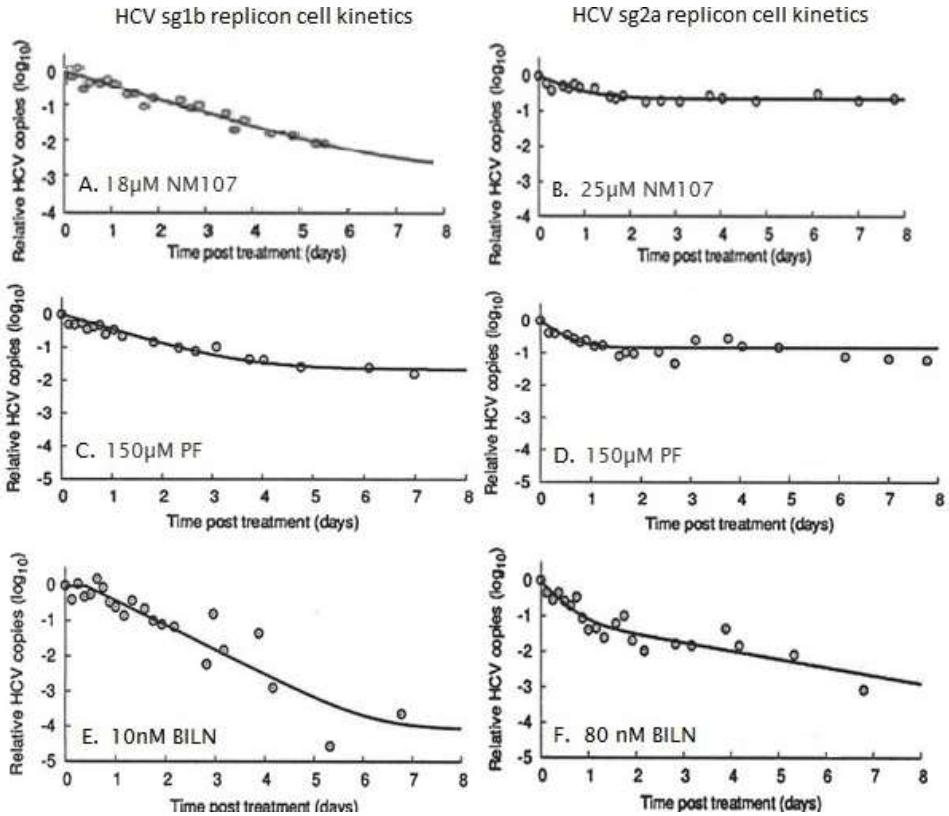

Figure 13. Different Potency of HCV DAA against HCV Genotype 1 and 2. Non-growing DMSO-Huh7 sg1b (panels A, C, and E) or sg2a replicon cells (panels B, D, and F) were treated with NM107 (panels A and B), PF254027 (panels C and D), BILN2061 (panels E and F), or diluent control (not shown). Triplicate wells were harvested at indicated times post-treatment (x-axis) and HCV RNA was quantified by RT-qPCR and normalized to cellular GAPDH levels. Open circles represent the average of triplicate samples graphed as the difference in HCV RNA cps/μg relative to the diluent treated control cultures at the corresponding time point. Solid line shows simulation by mathematical model fit to all data.

HCV Genotype	Drug	NM107	PF254027	BILN2061
sg1b	Dose	18 μM	150 μM	10 nM
	Efficacy	98%	98%	99.9%
sg2a	Dose	25 μM	150 μM	80 nM
	Efficacy	70%	88%	93%

Table 6. Replicon Model Estimates of Drug Efficacy. Efficacy is estimated as the ε_{in}, or percent inhibition of HCV RNA production

3.3 Discussion

These studies used mathematical modeling to analyze HCV replicon kinetics. The HCV replicon was chosen over the full infectious system in order to minimize the number of unknown parameters, thus increasing the parameter estimating sensitivity of the model. The mathematical model used for these studies had been published, but it had only been used to analyze data from growing cells, which did not maintain steady levels of HCV RNA, a critical necessity according to the assumptions built into the model. In these studies, we analyzed non-growing HCV replicon cell kinetics under treatment with IFN or direct acting antivirals, specifically HCV NS5b polymerase and HCV NS3 protease inhibitors. The mathematical modeling analysis of these kinetic data provided estimates for the rate of HCV sgRNA degradation, drug efficacies, and response delays, as well as generating hypotheses about the mechanism of action of HCV antivirals. Experiments were also conducted to compare efficacy of HCV NS5b polymerase and HCV NS3 protease inhibitors against HCV genotypes 1b and 2a.

Modeling perturbation of viral steady-state provides an enormous advantage due to the inherent information provided by the nature of a steady-state system (i.e. that production equals clearance). This simple fact enables different viral parameters to be expressed relative to each other, allowing a reduction in equation unknowns. However, it has been shown that HCV infection levels fluctuated in growing Huh7 cells following the growth rate of the cells.[90] Hence, it was critical for us to adapt our modeling efforts to the non-growing DMSO Huh7 system which had been shown to establish a long term, stable, steady-state HCV infection.[83] Equally important,

these non-growing Huh7 cells are more physiologically relevant in terms of hepatocyte biology and HCV infection dynamics. Transitioning Huh7 cells are into a non-growing state makes them more similar to liver hepatocytes in several ways: they are growth-arrested and polarized like hepatocytes, they have increased liver-specific gene expression that is closer to hepatocyte gene expression profiles, and the non-growing state induces drug metabolism.[88] Additionally, the non-growing cells are able to maintain steady-state HCV infection similar to what is seen in chronically infected patients. [83,84]

The studies presented here show that our published replicon model not only fit the data from non-growing DMSO Huh7 experiments well, but also yielded parameter estimates that were consistent with published results from the growing Huh7 cell system (Table 2). Fortuitously, the non-growing DMSO Huh7 cultures have several additional technical advantages over growing cell cultures that further facilitate modeling efforts. The non-dividing state of the cells means that they do not need to be passaged, allowing for longer experiment time courses with cells plated in smaller wells (96-well plates) facilitating the management of high number of parallel wells needed for the frequent sampling of replicate cultures that is necessary for kinetic experiments (as demonstrated in figs 9 vs 10). All of these factors contribute to enhanced rigor (number of replicates) and reduced well-to-well variability [79,84]

Once we validated the use of the model in our non-dividing DMSO Huh7 cells, we proceeded to utilize the model to analyze HCV treatment response to direct acting antivirals. The mathematical model was instrumental for estimating unknown HCV replicon parameters. By

analyzing HCV RNA kinetics during treatment with HCV NS5b polymerase inhibitors, which have a well-characterized single mechanism of action, we were able to estimate drug efficacies in blocking HCV RNA synthesis and the intrinsic rate of HCV RNA degradation (Tables 3 and 4). This work also confirmed how essential frequent sampling is for accurate modeling (Fig. 9).

While the HCV NS5b polymerase has a singular role in the HCV viral lifecycle, at the time it was being discovered that the viral NS3 protease has multiple possible roles not only cleaving the viral polyprotein into its essential functional protein subunits, but also cleaving host innate signaling molecules to render them non-functional for HCV detection. For this reason, an NS3 inhibitor could have multiple possible mechanisms of action against HCV. Our experiments demonstrated that the protease inhibitor was able to reduce HCV RNA to a greater extent than the 98% effective dose of the polymerase inhibitor (4 logs versus 2) and mathematically modeling a complete (100%) block of RNA production alone was unable to simulate the rapid and profound decrease in HCV RNA levels that were seen empirically.

This result and the mathematical modeling of the data thus strongly suggested that protease inhibitors do have multiple mechanisms of action to reduce HCV RNA. Specifically our model predicted that BILN2061 reduces HCV RNA by both blocking production and enhancing RNA degradation, which may be connected to its effect on thwarting a primary mechanism by which HCV blocks intracellular IFN antiviral signaling (Table 5). This is consistent with more recent modeling analyses of HCV kinetics in patients who were treated with HCV protease inhibitor danoprevir which project that danoprevir significantly blocks intracellular viral production (with

mean effectiveness 99.2%) and enhances intracellular viral RNA degradation about 5-fold.[91] Thus our *in vitro* modeling support these *in vivo* modeling results in which intracellular HCV RNA kinetics are lacking.

Statistically, the 95% confidence intervals for the delay estimates before sg1b declined from baseline were identical for polymerase inhibitors and protease inhibitors. However, the data suggested that the best estimate for the polymerase inhibitors was 0-6 hours (Table 4), and for the protease inhibitor it was 10 hours (Table 5). If the delay were proven to be longer for the protease inhibitor than for the polymerase inhibitor, it may reflect the time that it takes for existing replication complexes to degrade, because the protease inhibitor reduces HCV RNA by interfering with the supply of cleaved protein units that replace the replication complexes (compared to the polymerase inhibitor, which reduces RNA production more directly by blocking polymerase activity). Another possibility is that any RNA reduction caused by a restoration of the host's innate immune signaling pathways will not be apparent until the host cell creates signaling proteins to replace those cleaved by the protease.

Finally, before proceeding to the HCV genotype 2a infection, we used our model to compare the efficacy of HCV DAAs against HCV sg1b and sg2a replicons, which was of interest because these direct acting antivirals were developed against HCV genotype 1 and were expected to be more effective against sg1b. The results (Fig. 13 and Table 6) confirmed that both polymerase inhibitors (NM107 and PF254027) and protease inhibitors (BILN2061) are more effective at reducing sg1b HCV RNA, consistent with what was observed clinically.

In the future, this mathematical model could be adjusted to include more HCV lifecycle details in order to generate more detailed hypotheses about antiviral mechanism of action. For example, the model could incorporate the polyprotein translation step, including rate coefficients for initiation, elongation, and termination and/or synthesis of negative and positive strand RNAs. In order to reduce the number of unknown parameters estimated by the model, some of these rates could be measured experimentally or taken from literature. Likewise, the use of the subgenomic replicon model rather than full HCV infection model would facilitate such efforts as it would help keep the model complexity to a minimum. Such a model would be ideal for studying the details of HCV replication, however, because our interest was primarily in antiviral drug development our future efforts turned to the *in vitro* HCV infection system (see Chapters 4 and 5).

4. MODELING HCV INFECTION STEADY-STATE DYNAMICS

4.1 Introduction

After successfully mathematically modeling HCV replicon drug treatment response kinetics and utilizing this quantitative analysis to estimate HCV RNA half-life in the context of the replicon environment, we wanted to apply the same quantitative analysis to data generated in the cell culture HCV infection system, which had been first published by my thesis lab and others in 2006.[13-15] Unlike the HCV replicon system, the cell culture HCV infection system recapitulates the entire viral life cycle and mathematically modeling this full life cycle would allow analysis of antivirals that target not only HCV RNA synthesis and polyprotein cleavage steps completed in the replicon system, but also the entry and assembly/secretion steps of the viral life cycle. Thus, we adapted the simple mathematical model (Eq. 1 in Chapter 3) of the HCV replicon system in order to describe the full viral life cycle of the cell culture HCV infection system. In this chapter, we will discuss the first iteration of this model, the adjustment/hypothesis it generated, and the revised model that reflects the resulting change in our understanding of HCV steady-state dynamics.

4.2 RESULTS

4.2.1 Creating the Hepatitis C Virus Cell Culture Infection Model

Unlike the replicon system, in which virus levels are measured by the single parameter of intracellular HCV RNA, in the HCV cell culture (HCVcc) infection model we include three experimentally measurable viral parameters: intracellular viral RNA, extracellular viral RNA (i.e. total virions), and extracellular titer (i.e infectious virions). In the model schematic below (Fig. 14A), the large oval represents a cell permissive to HCV infection. Infectious viral particles (V_i) can enter the cell with an entry rate coefficient of k_{in}. Then, new copies of HCV RNA (R) are made with production rate α_0.

The accumulating HCV RNA (R) then degrades at rate constant μ or is assembled and secreted at rate constant k_s. A portion of these secreted particles (ρ, a constant with possible values between 0 and 1) will be infectious (V_i), and the remainder ($1-\rho$) will be non-infectious (V_{ni}). Infectious particles (V_i) are degraded into non-infectious particles (V_{ni}) with rate coefficient k_{loss} and total encapsidated RNA, V_{tot}, is degraded with rate constant c. It is worth noting here that experimentally we measure total extracellular HCV RNA (V_{tot}) which represents both infectious and non-infectious extracellular HCV particles (i.e. V_i+V_{ni}) by RT-qPCR and V_i by titer assay, but non-infectious extracellular HCV particles are not measured directly.

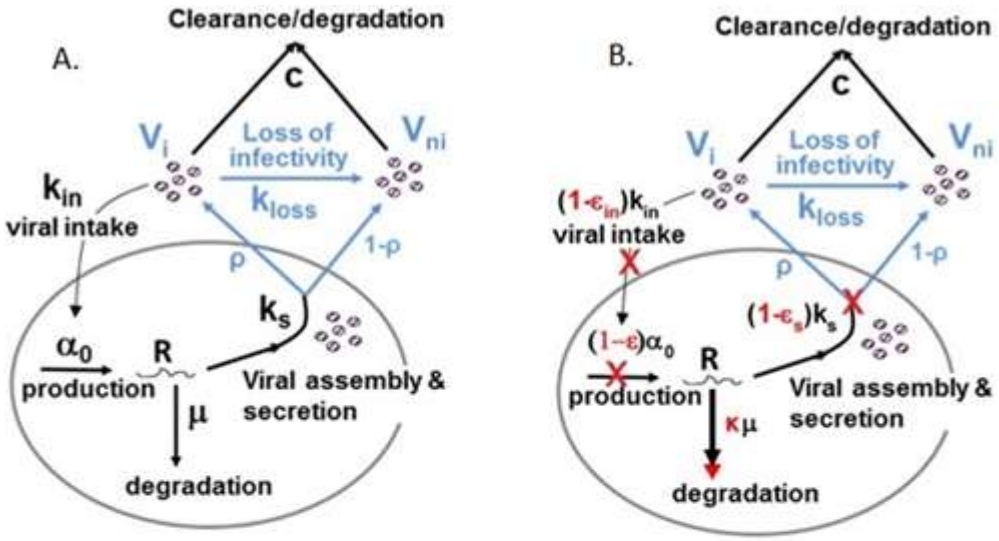

C.

$$\frac{dR}{dt} = (1-\varepsilon)\alpha_0 + k_{in}V_i - \kappa\mu R - (1-\varepsilon_z)k_z R$$

$$\frac{dV_i}{dt} = (1-\varepsilon_z)k_z R\rho - (k_{loss} + c)V_i - k_{in}V_i$$

$$\frac{dV_{ni}}{dt} = (1-\varepsilon_z)k_z(1-\rho)R + k_{loss}V_i - cV_{ni}$$

$$V_{tot} = V_i + V_{ni}$$

Fig 14. Initial HCVcc Mathematical Model Schematic. A) Schematic representing the HCV viral lifecycle in an individual cell. B) Schematic representing the HCV viral lifecycle and possible antiviral effects marked in red. C) Equations that comprise the mathematical model.

Below the schematics are the equations that make up the mathematical model (Fig. 14C). Analogous to the replicon model (Eq. 1 in Chapter 3), the corresponding differential equations are constructed by combining the additive and subtractive forces that affect the levels of intracellular HCV RNA over time (dR/dt), extracellular infectious particles over time (dV_i/dt), and extracellular non-infectious particles over time (dV_{ni}/dt). In order to simulate inhibition of any of the viral lifecycle steps that are included in the schematic –viral entry, RNA production, or assembly/secretion– the rate coefficient of that step in the equation is multiplied by an inhibition coefficient expressed as $(1-\epsilon)$, where ϵ is a value equal to or greater than 0 and smaller than 1, reflecting the percentage or efficacy of inhibition. In this set of equations, ϵ represents efficacy in blocking HCV RNA synthesis and ϵ_s represents efficacy in blocking viral assembly/secretion. In order to simulate a condition that enhances the degradation rate of intracellular HCV RNA (R), the degradation rate $\mu*R$ is multiplied by κ, which can be set to a number equal to or greater than 1.

Because studies in cell culture and in patients have documented relatively small fluctuations in HCV levels over time during chronic infection, revealing that the virus exists at steady-state levels, we can use what we know about the dynamics of chronic HCV infection to minimize the number of unknown parameters in the model. Specifically, we express this knowledge mathematically by setting all viral inhibition parameters in our model to equal zero (and κ to 1) and setting the differential equations that describe the change in viral levels to zero for intracellular HCV RNA, extracellular HCV RNA, and extracellular titer (dR/dt, dV_{ni}/dt, and $dV_i/dt = 0$).

With this information added, the mathematical model equations during steady-state become

$$0 = \alpha_0 + k_{in}V_i - \mu R - k_s R$$

$$0 = k_s R\rho - (k_{loss} + c)V_i - k_{in}V_i \qquad \text{(Eq. 3)}$$

$$0 = k_s(1-\rho)R + k_{loss}V_i - cV_{ni}$$

Algebraic rearrangement of these equations (steps described in Fig. 15) then allows us to link some of the unknown parameters to each other, in other words to express certain parameters in terms of others, so that the number of unknowns is functionally reduced and the model can be used to simulate steady-state with the incorporation of equations 4-7 (Fig. 15).

$$set\ \frac{dR}{dt} = 0 \qquad result\ after\ algebraic\ rearrangement: a0 = (\mu + k_s)R_0 - k_{in}V_{i0} \qquad \text{(Eq. 4)}$$

$$set\ \frac{dV_{ni}}{dt} = 0 \qquad result\ after\ algebraic\ rearrangement: V_{ni0} = \frac{(k_s(1-\rho)R_0 + k_{loss} * V_{i0})}{c} \qquad \text{(Eq. 5)}$$

$$set\ \frac{dV_i}{dt} = 0 \qquad result\ after\ algebraic\ rearrangement:\ k_s = \frac{(k_{in} + c + k_{loss})V_{i0}}{\rho * R_0} \qquad \text{(Eq. 6)}$$

$$replace\ k_s\ in\ Eq.5\ with\ right\ half\ of\ Eq.6\ and\ replace\ V_{ni0}\ with\ V_{toto} - V_{i0}$$

$$result\ of\ algebraic\ rearrangement: k_{in} = -c - \frac{k_{loss}}{(1-\rho)} + \frac{c * \rho}{(1-\rho)} * \frac{V_{toto} - V_{i0}}{V_{i0}} \qquad \text{(Eq. 7)}$$

Figure 15. Using HCV Equilibrium to Reduce Unknown Model Parameters. Parameters a_0 (intracellular HCV RNA synthesis rate), V_{ni0} (pre-treatment V_{ni} level) and K_{in} (viral entry rate constant), and k_s (assembly/secretion rate constant) as a function of other model parameters. V_{tot0}, measured pre-treatment extracellular HCV RNA level; Vi0 (measured pre-treatment titer. R_0, pre-treatment intracellular HCV RNA (Table 8).

4.2.2 Empirically Measuring Unknown Viral parameters

To further reduce the number of unknown parameters in our HCVcc Infection Model, we directly quantified those parameters which could be readily measured empirically. Specifically, we measured the decay rate of particle infectivity [i.e. infectious particles decay (k_{loss})] and of total extracellular HCV RNA [i.e. decay of RNA containing particles (c)]. To do this, we emulated our standard experiment conditions by diluting stock virus in cell culture medium to a concentration representative of that measured during our experiments and incubating it at the same

temperature as the kinetic experiments, 37℃. We harvested aliquots over time and measured the infectious titer and total HCV RNA to monitor decay (Fig. 16).

The value for the rate coefficient for the loss of infectivity (k_{loss}) in the mathematical model was found by plotting these data on a graph that had an x-axis of time (days) and a y-axis of the negative natural log of the FFU [-ln(FFU)], then adding a linear trend line whose slope value of 2.64 day^{-1} was taken as the decay rate coefficient value. Analogously, the slope of the transformed RNA decay data gave the rate coefficient of 0.13 day^{-1} for the degradation of extracellular HCV particles that encase the viral RNA (c). The corresponding half-life for the infectivity at 37℃ is 6.3 hours, which is significantly less than the half-life of the particle that protects the HCV RNA, which is 127 hours.

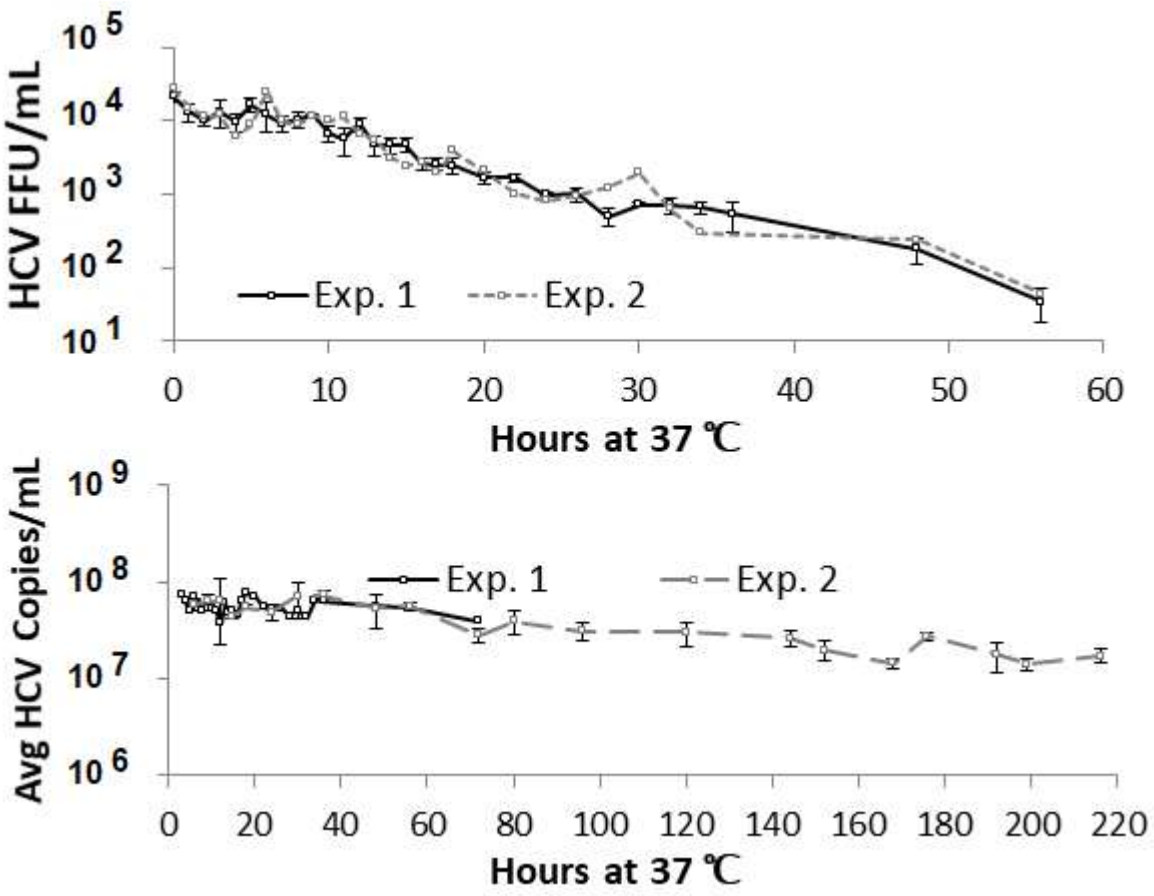

Figure. 16. Kinetics of extracellular HCV viral particle decay. Aliquots of virus were incubated at 37℃ for the indicated times (x-axis). **A**) Loss of particle infectivity. Samples were titered by limiting-dilution titer assay. Focus-forming units or infectious particles per mL is graphed (y-axis). **B**) Loss of HCV particle integrity. HCV RNA copies per mL was/were quantified by RT-qPCR (y axis). Two independent experiments are graphed. Each data point represents the average of duplicates taken at each time point.

4.2.3 Preliminary Model Fits to Inhibition Data Reveal Missing Pathway in Mathematical Model

After building the mathematical model to include HCV steady-state infection and all directly measured parameters, we wanted to determine whether the model could predict the behavior of the system. To do this we performed HCV steady-state inhibition experiments and determined if the model could simulate the empirical data. Similar to the replicon experiments, we started by using HCV antivirals with well-defined, single mechanisms of action – an HCV NS5b polymerase inhibitor and an HCV secretion inhibitor. Specifically, we established non-growing Huh7 cultures (Fig. 17A), infected them with HCVcc, and allowed infection to progress to steady-state (Fig. 17B). To perturb steady-state, we treated these chronic infections with either NM107, a nucleoside-analog inhibitor of the viral polymerase (NS5b), or Naringenin, a grapefruit extract/flavonoid that blocks HCV secretion by inhibiting very low density lipoprotein (vLDL) secretion through activation of peroxisome proliferator-activated receptor (PPARα)[56,92]. Frequent samples were harvested to monitor intracellular HCV RNA, extracellular HCV RNA, and extracellular HCV titers (Fig. 18).

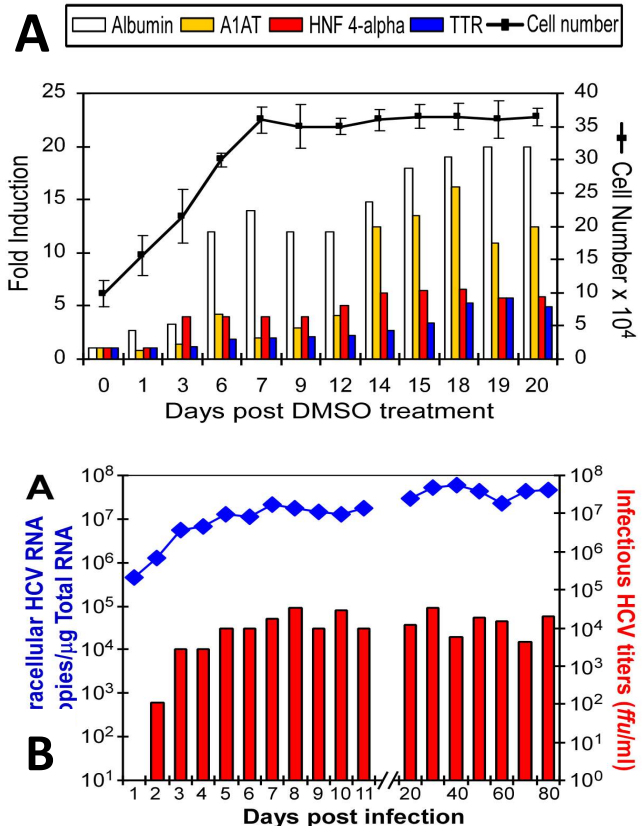

Figure 17. Steady-State HCV Infection in Non-Growing Huh7 Cells. (A) Establishment of non-growing Huh7 cells. Huh7 cells were plated on collagen and 1% DMSO was added to the media at confluence. At indicated times (x-axis), cells were harvested for counting (right y axis) and RNA extraction. RT-qPCR was performed to quantify the relative expression if the indicated hepatocyte-specific genes which are graphed as fold induction (left y-axis) over that observed in growing Huh7 cells **(B)** HCV infection. At day 20 post-DMSO treatment, cultures were infected with HCV at a MOI of 0.01 foci forming units (*ff*u)/cell. Culture media and cell RNA were harvested at various times post-infection (p.i.) and the kinetics of infection was monitored by titration and RT-qPCR, respectively.

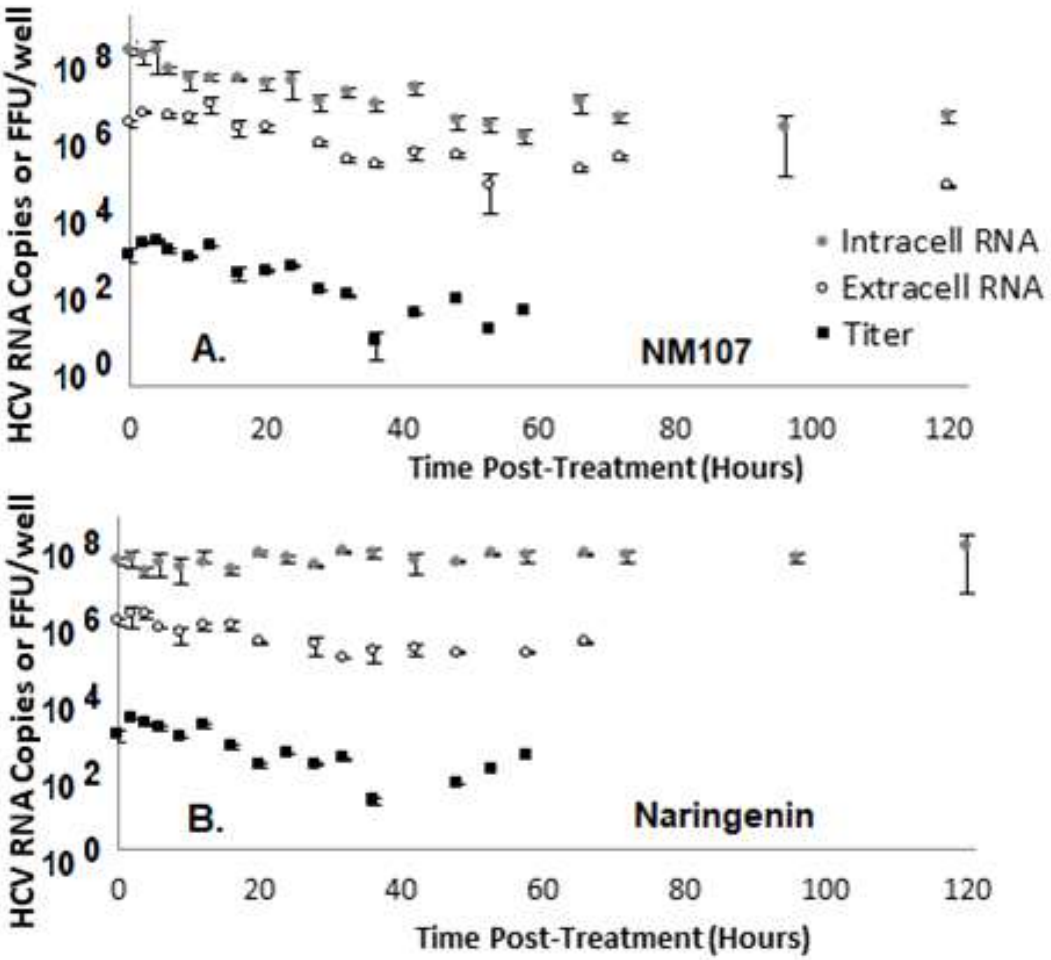

Figure 18. HCVcc Kinetics During Treatment with Direct Acting Antivirals. DMSO growth-arrested Huh7 cells with steady-state HCV RNA levels were treated with **A)** 25 μM NM107 or **B)** 200 μM Naringenin or diluent control (not shown). Cell lysate and culture supernatant were harvested at the indicated time points post-treatment (x-axis). Intracellular HCV RNA was quantified by RT-qPCR and the average of triplicate samples is graphed as HCV RNA copies per well (gray circles). Extracellular HCV RNA was quantified by RT-qPCR and the average of duplicate samples is graphed as HCV RNA copies per well (white circles). HCV titer was determined by titration on naïve Huh7 cells and the average of duplicate samples is graphed as FFU per well (black squares). All data points are graphed relative to the diluent treated control cultures at the corresponding time point (as described in Materials and Methods). Error bars represent the standard of deviation of measured values among the replicate wells.

Inhibition of intracellular HCV RNA by the polymerase inhibitor, NM107, started to occur between 4 and 6 hours and dropped nearly one log by 9 hours after initiation of treatment. The decline slowed after 9 hours with HCV RNA being reduced by an additional log by 48 hours (Fig. 18A, gray circles). The amounts of extracellular HCV RNA (white circles) and extracellular infectious titers (black squares) were also reduced by NM107, although this reduction was slower beginning after 12 hours of antiviral treatment presumably due to the time required for intracellular RNA levels to be reduced to the point that it would affect assembly. Both extracellular HCV RNA and titer were reduced by a log after 36-42 hours of treatment. During treatment with the HCV secretion inhibitor, as expected intracellular HCV RNA levels were not reduced (Fig. 18B, gray circles). In contrast, extracellular HCV RNA and titer (white circles and black squares, respectively) were each reduced by 1 log by 32 hours after initiation of treatment, which is consistent with the treatment affecting the secretion of HCVcc without affecting HCV RNA production. The delay lasted for 12-16h, which may reflect the time that is required for vLDL secretion to be reduced.

To determine if our new HCVcc infection model could simulate the behavior of the system after perturbation from steady-state, we fit the model to these empirical data and assessed the quality or closeness of these fits. Looking at the polymerase data, the model simulation (Fig. 19A, solid gray line) recapitulated the intracellular HCV RNA inhibition kinetics (gray circles) giving a satisfactory fit. However, the fit to the extracellular titer data (Fig. 19A, dashed gray line and black squares, respectively) was not accurate; it seemed to fit between 0 and 24 hours of treatment but then only predicted a ¾ log reduction which was significantly less than the empirical

data (black squares). Most problematic, the simulation of the extracellular RNA level (V_{tot}) (Fig. 19A, dashed black line) showed no significant reduction over time, even though the empirical data (Fig. 19A, white circles) showed a reduction greater than one log during the course of treatment. The mathematical model was also unable to fit the secretion inhibitor data, even if the simulation blocked secretion by 99.99%. Again, simulating intracellular RNA was not a challenge, but model simulations with fixed $c=0.13$/day and $k_{loss}=2.64$/day (Fig. 16) for extracellular HCV RNA were only reduced by ¼ log even though empirical levels were reduced by ¾ log and simulations for HCV titer were only reduced 1/3 log even though empirical levels were reduced by ¾ log (Fig. 19B).

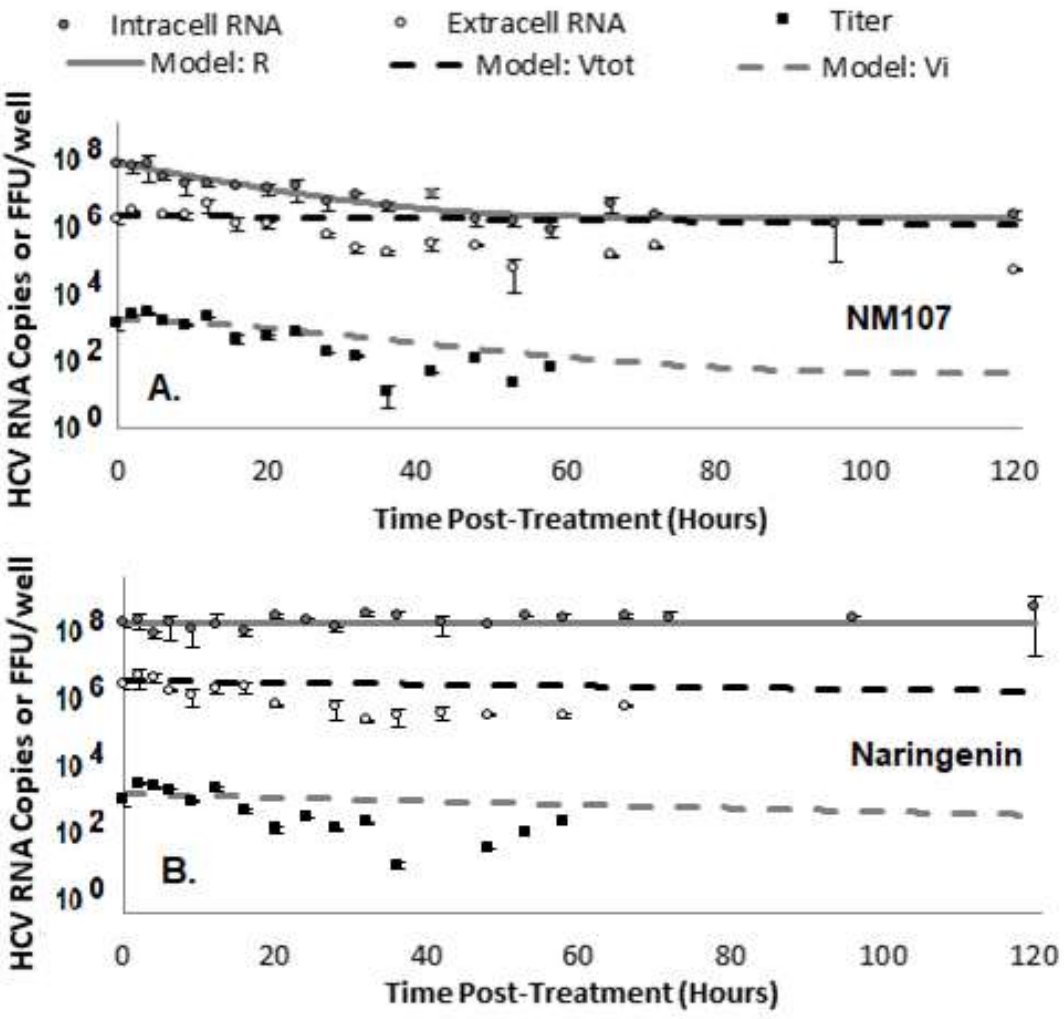

Figure 19. Initial HCVcc Infection Model Data Fits. The mathematical model was used to fit the empirical data in Fig. 18 using Berkeley Madonna software. **A)** NM107 HCV NS5b polymerase inhibitor data. **B)** Naringenin HCV secretion inhibitor data. Solid or dashed lines represent mathematical model fits to corresponding datasets. Model parameter values used for plotting the curves: E_p=97% for NM107 (0 for Naringenin). E_{in}=0. E_s=99.99%. R_0=5.86x10^7, $Vtot_0$=1.7x10^6, Vi_0=1600, t_0=0.1 days for NM107 or 0.67 days for Naringenin, c=0.13/day, μ=2.77/day, K_{loss}=2.64/day, ρ=0.0022

Looking at the schematic (Fig. 14A-B) and equations (Fig. 14C), the reason the model was unable to simulate the data became apparent. The only pathway in the mathematical model able to reduce extracellular HCV RNA was degradation, but based on our empirically measured HCV degradation rate, that process is too slow to account for the rate of reduction that was seen in the experiments as the stability of the particle protecting the HCV RNA in the media is extremely high with a half-life of 127 hours (Fig. 16A). In these inhibition experiments, the extracellular HCV RNA was reduced ~6 times as fast, with a half-life of 18.7 hours and 19.9 hours for the polymerase and secretion inhibitor experiments, respectively. Based on the MOA of these two antiviral drugs we expect them to reduce progeny virus secretion without enhancing the degradation rate of HCV particles and the RNA contained inside, thus the inability of the model to simulate the empirical data suggested that our understanding of the system was incomplete. Therefore, we hypothesized that there was another mechanism for clearing HCV particles/RNA from extracellular media and we designed experiments to investigate this model-derived hypothesis.

4.2.4 Investigating Mechanisms by Which Extracellular Hepatitis C Virus Ribonucleic Acid is Reduced during the Hepatitis C Virus Cell Culture Lifecycle

Because experimental data was indicating that degradation of extracellular virions encapsidating HCV RNA is about 6 times too slow to explain the reduction seen in our inhibition

experiments, this indicated that something was missing from our model. Specifically, there had to be an additional pathway by which extracellular RNA-containing viral particles were being removed from the extracellular milieu. First, we tested the possibility that the cells might be secreting a product that enhances the degradation of extracellular HCV particles and the rate of extracellular HCV RNA reduction, we treated stock virus with either fresh/unused media or media taken from uninfected cells, cells infected by adenovirus, or cells treated with IFN to induce an immune response analogous to HCV.

At every time point, we froze aliquots, and added fresh or spent media to the remaining aliquots. At the end of the experiment, RNA was isolated from all samples to determine HCV RNA levels over time when exposed to these differently conditioned media. Within the 25 hour assay, HCV RNA levels were not decreased significantly by any of treatments, indicating that HCV RNA degradation was not enhanced by spent media and suggesting that cells are not secreting products that enhance the loss of extracellular HCV RNA in the media (Fig. 20). In conclusion, this mechanism is not likely to be responsible for reducing the extracellular HCV RNA during HCVcc infection, and the next option that we considered was cellular uptake.

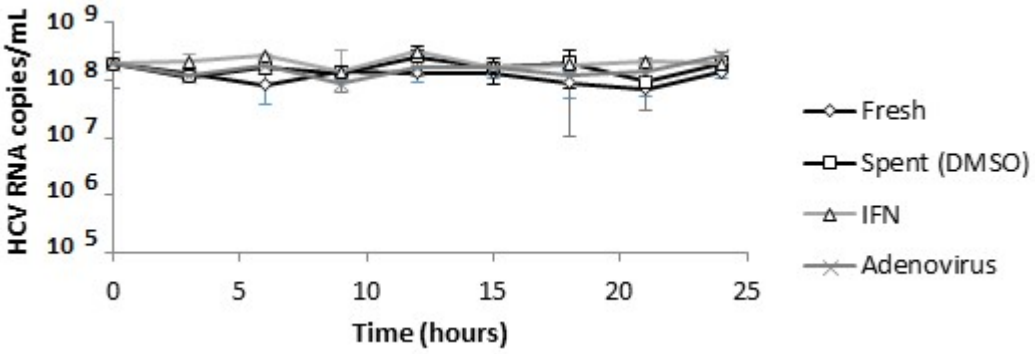

Figure 20. Extracellular HCV RNA Stability in Differently Conditioned Media. Virus aliquots were incubated with media from uninfected cells (squares), IFN-treated cells (triangles), adenovirus infected cells (crosses) or fresh media (diamonds) at 37C for the indicated time. HCV RNA was isolated, quantified by RT-qPCR, normalized to spiked carrier RNA and is graphed as HCV copies/mL.

4.2.5 *In vivo* Evidence that Hepatitis C Virus Entry into Hepatocytes Plays a Major Role in Hepatitis C Virus Steady-State

We often perform *in vitro* experiments to test mathematical model predictions/hypotheses generated when modeling clinical data, however in this case we happened to independently make an interesting observation while monitoring HCV levels in patients during liver transplantation

that provides *in vivo* evidence to support our *in vitro* model hypothesis that viral entry into hepatocytes may play a role in HCV steady-state.

In a collaboration with Dr. Forns, we were monitoring viral kinetics during liver transplantation to evaluate the function of the liver in clearing free virus from the circulation. The idea was to measure HCV levels in the blood during the anhepatic phase (AH) when no liver is present and then during early post-reperfusion phase (RP) after the new liver had been introduced. In total, 5 patients (P1-P5) with median age 60 years (range, 49-68) and median BMI 30 (range, 19-34) underwent liver transplantation (Table 7). Blood samples were taken before liver transplantation, every 5-15 minutes during the anhepatic phase (AH) and every 3.6 minutes to 2 hours until 4 hours after graft reperfusion (RP), during which we assume that there is no production of new virions from the HCV-negative donor liver. Thereafter, HCV RNA was measured intermittently (Fig. 21). Transfusion of blood products and albumin infusion were recorded.

Patient	Gender	Weight (kg)	BMI	Age at LT	Donor age	Donor gender	HCV genotype
1	M	90	29	49	29	M	1b
2	M	88	30	68	72	M	1b
3	F	70	31	66	33	M	1b
4	M	87	34	56	69	M	3
5	F	43	19	60	73	F	1b
Median (range)		87 (43–90)	30 (19–34)	60 (49–68)	69 (29–73)		

Table 7. Characteristics of HCV Infected Liver Transplant Patients

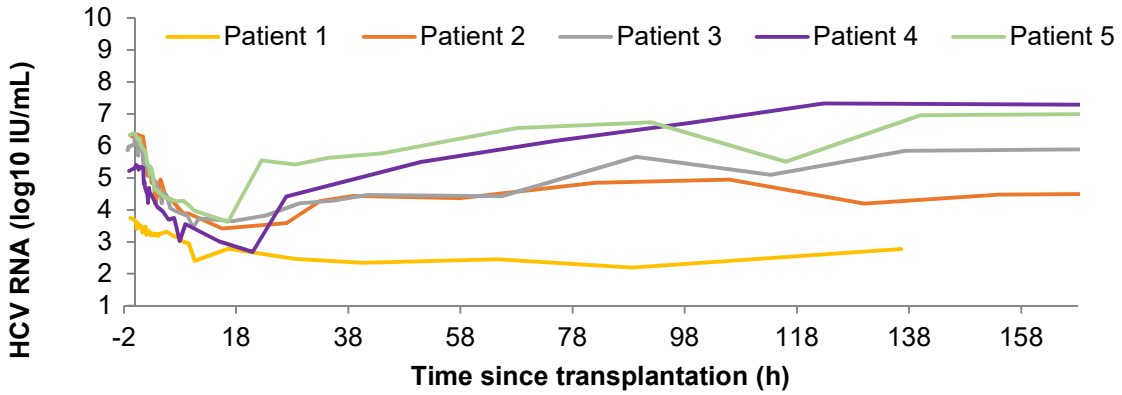

Figure 21: HCV Kinetics before, during, and after Liver Transplantation.
Surgery was initiated at $t = 0$.

The median viral load across all 5 patients before AH phase was 6.04 (range 3.71–6.40) $\log_{10}$ IU/mL. The AH phase lasted 1.25 h – 1.90 h in duration. During that time virus levels were flat in three patients (P2, P3 and P4). In the other two patients (P1 and P5), serum HCV half-live was 1.93 h and 0.95 h, respectively (Fig. 22). Although the calculations were adjusted/corrected for fluid input, it is perhaps noteworthy that patients 1 and 5 received the largest volume of fluid during the procedure consisting of 500 and 750 mL respectively. During the first 4 hours after graft reperfusion, Patient 1 experienced a plateau in viral load while Patients 2–5, exhibited HCV RNA decline with slopes 0.34, 0.36, 0.24, and 0.39 log10 IU/mL per day ($p < 0.01$), corresponding to viral half-lives of 0.9 h, 0.83 h, 1.23 h, and 0.78 h respectively. While it was expected that HCV RNA levels would drop once the infected liver was removed because no more HCV particles

would be generated, the observation that the HCV levels remained unchanged during the anahepatic phase in three of five patients (Fig. 22) suggests that the liver was not only the main producer of HCV, but also the main route by which HCV is cleared from the serum.

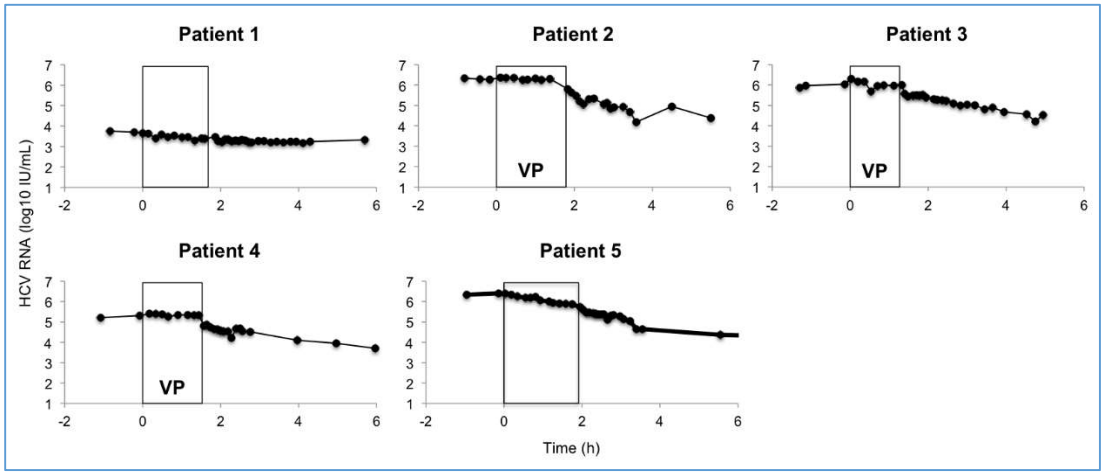

Figure 22: HCV RNA Kinetics during Liver Transplant. Blood samples were taken from five HCV infected patients before and during the anhepatic phase (rectangles), and 4 hours after liver graft reperfusion. HCV RNA measurements are shown with circles connected by straight lines. Patients 2, 3 and 4 experienced a viral plateau (VP) during AH. The boxed region represents the anhepatic phase and VP indicates which patients had a viral load plateau during the anhepatic phase.

4.2.6 Updating Mathematical Model to Include Non-Productive Cellular Uptake of Hepatitis C Virus Particles

Based on *in vitro* observations that Huh7 cells were not secreting something that enhances HCV particle degradation and *in vivo* observations during liver transplant that suggest the infected liver is the main route by which HCV is cleared from the serum of infected patients, we added a pathway to the model that allows not only infectious particles (V_i), but now also non-infectious virus particles (V_{ni}) to enter infected cells (albeit all this entry is likely non-productive due to super-infection exclusion[93]) (Fig. 23).

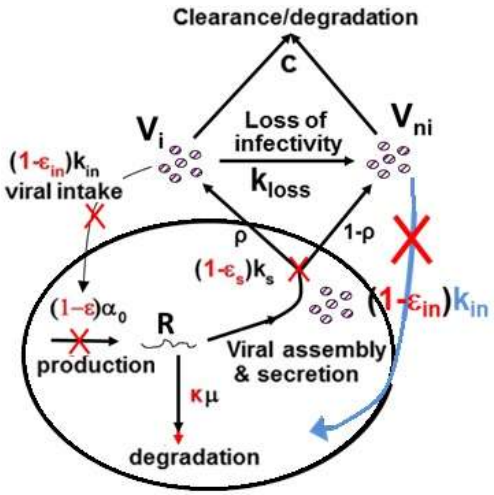

$$\frac{dR}{dt} = (1-\varepsilon)\alpha_0 + (1-\varepsilon_{in})k_{in}V_{tot} - \kappa\mu R - (1-\varepsilon_s)k_s R$$

$$\frac{dV_i}{dt} = (1-\varepsilon_s)k_s R\rho - (k_{loss}+c)V_i - (1-\varepsilon_{in})k_{in}V_i$$

$$\frac{dV_{ni}}{dt} = (1-\varepsilon_s)k_s(1-\rho)R + k_{loss}V_i - cV_{ni} - (1-\varepsilon_{in})k_{in}V_{ni}$$

$$V_{tot} = V_i + V_{ni}$$

Fig 23. Revised HCVcc Mathematical Model. This schematic represents the viral life cycle described by the mathematical model, with the inclusion of an additional pathway so that now any viral particle in theory (V_i and V_{ni}) can enter infected cells (highlighted in blue). Specifically, V_{ni} is now able to enter the cell with the same entry rate coefficient k_{in} as V_i. The model also allows inhibition of entry ϵ_{in} for both species of extracellular HCV particles. The corresponding mathematical model equations are to the right of the schematic.

4.2.7 Updated Hepatitis C Virus Cell Culture Model Fits Empirical Data, Consistent with Viral Entry Playing a Role in Maintaining Hepatitis C Virus Steady-State

After changing the mathematical model to allow any virus (V_i or V_{ni}) to non-productively enter infected cells, it was necessary to determine whether this updated model could simulate HCVcc inhibition kinetics and estimate HCVcc infection parameters. We allowed Berkeley Madonna software to find a best fit for the updated mathematical model (Fig. 23) and empirical HCVcc kinetics during treatment with both NM107 and Naringenin, (Fig. 24). For both sets of

inhibition kinetics, the model was able to accurately fit all three measured HCVcc parameters throughout the time course.

With these new fits, we proceeded to calculate confidence intervals for parameter estimations made by the mathematical model (Table 8). This analysis is important as it reveals how robust the model parameter estimates are. As indicated, when appropriate, we fixed parameters that were estimated directly from designed *in vitro* experiments or for mechanisms of inhibition that are not relevant when considering the target of the antiviral being used. As can be seen by the tight confidence intervals and p-values below 0.05, this analysis revealed that the model is sensitive to all parameters estimated (Table 8). This analysis also provided a quantitative assessment of how well the model fit the data. Specifically, the residual sum of squares/sum of squared residuals or RRS is calculated by squaring the distance from each data point to the closest point in the simulation then taking the square root of the sum of those squares. Compared to the very large "bad fit" RSS values of 90.5 (NM107 dataset) and 84.8 (Naringenin dataset) calculated when fitting our original HCVcc infection model (Fig. 14) to these same datasets (Fig. 18), the 4x lower RSS values of 19.2 (NM107 dataset) and 21.9 (Naringenin dataset) calculated when fitting the revised HCVcc infection model reveal a much closer fit (Table 8).

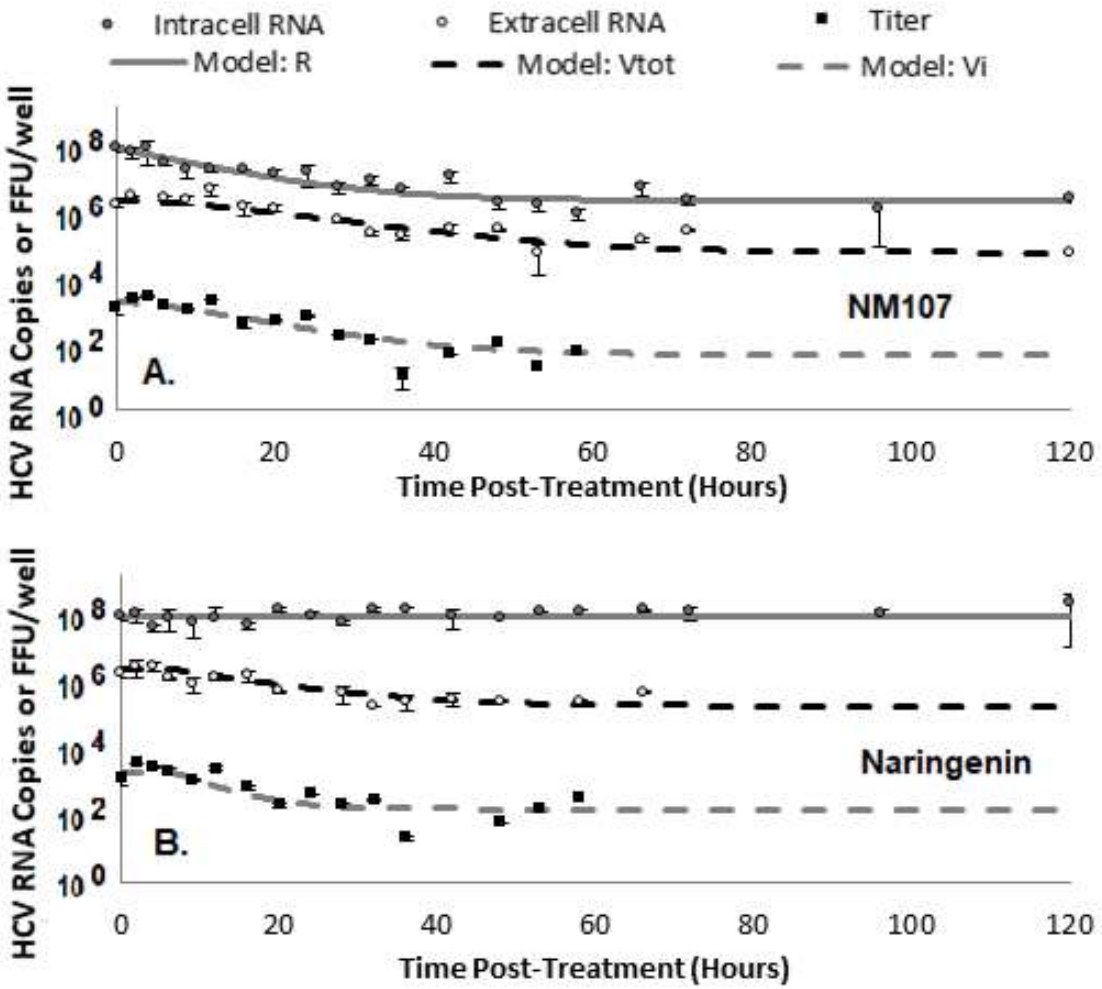

Figure 24. Revised HCVcc Infection Model Data Fits. The mathematical model was used to fit the empirical data in Fig. 18 using Berkeley Madonna software. **A)** NM107 HCV NS5b polymerase inhibitor data or **B)** Naringenin HCV secretion inhibitor data. Solid or dashed lines represent mathematical model fits to corresponding datasets. Model parameters are described in Table 8.

Biological Definition		NM107 Values [95% C.I.]	Naringenin Values [95% C.I.]	Source
	Experiment data points	49	49	
	Number of model estimates	3	2	
R_0	Initial intracellular HCV RNA	$5.86x10^7$ copies/well	$5.86x10^7$ copies/well	Experimentally measured
$Vtot_0$	Initial extracellular HCV RNA	$1.7x10^6$ copies/well	$1.7x10^6$ copies/well	Experimentally measured
Vi_0	Initial extracellular infectious HCV particles	1600 FFU/well	1600 FFU/well	Experimentally measured
Vni_0	Initial extracellular non-infectious HCV particles	1,698,400 /well	1,698,400 /well	Experimentally estimated as $Vtot_0$-Vi_0
(RSS)	Distance between data and simulation (natural log)	19.201	21.914	Calculated by DEDiscover
(ρ)	Portion of infectious virions	0.0021 [0.0016-0.0026]	0.0023 [0.0017-0.0030]	Estimated using DEDiscover
(μ)	RNA degradation rate constant (/day)	2.7782 [2.0798-3.4767]	2.7782 (fixed)	Estimated by fitting model to NM107 data
c	Non-infectious particle degradation rate constant	0.13/day	0.13/day	Experimentally measured
k_{loss}	Loss of infectivity rate constant	2.64/day	2.64/day	Experimentally measured
α_0	Intracellular HCV RNA synthesis rate constant	$1.78x10^8$/day	$1.78x10^8$/day	Determined by fitting in Berkeley Madonna
k_{in}	Viral entry rate constant	1.84/day	1.84/day	Determined by fitting in Berkeley Madonna
k_s	Assembly/secretion rate constant	0.06/day	0.06/day	Determined by fitting in Berkeley Madonna
t_0	delay	0.1 days	0.67 days	Estimated by Berkeley Madonna software
(ϵ)	RNA production Inhibition	0.9726 [0.9605-0.9846]	0 (fixed)	Estimated by fitting model to NM107 data
(ϵ_s)	assembly/secretion Inhibition	0 (fixed)	0.9217 [0.8864-0.9569]	Estimated by fitting model to Ng data
ϵ_{in}	Entry inhibition	0 (fixed)	0 (fixed)	Fixed

Table 8. Revised HCVcc Model Parameter Estimations. The estimated value for a parameter is followed by its 95% confidence interval in brackets. If the parameter was not estimated by the model, that is indicated by writing the word "fixed" after a parameter estimate.

Another important consideration is whether the mathematical model gives parameter estimates within the range of accepted biological norms. For example, having estimates for the portion of secreted HCV particles that are infectious around 1 in 500 [within a 95% confidence interval of 1/333-1/625] is consistent with empirically measured specific infectivity values in our laboratory and others. Likewise, the estimated values for the inhibition efficacies of these antivirals against their respective viral lifecycle targets being around 90% or greater is expected because these antivirals have been reported to be potent inhibitors of HCV. The estimate for the degradation rate coefficient of intracellular HCV RNA is between 2- 3-times faster than reported in the sg1b replicon system, but this is perhaps also expected due to the longer length and possibly lower stability of the viral RNA in the infection system does not stay perpetually associated with and protected by replication complexes (as it would in the replicon system), but rather must be transported to site of assembly which presumably would involve exposing it to degradation mechanisms. Importantly, this analysis confirms that the model estimates are all within accepted biological norms and further supports the hypothesis that non-productive cellular uptake of viral particles is a component of HCVcc infection dynamics.

4.3 Discussion

With the availability of a robust *in vitro* HCV infection that achieves long-term steady-state chronic infection, we have created the first data-driven, multi-scale (i.e intracellular and extracellular) mathematical model of HCV infection for understanding the dynamics of HCV

infection and treatment response *in vitro*. The initial model was based on our basic understanding of the HCV lifecycle (Fig. 14) and empirically measured viral parameters (Fig. 16). While we were able to generate model equations that represented HCV steady-state (i.e. no antiviral inhibition and no change in viral load), which allowed us to reduce the number of unknown parameters, this initial model was unable to predict the behavior of the system and simulate HCV inhibition kinetics under treatment with antivirals with single, known mechanisms of action (Fig. 18). By assessing the inadequacies of the model, we hypothesized that extracellular HCV RNA must have an additional mechanism of clearance we originally did not anticipate. Through empirical observations *in vitro* (Fig. 20) and *in vivo* (Fig. 22), we obtained data consistent with non-productive viral uptake into infected cells playing a role in the maintenance of HCV steady-state infection dynamics. Consistent with this hypothesis, expanding our HCV infection model to include this new aspect of HCV steady-state (Fig. 23) allowed for accurate simulation of the empirical data (Fig. 24; Table 8).

Expanding our replicon model entailed adding additional steps of the viral life cycle (e.g. entry, assembly/secretion, and degradation of each species of extracellular HCV particle) that include not only intracellular HCV RNA levels (analogous to the replicon model), but also extracellular HCV RNA and titer in the culture media. Therefore, in these experiments, we collected culture supernatants and cell lysates and expressed all measured parameters on the same scale, e.g. per experimental well to allow all HCV parameters to be interconnected in the mathematical model equations. Most importantly, adapting the mathematical model from the HCV replicon system to the *in vitro* HCV infection system has two significant advantages. First,

the mathematical model allows us to study antivirals that target viral lifecycle steps such as entry, assembly, and egress, which are not recapitulated by the HCV replicon system. Second, the inclusion of extracellular HCV RNA data/predictions is more readily comparable to patient data (i.e. serum levels of HCV RNA) and thus is more directly clinically relevant/informative.

One technical challenge we faced trying to quantify HCV extracellular titer in the context of HCV inhibition experiments was the presence of the HCV inhibitors in our collected media samples. This required kinetic analysis to determine how long the inhibitor containing inoculum had to be left on the cells to allow the buoyant HCV particles to reach the cells and initiate HCV and careful titration of the samples to reduce the concentration of the inhibitors to non-interfering doses without reducing the titer of the HCV present to below our quantification limits. While samples harvested early during the experiment have enough FFU to allow for adequate dilution, this can be problematic for samples taken later after antiviral inhibition. While we tried other, more complex, strategies such as filtering and dialysis, we ultimately settled on determining the maximum concentration of each drug that could be incubated with the cells for the 9 hours required for efficient HCV infection initiation (see Materials and Methods). Since the studies in this thesis were completed, our lab group has adapted this titer assay to 24-well plates to allow a higher volume of sample per well which increases the number of countable foci and results in a lower limit of detection.

The mathematical modeling also highlighted a few interesting observations during the analysis of HCVcc response kinetics during treatment with a well-characterized HCV NS5b

polymerase inhibitor NM107. Because the HCV polymerase inhibitor was blocking HCV RNA synthesis, we expected a decline in intracellular HCV RNA and we did see a decrease that was two-logs (99%) lower than the initial levels (Fig. 24A). The decline in intracellular HCV RNA was followed by a one-log (90%) decline in extracellular HCV particles, presumably as a secondary effect of the polymerase inhibition, due to less intracellular HCV RNA being available for packaging into progeny HCV particles that can be secreted. Notably, this delay was simulated by the model without inserting an artificial delay in any equations that describe the effect of the polymerase inhibitor on extracellular HCV parameters. Importantly, the model also recapitulated the smaller reduction in extracellular HCV RNA compared to intracellular (90% vs 99%). One explanation for this observed inhibition pattern is that HCV RNA is likely synthesized in excess of the amount that ultimately gets packaged for secretion as Huh7 cells are limited in the lipoprotein synthesis required to support efficient HCV assembly and secretion.

Because HCV superinfection exclusion has been reported for HCV[93], in our initial model we assumed extracellular HCV steady-state RNA levels were maintained solely by HCV particle degradation balanced by HCV particle production. However, this initial model proved unable to simulate our empirical HCV inhibition kinetics (Fig. 19) and the discrepancies between the model and the data revealed that there must be an additional mechanism of extracellular HCV RNA clearance. While HCV clearance from the blood in patients has always been presumed to be immune-mediated, this mechanism is not present *in vitro*. In the absence of *in vitro* evidence supporting enhanced degradation (Fig. 20) and the presence of *in vivo* evidence supporting liver uptake (Fig. 22), we adjusted our mathematical model to include a cellular uptake pathway that

reduces extracellular HCV RNA (Fig. 23). Importantly, this is not inconsistent with the previously reported super-infection exclusion as there are many possible mechanisms by which a virus can block a productive super-infection post-viral entry (e.g. preventing fusion, uncoating, or translation of the incoming virus). While the model does not specify whether this entry pathway signifies the canonical HCV cellular entry pathway, or some other non-specific cellular uptake, the model does not include a mechanism for this secondary uptake to increase HCV RNA synthesis and any increase in intracellular RNA levels caused by cellular uptake is miniscule compared to that caused by the amplification of RNA synthesis, hence this entry is likely non-productive, consistent with superinfection exclusion. Importantly, the updated model accurately simulated NM107 and NG inhibition data yielding robust parameter estimates that are within biologically relevant ranges (Fig. 24 and Table 8). Hence, while future experiments are needed (see Chapter 6), the revised model supports the unexpected conclusion that cellular uptake of HCV RNA is important for HCVcc infection dynamics.

5. MODELING HEPATITIS C VIRUS TREATMENT RESPONSE TO ELUCIDATE DRUG MECHANISM OF ACTION

5.1 Introduction

Initial HCV direct acting drug development efforts focused on the standard viral enzymatic targets, such as the NS3/4A protease and the NS5B polymerase. However, using a non-biased screening approach, Bristol Myer Squibb identified a NS5A inhibitor, which they named BMS-790052 or daclatasvir.[94] The clinical efficacy of daclatasvir was confirmed in a single dose study which surprisingly revealed that inhibiting this protein resulted in a more rapid reduction in serum HCV levels than had previously been seen with any other treatment.[94] Not only was this exciting from a clinical perspective, but it was also interesting mechanistically for two reasons. First, it was of interest because the functions of HCV NS5a were not well defined and thus understanding the mechanism of action of this inhibitor could reveal insight into critical aspects of the HCV life cycle. Second, it was of interest because NS5a has no known enzymatic activity, making it an unusual and unexpected drug target.[95–99] As such, we sought to use mathematical modeling to elucidate the mechanism of action of this new NS5a inhibitor, BMS-790052 or Daclatasvir (DCV).

5.2 Results

5.2.1 Modeling HCV Treatment Response to Daclatasvir in Patients

Our 2013 manuscript (*Proc Natl Acad Sci* USA **110**, 3991–3996)(Appendix A), describes the first phase of this study in which the serum (extracellular) HCV RNA levels that had been measured in patients were analyzed by mathematical modeling to try and determine the mechanism of the rapid HCV decline observed. Although previous modeling of HCV inhibition kinetics in patients had been achieved with a simple mathematical model based solely on extracellular HCV serum kinetics, these efforts found that simulating the *in vivo* inhibition kinetics of daclatasvir required a "multiscale" model that also includes theoretical intracellular inhibitory effects which cannot be directly measured from available patient samples. While the model could fit the data assuming several possible mechanisms of action, only simulations hypothesizing that DCV **blocks viral RNA synthesis and virion assembly/secretion** were deemed valid because matching the data to other mechanism simulations required parameter values that were outside of acceptable biological ranges.

5.2.2 Confirming *in vivo* Model Predictions that Daclatasvir has Two Mechanisms of Action

Because measuring intracellular HCV parameters is not feasible in patients, we conducted an experiment *in vitro* with the same drug and measured both intracellular and extracellular levels of virus to examine whether the NS5a inhibitor was blocking both RNA production and

assembly/secretion. Specifically, chronically HCV infected non-growing Huh7 cells were treated with drug vehicle alone, DCV, or the HCV NS5b polymerase inhibitor, NM107. During treatment, samples were harvested frequently to monitor the inhibition of intracellular HCV RNA and extracellular infectious HCV titer over time. Both drugs reduced intracellular HCV RNA with identical kinetics, but titer was reduced by DCV much faster than by NM107, consistent with the model prediction that DCV in addition to blocking HCV RNA synthesis, also has an additional independent effect on HCV virion assembly/secretion (Appendix A, Pg. 138, Fig. 4).

5.2.3 Modeling Hepatitis C Virus Cell Culture Treatment Response to Daclatasvir *in vitro*

While the ability of the *in vivo* mathematical model to generate a hypothesis about drug mechanisms of action within the cell based on extracellular data alone is impressive, we decided to utilize our *in vitro* mathematical model to try and further dissect this novel mechanism of action on a molecular level. For this, chronically infected non-growing Huh7 cells were again mock-treated or treated with DCV, but this time samples were harvested to monitor intracellular HCV RNA, extracellular HCV titer, as well as extracellular HCV RNA over time. Similar to our published results, the NS5a inhibitor reduced intracellular HCV RNA (Fig. 25, gray circles), but titer was reduced more rapidly and to a larger extent (1 log versus 1.75 logs by 20 hours) (Fig. 25, black squares) consistent with DCV inhibiting HCV RNA synthesis and HCV virion assembly/secretion. The additional extracellular HCV RNA data (Fig. 25, white circles) revealed a reduction of ¾ log, parallel with the intracellular RNA reduction indicating that DCV treatment was altering the specific infectivity of the virus being produced.

Surprisingly, although our HCVcc model was able to fit well the data from the secretion inhibitor (NG) and the HCV NS5b polymerase inhibitor (NM107) (Chapter 4, Fig. 24), when we tried to simulate these DCV NS5a inhibition kinetics we found that the model was unable to fit the data (Fig. 25). Full ranges of biologically relevant values were tested for each biological parameter, but the best fits could not simultaneously simulate the inhibition kinetics of all three measured variables- intracellular HCV RNA, extracellular titer and extracellular total HCV RNA levels. The two best fits could fit the kinetic data for only two of the three variables, one fitting the intracellular HCV RNA and extracellular titer levels (Fig. 25A) and one fitting the intracellular HCV RNA and the total extracellular HCV RNA levels (Fig. 25B). When testing each unknown parameter within its biologically relevant range, it became apparent that the model always decreased infectious extracellular titer and total extracellular HCV RNA in parallel under every condition, despite the fact that the mathematical model has a nearly 10-fold difference between the rate coefficients of particle degradation (c) and the loss of infectivity (k_{loss}) which accounts for the difference in half-lives between these parameters. Because we know that viral infectivity can in theory be altered, this restriction in the model simulation dynamics suggested something was missing, likely due to the fact that we had left assembly and secretion coupled.

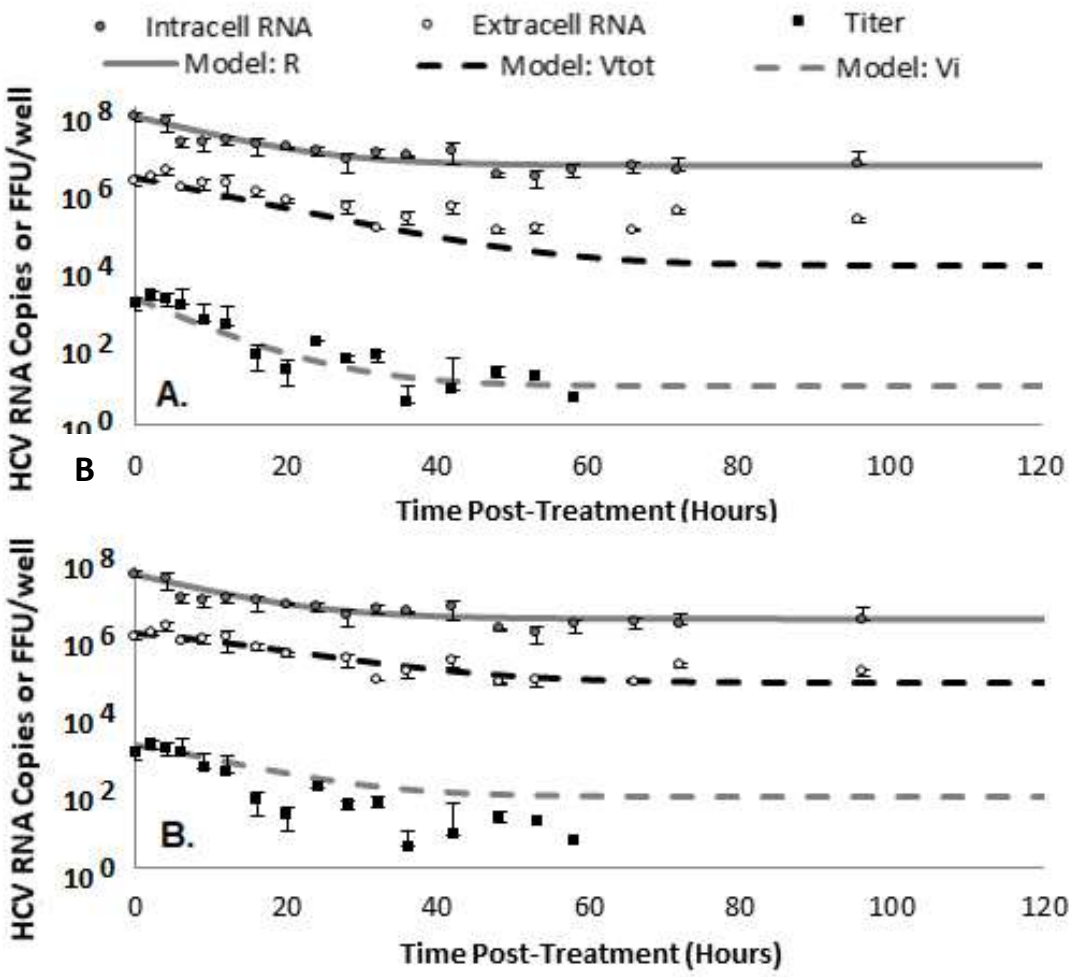

Fig 25. HCVcc Infection Model Data Fits to DCV Inhibition Kinetics. Growth-arrested Huh7 cells with steady-state, chronic HCV infection were treated with 1nM BMS-790052 or diluent control (not shown). Cell lysate and culture supernatant were harvested at the indicated time points post-treatment (x-axis). Intracellular HCV RNA was quantified by RT-qPCR and the average of triplicate samples is graphed as HCV RNA copies per well (gray circles). Extracellular HCV RNA was quantified by RT-qPCR and the average of duplicate samples is graphed as HCV RNA copies per well (white circles). HCV titer was determined by titration on naïve Huh7 cells and the average of duplicate samples is graphed as FFU per well (black squares). All data points are graphed relative to the diluent treated control cultures at the corresponding time point (as described in Materials and Methods, Fig. 4). Error bars represent the standard of deviation of measured values among the replicate wells. Solid and dashed lines represent mathematical model fits to corresponding datasets achieved with Berkeley Madonna software. **(A)** Best fit to intracellular HCV RNA and extracellular HCV titer. **(B)** Best fit to intracellular HCV RNA and extracellular HCV RNA.

5.2.4 Confirming Accurate Quantification of Extracellular Hepatitis C Virus RNA Levels

Before changing the model to account for DCV data, we first wanted to determine if there was a technical artifact that was causing the extracellular HCV RNA levels in our experimental system to remain high or if our assay was accurately measuring V_{tot}. In particular, it had been reported that HCV RNA can be found in extracellular exosomes raising the question of whether HCV may be transmitted by exosomes, and if perhaps this is one reason why antibodies against HCV particles are not optimally effective.[100–103] Hence, we wanted to determine whether the high levels of extracellular HCV RNA might be due to the secretion of exosomes containing viral RNA. However, separating exosomes from HCV particles is difficult because they are similar in size (exosomes being 50–90 nm[85] and HCV particles being 40–70 nm)[14,23,104–107]and HCV particles bind to CD–81[108], a prominent exosome marker[85]. Hence, we decided to modulated the amount of exosomes that were secreted by infected cells and investigated whether the amount of exosome secretion affected extracellular HCV RNA levels. The experimental approach we chose was to manipulate exosome secretion and determine if this affects extracellular HCV RNA levels. Hence, we treated chronically HCV infected, non–growing cells with exosome secretion inhibitor (GW4869) or the exosome secretion enhancer (A23187)[109,110] and monitored HCV levels as well as toxicity. Exosomes were isolated by ultracentrifugation and measured by Bradford assay and CD63 ELISA assay, indicating that exosomes in the supernatant were reduced by 40% and increased by 304% by these treatments, respectively (data not shown), but we did not observe any effect on extracellular HCV RNA levels (Fig. 26).

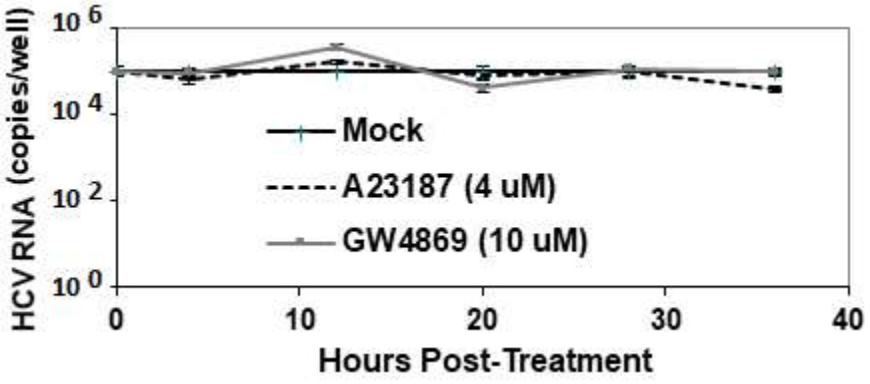

Figure 26. Extracellular HCV RNA Levels during Exosome Secretion Modulation. Growth-arrested Huh7 cells with steady-state, chronic HCV infection were treated with 10 μM GW4869 (dark gray line), 4 μM A23187 (black dashed line) or diluent control (black solid line). Culture supernatants were harvested at the indicated time points post-treatment (x-axis). Extracellular HCV RNA was quantified by RT-qPCR and the average of duplicate samples is graphed as HCV RNA copies per well. All data points are graphed relative to the diluent treated control cultures at the corresponding time point (as described in Materials and Methods, Fig. 4). Error bars represent the standard of deviation of measured values among the replicate wells.

Furthermore, when we treated chronically infected cells with a dose of an HCV-specific secretion inhibitor that blocks 92% of HCV secretion without altering the exosome secretion pathway (Chapter 3, Fig. 18B), we saw a 1-log reduction in extracellular HCV RNA, suggesting that 90% of the HCV RNA levels represent HCV particles and not exosomes. Additionally, if exosomes were artificially increasing extracellular HCV RNA levels in a way that caused them to

decline more slowly than extracellular titer levels, we would expect this phenomenon would have been equally apparent in our previous steady-state inhibition experiments. However, this had never been observed in our previous HCV secretion inhibitor (Chapter 3, Fig. 18B) or HCV polymerase inhibitor (Chapter 3, Fig. 18A) experiments, where we observed parallel decline in extracellular viral species, suggesting that exosomes were not artificially increasing levels of extracellular HCV RNA.

5.2.5 Mechanisms by Which Daclatasvir Could be Reducing Extracellular Hepatitis C Virus Titer Faster than Extracellular Hepatitis C Virus RNA

After confirming that our extracellular HCV RNA measurements are an accurate reflection of extracellular HCV particles, V_{tot}, we concluded that one of our model assumptions/hypotheses about the dynamics of HCV infection was incorrect or incomplete. When this occurs, it is an opportunity to determine where our gap in knowledge might be. After analyzing the model, we discovered two changes (i.e. hypotheses) that could allow extracellular titer to be reduced faster than total extracellular HCV RNA. One hypothesis that could be incorporated into the model would be to allow infectious and non-infectious particles to have distinct rates of entry, which we would model by having two separate entry rate coefficients for each species (k_i and k_{ni} instead of the single k_{in}) (Fig. 27A). This is biologically plausible because non-infectious particles could be less effective at entering a cell or perhaps enter through non-specific uptake at a distinct rate from infectious entry. However, this seems like an unlikely explanation because even if distinct entry

rates exist, NS5a is not thought to affect particle entry. A second hypothesis that could be incorporated into the model, and that would be consistent with our previous *in vivo* model predictions (Appendix A), is that the NS5a inhibitor disrupts/impairs some aspect of assembly/secretion such that an even larger percent of non-infectious virions are produced relative to infectious virions. We modeled this by including two distinct parameters that represent the efficacy of the drug in blocking assembly/secretion of the infectious virus vs. the non-infectious particles (Fig. 27B, having inhibition coefficients ϵ_{si} and ϵ_{sni}, instead of only having ϵ_s).

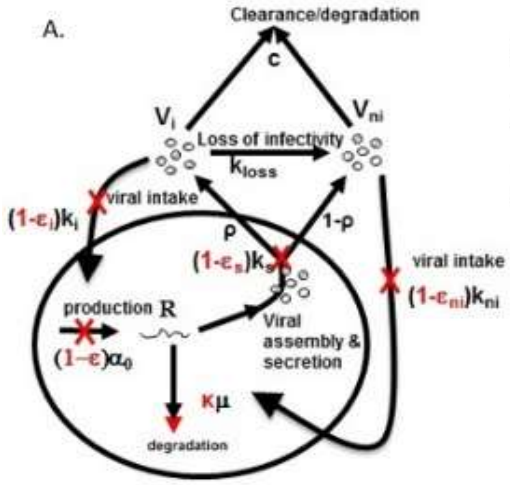

$$\frac{dR}{dt} = (1-\varepsilon)\alpha_0 + (1-\varepsilon_i)k_i V_i + (1-\varepsilon_{ni})k_{ni}V_{ni} - \kappa\mu R - (1-\varepsilon_s)k_s R$$

$$\frac{dV_i}{dt} = (1-\varepsilon_s)k_s R\rho - (k_{loss}+c)V_i - (1-\varepsilon_i)k_i V_i$$

$$\frac{dV_{ni}}{dt} = (1-\varepsilon_s)k_s(1-\rho)R + k_{loss}V_i - cV_{ni} - (1-\varepsilon_{ni})k_{ni}V_{ni}$$

B.

$$\frac{dR}{dt} = (1-\varepsilon)\alpha_0 + (1-\varepsilon_{in})k_{in}V_{tot} - (\kappa\mu + k_s((1-\varepsilon_{si})\rho + (1-\varepsilon_{sni})(1-\rho)))R$$

$$\frac{dV_i}{dt} = (1-\varepsilon_{si})k_s R\rho - (k_{loss}+c)V_i - (1-\varepsilon_{in})k_{in}V_i$$

$$\frac{dV_{ni}}{dt} = (1-\varepsilon_{sni})k_s(1-\rho)R + k_{loss}V_i - cV_{ni} - (1-\varepsilon_{in})k_{in}V_{ni}$$

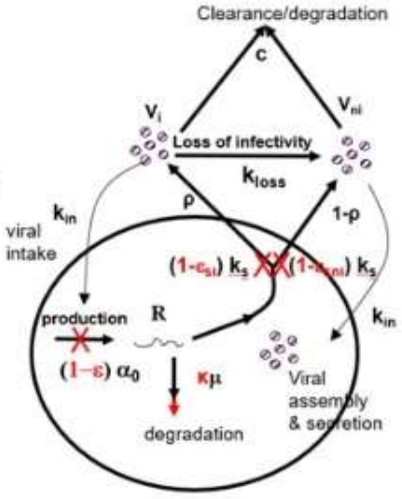

Figure 27. Mathematical Models Allowing Non-Parallel Extracellular HCV RNA and Infectivity Inhibition Kinetics. A) Distinct Entry Hypothesis Model. This model includes distinct entry rates k_i and k_{ni} and distinct entry inhibition coefficients ϵ_i and ϵ_{ni} for V_i and V_{ni}, respectively. B) Distinct Assembly/Secretion Hypothesis Model. This model includes two distinct inhibition coefficients for assembly/secretion of infectious and non-infectious HCV.

After incorporating these two different hypotheses into the model, both were able to simulate a non-parallel reduction in the two extracellular virus parameters. The models were sensitive to all parameters tested, as demonstrated by the relatively narrow 95% confidence intervals, except in the case of ϵ_{si} by the distinct assembly/secretion model (Table 8). However, the model proposing two distinct rates of entry for infectious and non-infectious particles was only able to fit the early NS5a data (0-36 hours), but then failed to simulate the later kinetics for the extracellular HCV RNA (Fig. 28A). In contrast, the model proposing that the NS5a inhibitor impairs infectious virus assembly/secretion modeled the data well with a greater goodness of fit (i.e., lower RSS) of model "assembly/secretion" compared to model "Entry", while both models have the same number of unknown parameters consistent with the NS5a inhibitor DCV inhibiting both HCV replication and assembly/secretion (Table 9; Fig. 28B).

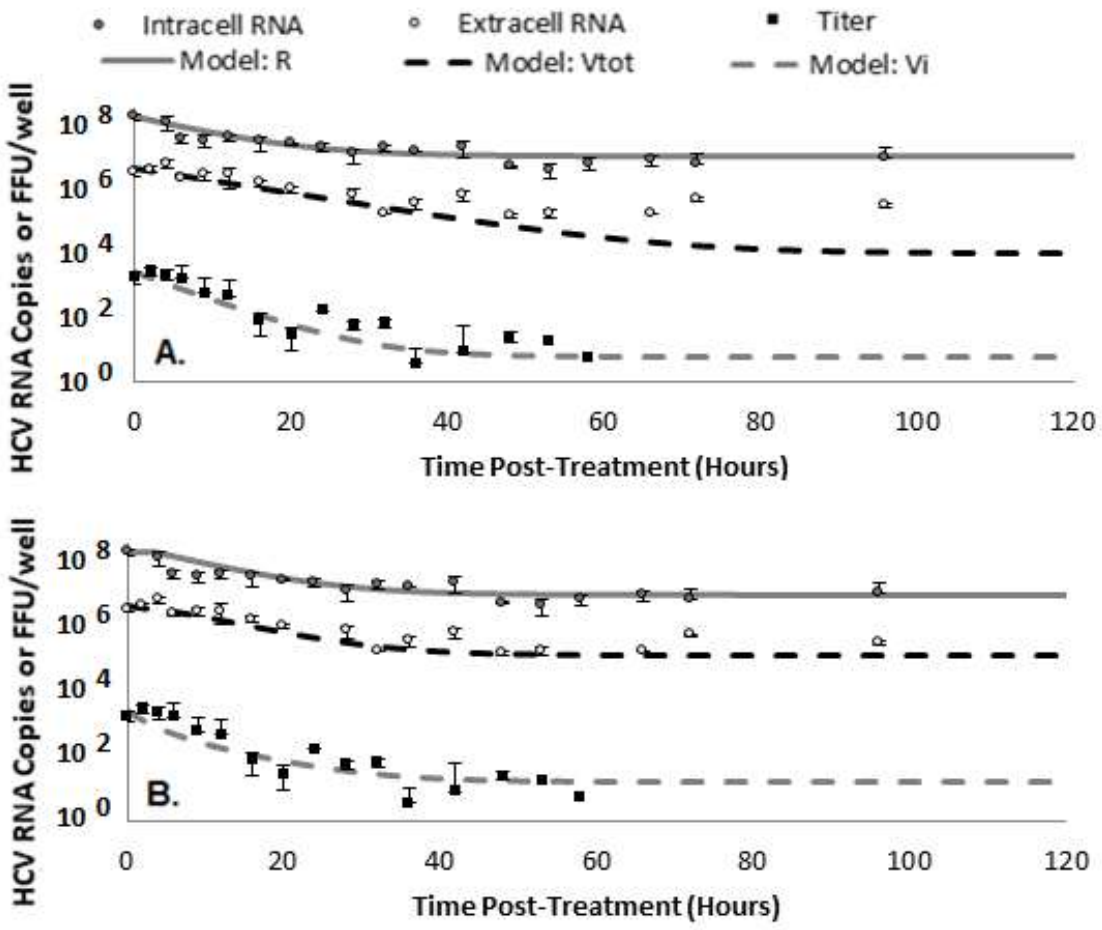

Figure 28. **Revised HCVcc Infection Model Data Fits to NS5a Inhibitor Data. A)** The mathematical model with distinct entry rates (Fig. 27A) or **B)** the mathematical model that allows an antiviral inhibition of assembly/secretion to have distinct effects on the two extracellular viral particle populations (Fig. 27B) were used to fit the empirical NS5a inhibition data in Figure 25 using Berkeley Madonna software. Solid and dashed lines represent mathematical model fits to corresponding datasets. Model parameters described in Table 9.

Model	Assembly/Secretion	Entry
Residual Sum of Squares (RSS)	20.2490	26.0254
T_0 (delay)	0.147 days (fixed)	0.01 days (fixed)
ϵ (efficacy of blocking RNA synthesis)	0.94 [0.9143–0.9603]	0.93 [0.9167–0.9561]
ϵ_{si} (efficacy of blocking Vi assembly/secretion	0.85 [0.0127–0.9381]	0.95 [0.9473–0.9911]
ϵ_{sni} (efficacy of blocking Vni assembly/secretion	0.34 [0.3142–0.3573]	N/A
K_i (Vi entry rate)	6.79 (fixed)	2.0 [1.9673–2.1047]
K_{ni} (Vni entry rate)	N/A	1.9 (fixed)

Table 9. Parameter Calibration Analysis for Distinct Entry and Assembly/Secretion Models. The two models were fit to the data generated by treatment with the HCV NS5a inhibitor Daclatasvir (DCV, BMS-790052). Estimated parameter values followed by 95% confidence intervals are shown. The residual sum of squares (RSS) is calculated by taking the shortest distance between each experimental data point and the model simulation, squaring each distance, summing the squares and taking the square root of the sum. If a value was estimated by curve fits in Berkeley Madonna or by the equilibrium/steady-state equations, no C.I. is available. N/A, this parameter does not exist in the model.

The distinct assembly/secretion model was also able to fit both the secretion inhibitor (NG) and polymerase inhibitor (NM107) kinetics as well as the previous model (data not shown), demonstrating that the adjustment to the model did not invalidate it for other classes of HCV inhibitors. However, it is important to note that the simpler model used to fit the secretion and polymerase inhibitor kinetics in the previous chapter (Chapter 4, Fig. 23) has the advantage of estimating fewer unknown parameters, giving the model more power.

5.2.6 Investigating Whether the Reduced Infectivity Observed During Daclatasvir Treatment is Specifically Related to Inhibiting Non-Structural Protein 5a

After getting the mathematical model to fit the NS5a inhibitor data and determining that DCV was affecting the specific infectivity of the progeny HCVcc produced, we were interested to further dissect the mechanism involved. Specifically, this raised the question whether the severe reduction in titer is specific to inhibition of HCV NS5a protein, or whether the dramatic reduction in virus titer is a compound effect caused by the inhibitor blocking both HCV synthesis and HCV assembly/secretion (e.g. perhaps reducing the amount of intracellular HCV RNA available for assembly/secretion making the process more error-prone). To address this question, we performed a chronic HCV inhibition experiment in which we compared the kinetics of DCV inhibition relative to a two-drug combination treatment with the polymerase inhibitor, NM107, plus the secretion inhibitor, Naringenin. As controls, NM107 and Naringenin monotherapy

treatments were assessed in parallel (Fig. 29). While DCV, NM107, and the combination NM107 + Naringenin therapy all reduced intracellular HCV RNA with similar kinetics, there were clear differences in kinetics of HCV titer inhibition. NM107 and Naringenin did not start reducing HCV titer until 4 hours eventually causing a 0.5 log reduction after 20 hours of treatment. However, like DCV and the combination NM107 + Naringenin treatment reduced HCV titer earlier and to a larger degree, starting after 2 hours and reducing titer by 1.5 logs after 20 hours of treatment. While these preliminary results suggest that the key to DCV potent antiviral affect in reducing extracellular HCV titer lies not in targeting NS5a, but in targeting both RNA replication and assembly/secretion steps of the lifecycle simultaneously, this experiment must be repeated before any conclusions are drawn.

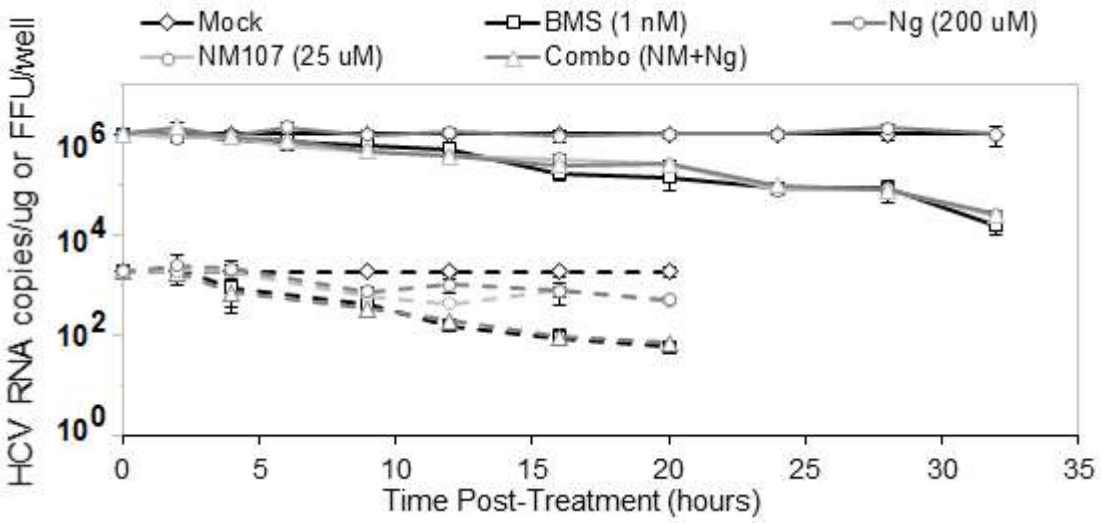

Figure 29. Comparison of HCV Inhibition Kinetics under DCV versus NM107 + Narengenin Combination Treatment. Non-growing, steady-state infected Huh7 cells were treated with 1nM BMS-790052 (black squares), 200 μM Naringenin (dark gray circles), 25 μM NM107 (light gray circles), 200 μM Naringenin +25 μM NM107 (dark gray triangles), or diluent control (black diamonds). Cell lysate and culture supernatant were harvested at the indicated time points post-treatment (x-axis). Intracellular HCV RNA was quantified by RT-qPCR and the average of triplicate samples is graphed as HCV RNA copies per well (solid lines). HCV titer was determined by titration on naïve Huh7 cells and the average of duplicate samples is graphed as FFU per well (dashed lines). All data points are graphed relative to the diluent treated control cultures at the corresponding time point (as described in Materials and Methods). Error bars represent the standard of deviation of measured values among the replicate wells.

5.3 Discussion

The work in this chapter focused on analyzing the unexpectedly rapid and potent HCV inhibition kinetics of NS5a protein inhibitor daclatasvir. Initial analysis of *in vivo* patient response kinetics revealed that a multiscale model was needed to explain the inhibition pattern observed and yielded the hypothesis that daclatasvir inhibited two distinct steps of the HCV life cycle- HCV RNA synthesis and HCV particle assembly/secretion (Appendix A). While *in vitro* experiments confirmed this hypothesis (Appendix A), we applied our *in vitro* HCVcc mathematical model to further dissect the molecular basis of this inhibition. Unexpectedly, our *in vitro* HCVcc model was not able to simulate *in vitro* HCV NS5a inhibitor kinetics, revealing a limitation of the model (i.e. the inability to alter the infectivity of the progeny virus produced) (Fig. 25). Testing alternative models/hypotheses to explain the observed reduced infectivity of extracellular HCV once again led to the conclusion that daclatasvir inhibits HCV RNA synthesis as well as assembly/secretion specifically reducing the ratio of infectious virus secreted relative to non-infectious virus.

The ability to generate a hypothesis about DCV mechanism of action within the cell based solely on extracellular patient data (Appendix A) illustrates the strength of mathematical modeling. Importantly however, the premise of our dual experimental/modeling approach is that model hypotheses should be experimentally tested to the extent possible. That being said, because mathematical models can test multiple hypotheses simultaneously and rapidly while also revealing which parameters in a system contribute the most to the outcome, they allow for in-depth analysis of experimental data and are very efficient tools for guiding not only the way we

think about biological systems, but also experimental design. As such, this interplay/crosstalk between empirical and theoretical efforts can serve to streamline research efforts.

We can utilize our models not only to generate hypotheses, but test them as well. Here, we used our HCVcc mathematical model to test different hypotheses that would account for the more rapid reduction in extracellular HCV titer compared to total extracellular HCV RNA. Consistent with our *in vivo* model predictions that DCV was acting at viral assembly/secretion, we found that the *in vitro* model hypothesis proposing this mechanism of action was able to best fit the experimental data. In hindsight however, we believe the modifications we made to the model to allow for changes in the infectivity of secreted virus are not as biologically accurate as they could be. Currently, we achieved this by artificially adding distinct assembly/secretion rates of infectious versus non-infectious virions, but biologically it is assumed that infectious and non-infectious particles are generated via the same pathways, albeit an inefficient/error-prone system that often generates defective (i.e. non-infectious) particles. Hence, future efforts are already underway to try and design the model to reflect this in a more biologically accurate way. Likewise, immediate future plans include separating the assembly and secretion steps of the HCV life cycle in our mathematical model, as this will allow finer dissection of the little-understood aspect of the viral life cycle. For this, we will adapt our kinetics experiments to also include measurements of intracellular infectious titer.

Most importantly, our findings that the NS5a inhibitor, DCV, reduces the infectivity of the extracellular HCV particles produced appears to explain a very unexpected and previously unexplained phenomena being observed in patients being treated with the new HCV DAAs. Specifically, it has been observed that many patients treated with HCV DAAs positive for serum HCV RNA at the end of their treatment, yet somehow go on to clear the virus after treatment has stopped.[111-115] This phenomenon, referred to as End of Treatment (EOT) HCV+, had never been seen previously with IFN-based therapies as any detectable HCV RNA at the end of treatment resulted in immediate HCV rebound and treatment failure. While there are other possible explanations for clearance in those who are EOT HCV+ (e.g. restored immune function), our *in vitro* data suggests that perhaps the majority of the HCV RNA present at the EOT may be non-infectious. In fact, while all published *in vivo* models to date predict HCV rebound if HCV RNA is present at the time treatment stops, we recently published a model incorporating the idea of non-infectious virus post-DAA treatment which is better able to predict HCV DAA treatment outcome (Appendix B).

6. DISCUSSION

6.1 Mathematical Modeling of Biological Systems

Recognizing an expanding need in biomedical research, in 2000 the NIH implemented "The Biomedical Information Science and Technology Initiative" to encourage the use of mathematical tools for understanding complex biological processes. Likewise, the mission of the National Centers for Biomedical Computing includes the creation of innovative software programs and other tools that will enable the biomedical community to integrate, analyze, model, and simulate data on human health and disease. The cross-disciplinary experimental and theoretical approach of this thesis is based on the same underlying premise that mathematical modeling can provide an effective research-enabling framework.

The use of mathematical modeling to simulate and understand complex biological systems has a long history, but is only recently becoming more mainstream as systems biology approaches in general have become more in vogue. Mathematical modeling of viral dynamics is a systems biology approach in that it can be used to analyze experimental results from complex biological systems with multiple factors and simultaneously integrate and test all major hypotheses about that biological system. In doing so, modeling can expedite the formulation of focused hypotheses that streamline experimental design and provide estimates for parameters that are difficult to isolate and measure empirically.

Mathematical models are valuable in understanding the dynamics of viruses that trigger both persistent infection (e.g. HIV-1[116-119], hepatitis B virus[120-122], hepatitis D virus[123,124], Theiler murine encephalomyelitis virus[125], herpes simplex virus[126] and HCV[87,127,128]) and acute infection

(e.g influenza A[129–131] and ebola virus.[132] Mathematical modeling is also improving our understanding of intracellular viral genome dynamics[53,75,76,133], T-cell dynamics, and the quantitative events that underlie the immune response to pathogens[116,119]. The standard model for HCV kinetics during treatment has provided many insights into the effectiveness and mechanism of action of interferon-alpha and ribavirin (reviewed in [134,135]). The models were able to retrospectively predict the duration of treatment needed for HCV eradication (cure)[73,136,137] and more recently used in real-time (during treatment) to predict the duration of IFN-free therapy with silibinin+ribavirin needed to achieve cure.[138]

While one might assume that recapitulating the dynamics of biological systems requires extremely complex models based on an elaborate system of differential equations, our group and others have demonstrated the value of simple data-driven models as a means to generate testable hypotheses and further knowledge[53,70,72,74,139]. By taking a truly integrated cross-disciplinary approach in which modeling is guided by experimental data that we tailor to the requirements of our mathematical model by our experimental design (Fig. 30), we are able to produce models with minimal unknowns, allowing for robust parameter estimation. Importantly, as illustrated in this thesis, the process of creating these data-driven models is knowledge generating. Thus, creation of the mathematical model is not simply a goal, but rather a tool that helps us better understand the biological system. The models developed herein, while still not complete, have helped us understand new aspects of HCV steady-state dynamics and investigate the mechanisms of action of clinically relevant HCV DAAs, including daclatasvir. Future efforts to refine the current HCVcc model and expand it to address additional molecular aspects of the viral

life cycle certainly will provide more opportunities to advance our knowledge in analogous ways.

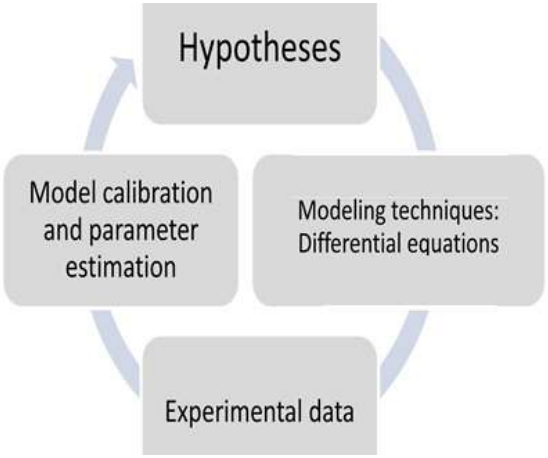

Fig. 30. The Experimental Modeling Cycle. Cycle in which we create models based on all major hypotheses about the biological system, test those models experimentally to determine if our understanding is correct and generate new hypotheses, then incorporate new information into the model in order to re-test via experiments again.

6.2 Using Model/Data Discrepancies to Further Knowledge

In Chapter 3, we utilized an already established HCV replicon mathematical model (Fig. 5; Eq. 2), and moving forward to use this to assess new HCV DAAs revealed the first model/data discrepancy, which informed our understanding of HCV biology. Specifically, because HCV NS3 protease inhibitors are expected to interfere with cleavage of the HCV polyprotein, reducing the amount of proteins required for HCV RNA synthesis, we expected the model to predict the inhibition kinetics of BILN2061 by reducing HCV RNA synthesis. However, we had to allow the model to also enhance HCV RNA degradation in order to simulate the rapid decline in HCV RNA that was observed empirically during these inhibition experiments (i.e. a 99.99% block in RNA synthesis simulated HCV RNA decline of 4 logs in 10 days while BILN2061 achieved this empirically in just 6-7 days).

Notably, this intracellular *in vitro* data-driven prediction is in agreement with our subsequent serum data-driven *in vivo* model prediction based on data from patients treated with protease inhibitor danoprevir.[91] While this simple model does not tell us if or how inhibition of NS3 might impact HCV RNA degradation, it is known that the HCV NS3 protease cleaves a cellular protein known as mitochondrial antiviral signaling protein/MAVS (also known as Cardif or IPS-1) and prevents this cellular protein from activating RIG-I/IFN signaling pathways that would reduce HCV[140,141,142] and others subsequently reported that one effect of IFN is to enhance HCV RNA degradation.[143] Hence, the model suggests that inactivation of HCV NS3 not only directly reduces HCV replication, but likely restores an important aspect of the host cell antiviral defense machinery.

In order to experimentally test this hypothesis and determine whether reactivation of MAVS is a major contributing factor to the rapid reduction in HCV RNA under HCV NS3 protease inhibitor BILN2061 treatment, we can repeat the kinetics experiment in our normal Huh7 cells and in Huh7.5 cells, which contain an inactivating mutation in MAVS. If the cells without functional MAVS do not show the same dramatic BILN20161 induced HCV inhibition and the mathematical model can simulate the RNA reduction kinetics in MAVS-deficient cells without requiring that the protease inhibitor increases HCV RNA degradation, then we could conclude that the reactivation of MAVS signaling is the explanation for the rapid protease inhibitor response kinetics. Notably, this would also allow us to potentially incorporate the effects of MAVS and NS3 inhibition of MAVS into the mathematical model.

After creating our initial infectious HCVcc mathematical model (Fig. 14), we quickly realized that the model could not fit our HCV NS5b polymerase inhibitor (NM107) and HCV secretion inhibitor (Naringenin) data because the model was unable to reduce extracellular HCV RNA levels as quickly as observed empirically. This discrepancy between the model and the data made us reconsider the assumptions that we had built into the model about clearance of extracellular HCV RNA during chronic HCVcc infection steady-state. The common perception is that during viral infections extracellular virus clearance is primarily immune-mediated. However, because this type of immune clearance does not occur *in vitro*, the only mechanism of extracellular HCV RNA clearance we had incorporated into the model was our empirically measured decay rate of particles containing HCV RNA. Because this sole mechanism was too slow to account for the reduction that we measured during antiviral treatment, this discrepancy led us

to investigate other possible mechanisms of extracellular HCV RNA clearance. Specifically, we investigated whether cells were secreting anything that would affect the rate of HCV RNA decay (as we had originally determined the stability of these particles in the absence of cells) and whether HCV declined in transplant patients during the anhepatic phase when the patient has no liver.

Because both of these experimental approaches provided evidence consistent with HCV uptake by hepatocytes, we added an additional pathway to our mathematical model that allowed not only infectious HCV particles (which was already intuitively present in the model), but also the much more abundant non-infectious HCV particles to enter cells. Importantly, this addition allowed the model to fit both the NM107 and Naringenin data, consistent with the conclusion that a significant amount of HCV entry into cells (regardless of infection status) is important to the steady-state dynamics observed, which raises questions regarding the nature of that entry.

Because most (if not all) the cells in our chronically infected cultures *in vitro* are already infected and superinfection exclusion has been reported for HCV, we assume this entry is non-productive (i.e. does not enhance HCV RNA synthesis) and speculate that it perhaps represents general supernatant sampling, by which the cell may be acquiring nutrients or clearing debris. To test the "non-productive" cellular uptake hypothesis we plan to perform experiments monitoring extracellular HCV RNA (i.e. virion) levels during incubation with: 1) no cells (negative entry control), 2) uninfected Huh7 cells (positive entry control), or 3) CD81 knockout cells (which are not permissive for infectious HCV entry). If there is an alternative non-productive route of HCV entry into cells, the CD81-negative cells should not become infected, but nonetheless should

result in a reduction of HCV RNA/particles in the media. If the results are unclear, we may need to expand the experiment to include an infected cell condition or alternative entry-blocking strategies, such as HCV neutralizing antibody or ezetimibe, which prevents HCV entry by blocking the internalization of the HCV entry factor NPC1L1.[33]

While our revised HCVcc mathematical model was able to fit HCV polymerase and HCV secretion inhibitor data (Fig. 24), when we tried to fit DCV inhibitor data (NS5a inhibitor) the model was unable to simulate the kinetics observed. The discrepancy brought to our attention that the model was unable to simulate non-parallel reduction in extracellular HCV titer and RNA, highlighting an important element missing from the model - a mechanism to alter progeny virus specific infectivity (i.e. the proportion of secreted viral particles that are infectious vs non-infectious). We could think of two different ways the model could be altered to allow changes in specific infectivity and thus created two models to test these two alternative hypotheses (e.g. the distinct entry hypothesis model versus the distinct assembly/secretion hypothesis model) (Fig. 27). While this approach confirmed the original *in vivo* model hypothesis that DCV was acting at the assembly/secretion step of the viral life cycle and further incorporated the empirically observed change in progeny virus specific infectivity, the current model still has limited ability to dissect the specific mechanism responsible. Hence, we would like to increase the amount of complexity in the model in order to increase the degree of detail in the hypotheses that can be generated by using the mathematical model to analyze kinetic data, particularly for drugs like HCV NS5a inhibitors.

6.3 Future Modeling Efforts

An important part of the process of increasing our model complexity will be to refine our HCVcc model so that the assembly/secretion step more accurately reflects the biology of these processes as we understand them. While the current model implies that assembly/secretion of V_i and V_{ni} are separate pathways, the assembly step of the HCV viral lifecycle is believed to be a single error-prone process which produces non-infectious virus simply because not all virions are perfect (e.g. Huh7 cells do not produce sufficient lipoproteins, making the virions produced more dense and less infectious). Drugs that interfere with the assembly step of the viral lifecycle may block assembly completely or perhaps make some aspect of the process even less efficient, enhancing the error rate and further decreasing the portion of secreted particles that are infectious. To try and dissect the MOA of these drugs, we have begun to develop an alternative assembly/secretion model in which the distinct effects of the drug on the extracellular populations of infectious vs. non-infectious particles would be achieved by allowing the drug to change the specific infectivity by a factor (represented by the parameter r) that is multiplied by ρ (Fig. 31A-B).

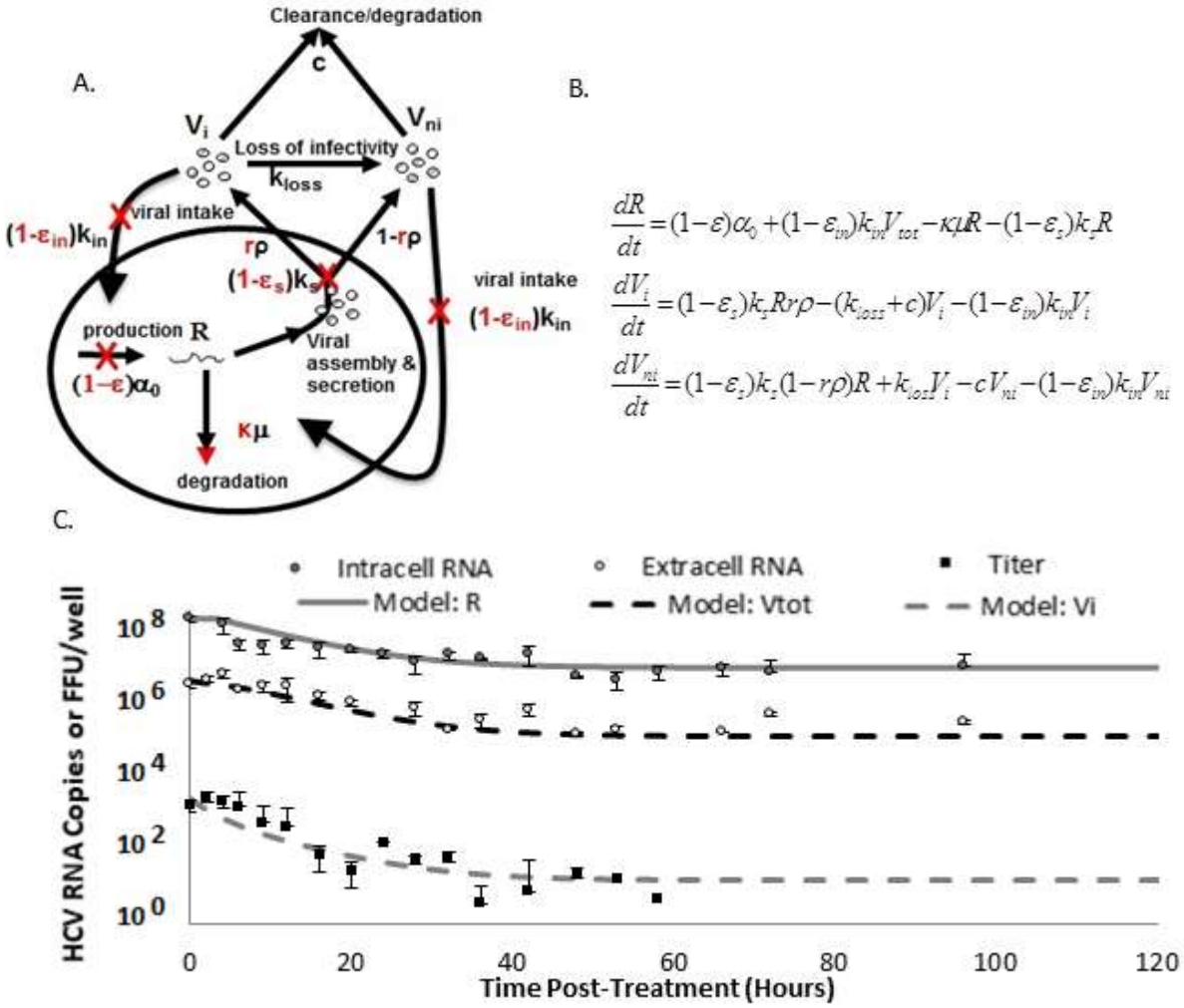

Figure 31. Preliminary HCVcc Specific Infectivity Model. **(A)** Model schematic allowing antiviral to change the specific infectivity ρ by a factor of r. **(B)** Equations comprising the mathematical model. **(C)** Preliminary fits of specific infectivity model to HCV NS5a inhibition data. Model parameters are described in Table 10.

Biological Definition		NM107 Values	Source
R_0	Initial intracellular HCV RNA	$5.86x10^7$ copies/well	Experimentally measured
$Vtot_0$	Initial extracellular HCV RNA	$1.7x10^6$ copies/well	Experimentally measured
Vi_0	Initial extracellular infectious HCV particles	1600 FFU/well	Experimentally measured
Vni_0	Initial extracellular non-infectious HCV particles	1,698,400 /well	Experimentally estimated as $Vtot_0-Vi_0$
(ρ)	Portion of infectious virions	0.0022	Estimated by fitting model to NM107 and Naringenin datasets
(μ)	RNA degradation rate constant (/day)	3.03/day	Estimated by fitting model to NM107 data
c	Non-infectious particle degradation rate constant	0.13/day	Experimentally measured
k_{loss}	Loss of infectivity rate constant	2.64/day	Experimentally measured
α_0	Intracellular HCV RNA synthesis rate constant	$1.78x10^8$/day	Determined by fitting in Berkeley Madonna
k_{in}	Viral entry rate constant	1.84/day	Determined by fitting in Berkeley Madonna
k_s	Assembly/secretion rate constant	0.06/day	Determined by fitting in Berkeley Madonna
t_0	delay	0.02 days	Estimated by Berkeley Madonna software
r	Factor by which drug alters specific infectivity	0.07	Estimated by Berkeley Madonna software
(ϵ)	RNA synthesis Inhibition	0.95	Estimated by Berkeley Madonna software
(ϵ_s)	assembly/secretion Inhibition	0.5	Estimated by Berkeley Madonna software
ϵ_{in}	Entry inhibition	0 (fixed)	Fixed

Table 10. Preliminary HCVcc Specific Infectivity Model Parameter Values.

Preliminary fits of this mathematical model have been promising (Fig. 31, Table 10) and additional work will be done to test/validate this model. While this model is mathematically indistinguishable from saying that the drug affects the assembly/secretion of one species more than another, one advantage to this model is that it is less likely that the drug mechanism will be misinterpreted and should allow the generation of more accurate hypotheses about assembly/secretion and drug mechanism(s) inhibiting this process. Another important mechanistic addition we hope to make in the future is to separate the assembly and secretion steps in the model and measure additional HCV parameters for that model by adapting our kinetics experiments to include measurements of intracellular infectious titer.

6.4 Patient Cure Despite End of Treatment Hepatitis C Virus RNA Positivity

HCV levels in patients need to be monitored during antiviral therapy to make decisions about treatment based on how quickly the levels are reduced. Because it is not possible to assess infectious titer in patients, extracellular (serum) HCV RNA levels are measured. For IFN-based therapies, detection of HCV RNA at the end of treatment (EOT) was a clear and absolute indicator of treatment failure.[144-146] However, since the FDA approval of HCV DAAs, numerous reports document that some patients treated with IFN-free DAA regimens achieved SVR (i.e. cure) despite having detectable viremia at end of treatment (i.e. EOT^{+}/SVR).[111-113,147-149]

One hypothesis offered for the phenomenon of EOT^{+}/SVR is immune-mediated clearance that occurs after treatment is completed.[150] The rationale for this hypothesis is compelling because unlike IFN treatment that continuously stresses the patient's immune response, DAAs directly

attack the virus, reducing viral loads and providing relief for the patient's immune system. However, our data suggest the additional hypothesis that DAAs (such as HCV NS5A inhibitors) promote the production of non-infectious viral particles as shown herein (Chapter 5).

Understanding EOT HCV RNA positivity is important for monitoring treatment success in order to make decisions about clinical care. With current HCV DAAs being unaffordable to many, it is important to be able to determine when treatment could be stopped. In this sense, it is particularly important to determine whether EOT^{+}/SVR is immune-mediated as this would imply the phenomenon might differ depending on host genetic factors, much like response to IFN treatment did, and thus the nature of the EOT HCV RNA is important for future modeling efforts.

In this regard, it is interesting to note that we recently incorporated the concept that DAAs (such as DCV) may alter the proportion of secreted viral particles that are infectious vs. non-infectious into an *in vivo* model developed to explain HCV cure after ultrashort DAA therapy (<28 days) (Appendix B). In this published study, we first showed that established models with measured longitudinal HCV viral loads indicated that in the two cases of ultrashort DAA therapy cure examined, cure would not have been predicted without an additional 3-6 weeks of therapy. We then developed a mathematical model that considers the fundamental concept that HCV RNA in serum represents both infectious virus (V_i) and non-infectious virus (V_{ni}). This new model fit the observed treatment outcomes by considering that in addition to slowing V_i and V_{ni} production ($\epsilon \sim 0.998$), these treatments further enhanced the ratio of V_{ni} to V_i, thus increasing the log (V_{ni}/V_i) from 1 at pre-treatment to 6 by the EOT.

While some are taking the approach of monitoring HCV patient immune responses during therapy to assess if the immune clearance hypothesis may be true, the current efforts in my thesis laboratory are focused on developing an infectivity test for clinical isolates which would allow us to test the infectivity of EOT HCV RNA directly to determine if the reduced infectivity we have observed *in vitro* also occurs in patients under DAA treatment. Another approach is to determine if the reduced infectivity of the HCV particle during DAA treatment *in vitro* corresponds to a physical change in the particles as this could possibly be monitored in patient serum instead of infectious titer.

6.5 Concluding Statements

Mathematical modeling facilitates comprehensive analysis of data as well as experimental design in complex experimental systems and experimentation provides a method for testing theoretical hypotheses generated by modeling, each investigative approach strengthening the other. The findings of this thesis work –estimates for parameters (for both the HCV replicon and HCVcc infection), the generation of mathematical models for analysis of HCVcc treatment kinetics, predictions about HCVcc infection dynamics and antiviral mechanisms of action, along with the application of these concepts to analysis of clinical data- now belong to a tradition of conclusions facilitated by mathematical modeling, especially in the context of viral kinetics.

True to the cyclical nature of data-driven mathematical modeling, this thesis work has not only answered inquiries but also raised questions and provided tools for future studies. Specifically, the mathematical modeling of HCV kinetics has led us to further investigate the

mechanisms of action of HCV NS3 protease inhibitors and HCV NS5a inhibitors. We expect these investigations to generate knowledge that further facilitates the analysis of clinical HCV treatment data, a process that has already begun.

REFERENCES CITED

1. Afdhal, N. H. The Natural History of Hepatitis C. *Semin. Liver Dis.* **24,** 3–8 (2004).

2. Poynard, T., Yuen, M.-F., Ratziu, V. & Lai, C. L. Viral hepatitis C. *Lancet (London, England)* **362,** 2095–100 (2003).

3. Gerlach, J. T. *et al.* Recurrence of hepatitis C virus after loss of virus-specific CD4(+) T-cell response in acute hepatitis C. *Gastroenterology* **117,** 933–41. (1999).

4. Mitruka, K. *et al.* Launch of a Nationwide Hepatitis C Elimination Program--Georgia, April 2015. *MMWR. Morb. Mortal. Wkly. Rep.* **64,** 753–7 (2015).

5. McAdam-Marx, C. *et al.* All-cause and incremental per patient per year cost associated with chronic hepatitis C virus and associated liver complications in the United States: a managed care perspective. *J. Manag. Care Pharm.* **17,** 531–46 (2011).

6. Tapper, E. B. *et al.* Direct costs of care for hepatocellular carcinoma in patients with hepatitis C cirrhosis. *Cancer* (2015). doi:10.1002/cncr.29855

7. Baldo, V., Baldovin, T., Trivello, R. & Floreani, A. Epidemiology of HCV infection. *Curr. Pharm. Des.* **14,** 1646–54 (2008).

8. Scull, M. A. *et al.* Hepatitis C virus infects rhesus macaque hepatocytes and simianized mice. *Hepatology* **62,** 57–67 (2015).

9. Zampino, R., Coppola, N., Sagnelli, C., Di Caprio, G. & Sagnelli, E. Hepatitis C virus infection and prisoners: Epidemiology, outcome and treatment. *World J. Hepatol.* **7,** 2323–30 (2015).

10. Messina, J. P. *et al.* Global distribution and prevalence of hepatitis C virus genotypes. *Hepatology* **61,** 77–87 (2015).

11. Houghton, M. Discovery of the hepatitis C virus. *Liver Int.* **29 Suppl 1,** 82–8 (2009).

12. Lohmann, V. *et al.* Replication of subgenomic hepatitis C virus RNAs in a hepatoma cell line. *Science (80-.).* **285,** 110–3. (1999).

13. Zhong, J. *et al.* Robust hepatitis C virus infection in vitro. *Proc Natl Acad Sci U S A* **102,** 9294–9299 (2005).

14. Wakita, T. *et al.* Production of infectious hepatitis C virus in tissue culture from a cloned viral genome. *Nat Med* **11,** 791–796 (2005).

15. Cai, Z. *et al.* Robust production of infectious hepatitis C virus (HCV) from stably HCV cDNA-transfected human hepatoma cells. *J Virol* **79,** 13963–13973 (2005).

16. Vercauteren, K., de Jong, Y. P. & Meuleman, P. Animal models for the study of HCV. *Curr. Opin. Virol.* **13,** 67–74 (2015).

17. Rijnbrand, R., Abell, G. & Lemon, S. M. Mutational analysis of the GB virus B internal ribosome entry site. *J. Virol.* **74,** 773–83 (2000).

18. Ramsay, J. D. *et al.* Experimental transmission of equine hepacivirus in horses as a model for hepatitis C virus. *Hepatology* **61,** 1533–1546 (2015).

19. Billerbeck, E. *et al.* Mouse models of acute and chronic hepacivirus infection. *Science* **357,** 204–208 (2017).

20. McLauchlan, J. Properties of the hepatitis C virus core protein: a structural protein that modulates cellular processes. *J Viral Hepat* **7,** 2–14 (2000).

21. Chan, S. W. & Egan, P. A. Hepatitis C virus envelope proteins regulate CHOP via induction of the unfolded protein response. *Faseb J* **19,** 1510–1512 (2005).

22. Andre, P. *et al.* Characterization of low- and very-low-density hepatitis C virus RNA-containing particles. *J Virol* **76,** 6919–6928 (2002).

23. Nielsen, S. U. *et al.* Association between hepatitis C virus and very-low-density lipoprotein (VLDL)/LDL analyzed in iodixanol density gradients. *J Virol* **80,** 2418–2428 (2006).

24. Uprichard, S. L. Hepatitis C virus experimental model systems and antiviral drug research. *Virol. Sin.* **25,** 227–245 (2010).

25. Pileri, P. *et al.* Binding of hepatitis C virus to CD81. *Science (80-.).* **282,** 938–941 (1998).

26. Zhang, J. *et al.* CD81 is required for hepatitis C virus glycoprotein-mediated viral infection. *J Virol* **78,** 1448–1455 (2004).

27. Monazahian, M. *et al.* Low density lipoprotein receptor as a candidate receptor for hepatitis C virus. *J.Med.Virol.* **57,** 223–229 (1999).

28. Agnello, V., Abel, G., Elfahal, M., Knight, G. B. & Zhang, Q. X. Hepatitis C virus and other flaviviridae viruses enter cells via low density lipoprotein receptor. *Proc. Natl. Acad. Sci. U. S. A.* **96,** 12766–12771 (1999).

29. Scarselli, E. *et al.* The human scavenger receptor class B type I is a novel candidate receptor for the hepatitis C virus. *EMBO J.* **21,** 5017–5025 (2002).

30. Zeisel, M. B. *et al.* Scavenger receptor class B type I is a key host factor for hepatitis C virus infection required for an entry step closely linked to CD81. *Hepatology* **46,** 1722–1731 (2007).

31. Evans, M. J. *et al.* Claudin-1 is a hepatitis C virus co-receptor required for a late step in entry. *Nature* (2007).

32. Zeisel, M. B., Barth, H., Schuster, C. & Baumert, T. F. Hepatitis C virus entry: molecular mechanisms and targets for antiviral therapy. *Front. Biosci. (Landmark Ed.* **14,** 3274–85 (2009).

33. Sainz, B. *et al.* Identification of the Niemann-Pick C1-like 1 cholesterol absorption receptor as a new hepatitis C virus entry factor. *Nat. Med.* **18,** 281–285 (2012).

34. Martin, D. N. & Uprichard, S. L. Identification of transferrin receptor 1 as a hepatitis C virus entry factor. *Proc. Natl. Acad. Sci. U. S. A.* **110,** 10777–82 (2013).

35. Lupberger, J. *et al.* EGFR and EphA2 are host factors for hepatitis C virus entry and possible targets for antiviral therapy. *Nat. Med.* **17,** 589–595 (2011).

36. Rijnbrand, R. C. A. & Lemon, S. M. in *The Hepatitis C Viruses SE - 5* (eds. Hagedorn, C. & Rice, C.) **242,** 85–116 (Springer Berlin Heidelberg, 2000).

37. Lin, C., Pragai, B. M., Grakoui, A., Xu, J. & Rice, C. M. Hepatitis C virus NS3 serine proteinase: trans-cleavage requirements and processing kinetics. *J Virol* **68,** 8147–8157 (1994).

38. Blight, K. J., McKeating, J. A. & Rice, C. M. Highly Permissive Cell Lines for Subgenomic and Genomic Hepatitis C Virus RNA Replication. *J. Virol.* **76,** 13001–13014 (2002).

39. Hijikata, M. *et al.* Proteolytic processing and membrane association of putative nonstructural proteins of hepatitis C virus. *Proc.Natl.Acad.Sci.USA* **90,** 10773–10777 (1993).

40. Hijikata, M. *et al.* Two distinct proteinase activities required for the processing of putative nonstructural precursor protein of hepatitis C virus. *J.Virol.* **67,** 4665–4675 (1993).

41. Grakoui, A., McCourt, D. W., Wychowski, C., Feinstone, S. M. & Rice, C. M. A second hepatitis C virus-encoded proteinase. *Proc.Natl.Acad.Sci.USA* **90,** 10583–10587 (1993).

42. Loo, Y. M. *et al.* Viral and therapeutic control of IFN-beta promoter stimulator 1 during hepatitis C virus infection. *Proc Natl Acad Sci U S A* **103,** 6001–6006 (2006).

43. Egger, D. *et al.* Expression of hepatitis C virus proteins induces distinct membrane alterations including a candidate viral replication complex. *J Virol* **76,** 5974–5984 (2002).

44. Zayas, M., Long, G., Madan, V. & Bartenschlager, R. Coordination of Hepatitis C Virus Assembly by Distinct Regulatory Regions in Nonstructural Protein 5A. *PLoS Pathog.* **12,** e1005376 (2016).

45. Appel, N. *et al.* Essential role of domain III of nonstructural protein 5A for hepatitis C

virus infectious particle assembly. *PLoS Pathog.* **4,** e1000035 (2008).

46. Hughes, M. *et al.* A conserved proline between domains II and III of hepatitis C virus NS5A influences both RNA replication and virus assembly. *J. Virol.* **83,** 10788–96 (2009).

47. Hughes, M., Griffin, S. & Harris, M. Domain III of NS5A contributes to both RNA replication and assembly of hepatitis C virus particles. *J. Gen. Virol.* **90,** 1329–34 (2009).

48. Masaki, T. *et al.* Interaction of hepatitis C virus nonstructural protein 5A with core protein is critical for the production of infectious virus particles. *J. Virol.* **82,** 7964–76 (2008).

49. Tellinghuisen, T. L., Foss, K. L., Treadaway, J. C. & Rice, C. M. Identification of residues required for RNA replication in domains II and III of the hepatitis C virus NS5A protein. *J. Virol.* **82,** 1073–83 (2008).

50. Paul, D., Madan, V. & Bartenschlager, R. Hepatitis C Virus RNA Replication and Assembly: Living on the Fat of the Land. *Cell Host Microbe* **16,** 569–579 (2014).

51. Masaki, T. *et al.* Involvement of hepatitis C virus NS5A hyperphosphorylation mediated by casein kinase I-α in infectious virus production. *J. Virol.* **88,** 7541–55 (2014).

52. Hiet, M.-S. *et al.* Control of temporal activation of hepatitis C virus-induced interferon response by domain 2 of nonstructural protein 5A. *J. Hepatol.* **63,** 829–37 (2015).

53. Guedj, J. *et al.* Modeling shows that the NS5A inhibitor daclatasvir has two modes of action and yields a shorter estimate of the hepatitis C virus half-life. *Proc Natl Acad Sci U S A* **110,** 3991–3996 (2013).

54. Wang, H. & Tai, A. Mechanisms of Cellular Membrane Reorganization to Support Hepatitis C Virus Replication. *Viruses* **8,** 142 (2016).

55. Vieyres, G., Dubuisson, J. & Pietschmann, T. Incorporation of hepatitis C virus E1 and E2 glycoproteins: the keystones on a peculiar virion. *Viruses* **6,** 1149–1187 (2014).

56. Nahmias, Y. *et al.* Apolipoprotein B-dependent hepatitis C virus secretion is inhibited by the grapefruit flavonoid naringenin. *Hepatology* **47,** 1437–45 (2008).

57. Moradpour, D., Penin, F. & Rice, C. M. Replication of hepatitis C virus. *Nat Rev Microbiol* **5,** 453–463 (2007).

58. Xiao, F. *et al.* Hepatitis C virus cell-cell transmission and resistance to direct-acting antiviral agents. *PLoS Pathog* **10,** e1004128

59. Graw, F., Martin, D. N., Perelson, A. S., Uprichard, S. L. & Dahari, H. Quantification of HCV cell-to-cell spread using a stochastic modeling approach. *J. Virol.* **89,** JVI.00016–15 (2015).

60. Dahari, H., Layden-Almer, J. E., Perelson, A. S. & Layden, T. J. Hepatitis C Viral Kinetics in Special Populations. *Curr Hepat Rep* **7,** 97–105 (2008).

61. Fried, M. W. *et al.* Peginterferon alfa-2a plus ribavirin for chronic hepatitis C virus infection. *N Engl J Med* **347,** 975–982 (2002).

62. Manns, M. P. *et al.* Peginterferon alfa-2b plus ribavirin compared with interferon alfa-2b plus ribavirin for initial treatment of chronic hepatitis C: a randomised trial. *Lancet* **358,** 958–965 (2001).

63. Ahmed, K. T., Almashhrawi, A. A., Ibdah, J. A. & Tahan, V. Is the 25-year hepatitis C marathon coming to an end to declare victory? *World J. Hepatol.* **9,** 921–929 (2017).

64. Liang, T. J. & Ghany, M. G. Current and future therapies for hepatitis C virus infection. *N. Engl. J. Med.* **368,** 1907–17 (2013).

65. Layden, T. J., Mika, B. & Wiley, T. E. Hepatitis C kinetics: mathematical modeling of viral response to therapy. *Semin. Liver Dis.* **20,** 173–83 (2000).

66. Layden, T. J., Lam, N. P. & Wiley, T. E. Hepatitis C viral dynamics. *Clin. Liver Dis.* **3,** 793–810 (1999).

67. Herrmann, E., Neumann, A. U., Schmidt, J. M. & Zeuzem, S. Hepatitis C virus kinetics. *Antivir. Ther.* **5,** 85–90 (2000).

68. Layden, J. E. *et al.* First phase viral kinetic parameters as predictors of treatment response and their influence on the second phase viral decline. *J. Viral Hepat.* **9,** 340–5 (2002).

69. Boulestin, A. *et al.* Twenty-four hour kinetics of hepatitis C virus and antiviral effect of alpha-interferon. *J. Med. Virol.* **78,** 365–71 (2006).

70. Chatterjee, A., Guedj, J. & Perelson, A. S. Mathematical modelling of HCV infection: what can it teach us in the era of direct-acting antiviral agents? *Antivir. Ther.* **17,** 1171–82 (2012).

71. Ribeiro, R. M. *et al.* Quantifying the Diversification of Hepatitis C Virus (HCV) during Primary Infection: Estimates of the In Vivo Mutation Rate. *PLoS Pathog.* **8,** e1002881 (2012).

72. Perelson, A. S. & Guedj, J. Modelling hepatitis C therapy--predicting effects of treatment. *Nat. Rev. Gastroenterol. Hepatol.* **12,** 437–45 (2015).

73. Guedj, J. & Perelson, A. S. Second-phase hepatitis C virus RNA decline during telaprevir-based therapy increases with drug effectiveness: implications for treatment duration. *Hepatology* **53,** 1801–8 (2011).

74. Goyal, A. *et al.* Modeling HCV cure after an ultra-short duration of therapy with direct acting agents. *Antiviral Res.* **144,** (2017).

75. Dahari, H., Ribeiro, R. M., Rice, C. M. & Perelson, A. S. Mathematical modeling of subgenomic hepatitis C virus replication in Huh-7 cells. *J Virol* **81,** 750–760 (2007).

76. Dahari, H., Sainz, B., Perelson, A. S. & Uprichard, S. L. Modeling subgenomic hepatitis C virus RNA kinetics during treatment with alpha interferon. *J. Virol.* **83,** 6383–6390 (2009).

77. Dahari Sainz, B. Jr., Perelson, A.S., Uprichard, S.L., H. Poster: Modeling subgenomic HCV RNA kinetics during interferon-α treatment. in *15th International Symposium on Hepatitis C Virus and Related Viruses* (2008).

78. Dahari, H., Ribeiro, R. M. & Perelson, A. S. Mathematical modeling of intracellular subgenomic HCV RNA kinetics during treatment in Huh-7 cells. *Hepatology* **42,** 564A (2005).

79. Yu, X. & Uprichard, S. L. Cell-based hepatitis C virus infection fluorescence resonance energy transfer (FRET) assay for antiviral compound screening. *Curr. Protoc. Microbiol.* **Chapter 17,** Unit 17.5. (2010).

80. Sainz, B. J., Barretto, N. & Uprichard, S. L. Hepatitis C virus infection in phenotypically distinct Huh7 cell lines. *PLoS One* **4,** e6561 (2009).

81. Uprichard, S. L., Chung, J., Chisari, F. V & Wakita, T. Replication of a hepatitis C virus replicon clone in mouse cells. *Virol J* **3,** 89 (2006).

82. Blight, K. J., Kolykhalov, A. A. & Rice, C. M. Efficient initiation of HCV RNA replication in cell culture. *Science (80-.).* **290,** 1972–5. (2000).

83. Sainz Jr., B. & Chisari, F. V. Production of infectious hepatitis C virus by well-differentiated, growth-arrested human hepatoma-derived cells. *J Virol* **80,** 10253–10257 (2006).

84. Yu, X., Sainz, B. & Uprichard, S. L. Development of a cell-based hepatitis C virus infection fluorescent resonance energy transfer assay for high-throughput antiviral compound screening. *Antimicrob. Agents Chemother.* **53,** 4311–9 (2009).

85. Théry, C., Clayton, A., Amigorena, S. & Raposo, G. Isolation and characterization of exosomes from cell culture supernatants. *Curr. Protoc. Cell Biol.* 3.22.1–3.22.29 (2006).

86. Franzen, C. a. *et al.* Characterization of uptake and internalization of exosomes by bladder cancer cells. *Biomed Res. Int.* **2014,** (2014).

87. Neumann, A. U. *et al.* Hepatitis C viral dynamics in vivo and the antiviral efficacy of interferon-alpha therapy. *Science (80-.).* **282,** 103–107 (1998).

88. Choi B. Sainz Jr., P. Corcoran, S.L. Uprichard, H. Jeong, S. Characterization of increased drug metabolism activity in DMSO-treated Huh7 hepatoma cells. *Xenobiotica* in press (2009).

89. Dahari, H. *et al.* Modeling inhibition kinetics of HCV sg1b RNA during IFN/DAAs treatment in non-growing Huh7 cells. in *62nd Annual Meeting of the American Association for the study of Liver Diseases* 54(Suppl): 538A (Hepatology, 2011).

90. Nelson, H. B. & Tang, H. Effect of cell growth on hepatitis C virus (HCV) replication and a mechanism of cell confluence-based inhibition of HCV RNA and protein expression. *J Virol* **80,** 1181-1190 (2006).

91. Rong, L. *et al.* Analysis of Hepatitis C Virus Decline during Treatment with the Protease Inhibitor Danoprevir Using a Multiscale Model. *PLoS Comput. Biol.* **9,** (2013).

92. Goldwasser, J. *et al.* Naringenin inhibits the assembly and long-term production of infectious hepatitis C virus particles through a PPAR-mediated mechanism. *J. Hepatol.* **55,** 963-71 (2011).

93. Schaller, T. *et al.* Analysis of hepatitis C virus superinfection exclusion by using novel fluorochrome gene-tagged viral genomes. *J Virol* **81,** 4591-4603 (2007).

94. Gao, M. *et al.* Chemical genetics strategy identifies an HCV NS5A inhibitor with a potent clinical effect. *Nature* **465,** 96-100 (2010).

95. Murray, C. L. & Rice, C. M. Hepatitis C: An unsuspected drug target. *Nature* **465,** 42-44 (2010).

96. Tse, M. T. Antiviral drugs: New oral HCV drug shows promise. *Nat. Rev. Drug Discov.* **9,** 432 (2010).

97. Tse, M. T. New oral HCV drug shows promise. *Nat. Rev. Microbiol.* **8,** 464 (2010).

98. Thompson, A. J., Clark, P. J. & McHutchison, J. G. Hepatitis C virus nonstructural protein 5A inhibitors: novel target-now for new trials and new treatment strategies. *Hepatology* **52,** 1162-1164 (2010).

99. Asselah, T. NS5A inhibitors: a new breakthrough for the treatment of chronic hepatitis C. *J. Hepatol.* **54,** 1069-1072 (2011).

100. Cosset, F.-L. & Dreux, M. HCV transmission by hepatic exosomes establishes a productive infection. *J. Hepatol.* **60,** 674-675 (2014).

101. Dreux, M. *et al.* Short-range exosomal transfer of viral RNA from infected cells to plasmacytoid dendritic cells triggers innate immunity. *Cell Host Microbe* **12,** 558-570 (2012).

102. Ramakrishnaiah, V. *et al.* Exosome-mediated transmission of hepatitis C virus between human hepatoma Huh7.5 cells. *Proc. Natl. Acad. Sci. U. S. A.* **110,** 13109–13113 (2013).

103. Bukong, T. N., Momen-Heravi, F., Kodys, K., Bala, S. & Szabo, G. Exosomes from hepatitis C infected patients transmit HCV infection and contain replication competent viral RNA in complex with Ago2-miR122-HSP90. *PLoS Pathog.* **10,** e1004424 (2014).

104. Heller, T. *et al.* An in vitro model of hepatitis C virion production. *Proc Natl Acad Sci U S A* **102,** 2579–2583 (2005).

105. Gastaminza, P., Kapadia, S. B. & Chisari, F. V. Differential biophysical properties of infectious intracellular and secreted hepatitis C virus particles. *J Virol* **80,** 11074–11081 (2006).

106. Lim, S. P. *et al.* Inducible system in human hepatoma cell lines for hepatitis C virus production. *Virology* **303,** 79–99 (2002).

107. Kanda, T. *et al.* Generation of infectious hepatitis C virus in immortalized human hepatocytes. *J Virol* **80,** 4633–4639 (2006).

108. Allander, T., Forns, X., Emerson, S. U., Purcell, R. H. & Bukh, J. Hepatitis C virus envelope protein E2 binds to CD81 of tamarins. *Virology* **277,** 358–67. (2000).

109. Xu, L., Han, C., Lim, K. & Wu, T. Cross-talk between peroxisome proliferator-activated receptor delta and cytosolic phospholipase A(2)alpha/cyclooxygenase-2/prostaglandin E(2) signaling pathways in human hepatocellular carcinoma cells. *Cancer Res.* **66,** 11859–11868 (2006).

110. Soo, C. Y. *et al.* Nanoparticle tracking analysis monitors microvesicle and exosome secretion from immune cells. *Immunology* **136,** 192–197 (2012).

111. Malespin, M. *et al.* Prevalence of end of treatment RNA-positive/sustained viral response in HCV patients treated with sofosbuvir combination therapies. *Therap. Adv. Gastroenterol.* **10,** 68–73 (2017).

112. Sidharthan, S. *et al.* Utility of hepatitis C viral load monitoring on direct-acting antiviral therapy. *Clin. Infect. Dis.* **60,** 1743–1751 (2015).

113. Kohli, A. *et al.* Virological response after 6 week triple-drug regimens for hepatitis C: a proof-of-concept phase 2A cohort study. *Lancet* **385,** 1107–1113 (2015).

114. Hasin, Y. *et al.* Hepatitis C virus cures after direct acting antiviral-related drug-induced liver injury: Case report. *World J. Hepatol.* **8,** 858–862 (2016).

115. Meissner, E. G. *et al.* Endogenous intrahepatic IFNs and association with IFN-free HCV treatment outcome. *J. Clin. Invest.* **124,** 3352–3363 (2014).

116. Perelson, A. S. Modelling viral and immune system dynamics. *Nat Rev Immunol* **2,** 28–36 (2002).

117. Ho, D. D. *et al.* Rapid turnover of plasma virions and CD4 lymphocytes in HIV-1 infection. *Nature* **373,** 123–126 (1995).

118. Perelson, A. S., Neumann, A. U., Markowitz, M., Leonard, J. M. & Ho, D. D. HIV-1 dynamics in vivo: virion clearance rate, infected cell life-span, and viral generation time. *Science (80-.).* **271,** 1582–1586 (1996).

119. Burg, D., Rong, L., Neumann, A. U. & Dahari, H. Mathematical modeling of viral kinetics under immune control during primary HIV-1 infection. *J. Theor. Biol.* **259,** 751–759 (2009).

120. Ciupe, S. M., Ribeiro, R. M., Nelson, P. W., Dusheiko, G. & Perelson, A. S. The role of cells refractory to productive infection in acute hepatitis B viral dynamics. *Proc Natl Acad Sci U S A* **104,** 5050–5055 (2007).

121. Dahari, H., Shudo, E., Ribeiro, R. M. & Perelson, A. S. Modeling complex decay profiles of hepatitis B virus during antiviral therapy. *Hepatology* **49,** 32–38 (2009).

122. Nowak, M. A. *et al.* Viral dynamics in hepatitis B virus infection. *Proc.Natl.Acad.Sci.U.S.A.* **93,** 4398–4402 (1996).

123. Koh, C. *et al.* Oral prenylation inhibition with lonafarnib in chronic hepatitis D infection: a proof-of-concept randomised, double-blind, placebo-controlled phase 2A trial. *Lancet. Infect. Dis.* **15,** 1167–1174 (2015).

124. Guedj, J. *et al.* Understanding early serum hepatitis D virus and hepatitis B surface antigen kinetics during pegylated interferon-alpha therapy via mathematical modeling. *Hepatology* **60,** 1902–1910 (2014).

125. Zhang, J., Lipton, H. L., Perelson, A. S. & Dahari, H. Modeling the acute and chronic phases of Theiler murine encephalomyelitis virus infection. *J. Virol.* **87,** 4052–4059 (2013).

126. Schiffer, J. T. *et al.* Frequent release of low amounts of herpes simplex virus from neurons: results of a mathematical model. *Sci. Transl. Med.* **1,** 7ra16 (2009).

127. Dahari, H. *et al.* A mathematical model of hepatitis C virus dynamics in patients with high baseline viral loads or advanced liver disease. *Gastroenterology* **136,** 1402–1409 (2009).

128. Dahari, H. *et al.* Mathematical modeling of primary hepatitis C infection: noncytolytic clearance and early blockage of virion production. *Gastroenterology* **128,** 1056–1066 (2005).

129. Baccam, P., Beauchemin, C., Macken, C. A., Hayden, F. G. & Perelson, A. S. Kinetics of influenza A virus infection in humans. *J. Virol.* **80,** 7590–7599 (2006).

130. Pawelek, K. A. *et al.* Modeling within-host dynamics of influenza virus infection including immune responses. *PLoS Comput. Biol.* **8,** e1002588 (2012).

131. Beauchemin, C. A. A. & Handel, A. A review of mathematical models of influenza A infections within a host or cell culture: lessons learned and challenges ahead. *BMC Public Health* **11 Suppl 1,** S7 (2011).

132. Madelain, V. *et al.* Ebola virus dynamics in mice treated with favipiravir. *Antiviral Res.* **123,** 70–77 (2015).

133. Neumann, A. U. *et al.* Novel mechanism of antibodies to hepatitis B virus in blocking viral particle release from cells. *Hepatology* **52,** 875–885 (2010).

134. Dahari, H., Shudo, E., Ribeiro, R. M. & Perelson, A. S. Mathematical modeling of HCV infection and treatment. *Methods Mol. Biol.* **510,** 439–453 (2009).

135. Dahari, H., Guedj, J., Perelson, A. S. & Layden, T. J. Hepatitis C Viral Kinetics in the Era of Direct Acting Antiviral Agents and IL28B. *Curr. Hepat. Rep.* **10,** 214–227 (2011).

136. Snoeck, E. *et al.* A comprehensive hepatitis C viral kinetic model explaining cure. *Clin. Pharmacol. Ther.* **87,** 706–713 (2010).

137. Dixit, N. M., Layden-Almer, J. E., Layden, T. J. & Perelson, A. S. Modelling how ribavirin improves interferon response rates in hepatitis C virus infection. *Nature* **432,** 922–924 (2004).

138. Dahari, H. *et al.* Sustained virological response with intravenous silibinin: individualized IFN-free therapy via real-time modelling of HCV kinetics. *Liver Int.* **35,** 289–294 (2015).

139. Nguyen, T. & Guedj, J. HCV Kinetic Models and Their Implications in Drug Development. *CPT pharmacometrics Syst. Pharmacol.* **4,** 231–42 (2015).

140. Liang, Y. *et al.* Antiviral Suppression vs Restoration of RIG-I Signaling by Hepatitis C Protease and Polymerase Inhibitors. 1710–1718 (2008). doi:10.1053/j.gastro.2008.07.023

141. Kalkeri, G. *et al.* Restoration of the Activated Rig-I Pathway in Hepatitis C Virus (HCV) Replicon Cells by HCV Protease , Polymerase , and NS5A. (2013). doi:10.1128/AAC.00399-13

142. Sumpter Jr., R. *et al.* Regulating intracellular antiviral defense and permissiveness to hepatitis C virus RNA replication through a cellular RNA helicase, RIG-I. *J Virol* **79,** 2689–99. (2005).

143. Pedersen, I. M. *et al.* Interferon modulation of cellular microRNAs as an antiviral mechanism. *Nature* **449,** 919–922 (2007).

144. Ferenci, P. *et al.* Peginterferon alfa-2a and ribavirin for 24 weeks in hepatitis C type 1 and 4 patients with rapid virological response. *Gastroenterology* **135,** 451–458 (2008).

145. Poordad, F. *et al.* Boceprevir for untreated chronic HCV genotype 1 infection. *N. Engl. J. Med.* **364,** 1195–1206 (2011).

146. Jacobson, I. M. *et al.* Simeprevir with pegylated interferon alfa 2a plus ribavirin in treatment-naive patients with chronic hepatitis C virus genotype 1 infection (QUEST-1): a phase 3, randomised, double-blind, placebo-controlled trial. *Lancet (London, England)* **384,** 403–413 (2014).

147. Sarrazin, C. *et al.* Importance of very early HCV RNA kinetics for prediction of treatment outcome of highly effective all oral direct acting antiviral combination therapy. *J. Virol. Methods* **214,** 29–32 (2015).

148. Harrington, P. R., Deming, D. J., Komatsu, T. E. & Naeger, L. K. Hepatitis C Virus RNA Levels During Interferon-Free Combination Direct-Acting Antiviral Treatment in Registrational Trials. *Clinical infectious diseases : an official publication of the Infectious Diseases Society of America* **61,** 666–667 (2015).

149. Maasoumy, B. *et al.* Frequency and predictive value of detectable HCV RNA at the end of treatment with ledipasvir/sofosbuvir ± ribavirin in a large real world cohort: Results from the German Hepatitis C-Registry (DHC-R). *Hepatology* **64,** 481–481A (2016).

150. Meissner, E. G. *et al.* Sustained Virologic Response for Chronic Hepatitis C Infection after 27 Days of Treatment with Sofosbuvir and Ribavirin. *Open forum Infect. Dis.* **1,** 13 (2014).

APPENDICES: APPENDIX A

Modeling shows that the NS5A inhibitor daclatasvir has two modes of action and yields a shorter estimate of the hepatitis C virus half-life

Jeremie Guedj[a,b,c,1], Harel Dahari[a,d,e,1], Libin Rong[f], Natasha D. Sansone[e,g], Richard E. Nettles[h,2], Scott J. Cotler[e], Thomas J. Layden[e], Susan L. Uprichard[d,e,g], and Alan S. Perelson[a,3]

[a]Theoretical Biology and Biophysics, Los Alamos National Laboratory, Los Alamos, NM 87545; [b]Institut National de la Santé et de la Recherche Médicale and [c]Université Paris Diderot, Sorbonne Paris Cité, Unité Mixte de Recherche 738, F-75018 Paris, France; [d]Department of Medicine, University of Illinois at Chicago, Chicago, IL 60612; [e]Division of Hepatology, Department of Medicine, Loyola University Chicago, Maywood, IL 60153; [f]Department of Mathematics and Statistics and Center for Biomedical Research, Oakland University, Rochester, MI 48309; [g]Department of Microbiology and Immunology, University of Illinois at Chicago, Chicago, IL 60612; and [h]Department of Discovery Medicine and Clinical Pharmacology, Bristol-Myers Squibb Research and Development, Princeton, NJ 08543

Edited* by Charles M. Rice, The Rockefeller University, New York, NY, and approved January 17, 2013 (received for review February 22, 2012)

The nonstructural 5A (NS5A) protein is a target for drug development against hepatitis C virus (HCV). Interestingly, the NS5A inhibitor daclatasvir (BMS-790052) caused a decrease in serum HCV RNA levels by about two orders of magnitude within 6 h of administration. However, NS5A has no known enzymatic functions, making it difficult to understand daclatasvir's mode of action (MOA) and to estimate its antiviral effectiveness. Modeling viral kinetics during therapy has provided important insights into the MOA and effectiveness of a variety of anti-HCV agents. Here, we show that understanding the effects of daclatasvir in vivo requires a multiscale model that incorporates drug effects on the HCV intracellular lifecycle, and we validated this approach with in vitro HCV infection experiments. The model predicts that daclatasvir efficiently blocks two distinct stages of the viral lifecycle, namely viral RNA synthesis and virion assembly/secretion with mean effectiveness of 99% and 99.8%, respectively, and yields a more precise estimate of the serum HCV half-life, 45 min, i.e., around four times shorter than previous estimates. Intracellular HCV RNA in HCV-infected cells treated with daclatasvir and the HCV polymerase inhibitor NM107 showed a similar pattern of decline. However, daclatasvir treatment led to an immediate and rapid decline of extracellular HCV titers compared to a delayed (6–9 h) and slower decline with NM107, confirming an effect of daclatasvir on both viral replication and assembly/secretion. The multiscale modeling approach, validated with in vitro kinetic experiments, brings a unique conceptual framework for understanding the mechanism of action of a variety of agents in development for the treatment of HCV.

direct-acting antiviral agents | mathematical modeling | viral dynamics

Hepatitis C virus (HCV) infection is a major health burden affecting about 150 million people worldwide (1) and ~4.1 million in the United States (2), where it is the primary cause of liver cirrhosis and liver cancer (1). Until 2011, the most advanced antiviral therapy was pegylated interferon-α (IFN-α) plus ribavirin (Peg-IFN/RBV), with a cure rate of 50% or less in patients infected with HCV genotype 1, the most prevalent in the Western world.

To obtain higher cure rates, drug development has focused mainly on inhibiting the function of nonstructural (NS) viral proteins with known enzymatic functions, such as the NS3-4A protease and the NS5B polymerase. Through the use of an innovative screening approach to search for nonenzymatic targets, daclatasvir (BMS-790052) was identified as a potent NS5A inhibitor (3). The functions of the NS5A protein are not fully elucidated, although in vitro studies suggest an essential role of NS5A in both viral replication (4–7) and assembly/release of infectious particles (8–11). The efficacy of daclatasvir as an antiviral agent was confirmed in a single ascending-dose study in which a mean 3.3-$\log_{10}$ reduction in viral load 24 h after drug administration was observed in patients receiving a 100-mg dose (3). More remarkably, 6 h after dosing, a mean 1.95-$\log_{10}$ viral load decline occurred. This decline is faster than has been observed with any other antiviral agent studied to date. Our goal is to uncover the biological basis of this extremely rapid viral decline and the in vivo mechanism of action (MOA) of daclatasvir through mathematical modeling.

Mathematical modeling of HCV infection and treatment has provided valuable insights into the mechanisms of action of IFN-based therapy (12). In these models, the infected cell is treated as a "black box" that produces/secretes virus particles, which then either are cleared or infect new target cells. Using this type of model, it was shown that IFN acts mainly to reduce the average rate of virion production/release per infected cell (12). As a consequence, the early viral decline in serum HCV RNA after treatment initiation was assumed to reflect the clearance of viral particles, which in the model occurs at rate c per virion. By fitting the HCV RNA decline during administration of high daily doses of IFN, Neumann et al. (12) estimated c in HCV genotype 1–infected patients as $6.2 \pm 1.8\ d^{-1}$, corresponding to a serum half-life ($t_{½}$) of 2.7 h. At this rate of virion clearance, it would take at least 17 h to achieve 1.95 $\log_{10}$ viral load reduction, not the 6 h observed.

Here, we analyze the early viral decay observed after one dose of 10 or 100 mg of daclatasvir (3). Using the standard model of HCV dynamics (12) or simple linear regression, we estimate the HCV $t_{½}$ to be about 0.7 h, i.e., 45 min. To explain the discrepancy with the prior $t_{½}$ estimate of 2.7 h during IFN treatment, we introduce a multiscale model of HCV viral dynamics that includes the effects of treatment on distinct intracellular processes of viral RNA production and virion assembly/secretion. We show that this model provides a conceptual framework for the origin of viral decline patterns. Further, the multiscale model fits data on viral declines in patients on IFN, daclatasvir, and the HCV protease inhibitor telaprevir (TVR) and allows us to decipher the mode of action of these drugs and estimate their in vivo antiviral effectiveness in blocking intracellular viral RNA production and in blocking virion assembly/secretion. This approach also shows why clearance rates derived from previous IFN-based studies are underestimates, and therefore it reconciles the two

Author contributions: J.G., H.D., S.L.U., and A.S.P. designed research; J.G., H.D., L.R., N.D.S., and A.S.P. performed research; R.E.N. and T.J.L. contributed new reagents/analytic tools; J.G., H.D., N.D.S., S.L.U., and A.S.P. analyzed data; and J.G., H.D., S.J.C., S.L.U., and A.S.P. wrote the paper.

Conflict of interest statement: R.E.N. was an employee of Bristol-Myers Squibb when this study was performed.

*This Direct Submission article had a prearranged editor.

[1]J.G. and H.D. contributed equally to this work.

[2]Present address: Janssen Services, LLC, Titusville, NJ 08560.

[3]To whom correspondence should be addressed. E-mail: asp@lanl.gov.

This article contains supporting information online at www.pnas.org/lookup/suppl/doi:10.1073/pnas.1203110110/-/DCSupplemental.

contradictory estimates of c and estimates the mean HCV $t_{½}$ as 45 min.

Results

Empirical Analysis of the Early Viral Decline. All nine patients treated with 10 or 100 mg of daclatasvir had a profound and rapid HCV RNA decline from baseline, with mean amplitudes of 0.27, 1.20, and 1.95 $\log_{10}$ international units (IU)/mL at 2, 4, and 6 h post dosing, respectively (Fig. S1). This translates into a mean rate of viral decline between 1 and 6 h of 23.2 d^{-1}, assuming the decline begins 1 h post dosing because of a pharmacological delay.

Analysis of Early Viral Kinetics Using the Standard Model of HCV Infection. In the five patients (Table 1) who did not have a viral load rebound over the first 3 d, the standard biphasic viral decline model introduced by Neumann et al. (12) (Eq. **1**) was fit to the data and well characterized the changes in HCV RNA (Fig. 1*A*). The mean antiviral effectiveness in blocking viral production/secretion, ε, was estimated as 0.997 (Table 1), and the mean rate of viral clearance, c, was estimated as 23.3 d^{-1}, similar to the empirical rate of viral decline estimated above. In addition, we observed a second phase of viral decline that allowed us to estimate the loss rate of infected cells, δ (mean 1.06 d^{-1}) (Table 1). Interestingly, although c and δ represent physiological quantities and therefore should not depend upon the antiviral strategy, these mean values are about four and seven times higher, respectively, than what was estimated previously in patients receiving IFN-based therapy (12, 13).

Analysis of Early Viral Kinetics Using a Multiscale Model. To resolve the discrepancy in the estimates of c and δ obtained when fitting viral load data during IFN-based therapy and daclatasvir therapy, we developed an HCV dynamic model that extends the standard model (Fig. 2*A*) by incorporating essential features of the viral lifecycle that may be targeted by daclatasvir. In this model, viral RNA (vRNA) is produced within infected cells at constant rate α, degraded with constant rate μ, and exported as virions into the circulation at rate ρ per vRNA (Fig. 2*B*). Moreover, the amount of vRNA per infected cell depends on the time elapsed since cell infection, which we call a, the age of an infected cell. Unlike the standard model that does not distinguish between vRNA production and virion secretion, this model allows us to distinguish three possible intracellular effects of antiviral therapy: blocking vRNA production with effectiveness ε_α, blocking vRNA packaging/secretion with effectiveness ε_s, and enhancing the vRNA degradation rate μ by a factor $\kappa \geq 1$.

Because the multiscale model contains several unknown parameters, several assumptions are necessary to make parameter identification possible when only short-term serum HCV RNA data are available. First, we assumed that the parameters c and δ do not depend on the type of treatment administered. Because we were interested in understanding the differences in the initial viral decay observed with daclatasvir vs. IFN-based therapies, we included in our analysis 20 patients who received different doses of daily IFN, and had frequent viral load measurements (12). Second, an approximate analytical solution of the multiscale model (Eq. **3**) may be obtained if one assumes that no new cell infections occur after treatment initiation. We found that the approximate solution (Eq. **3**) and the numerical solution of the full model (Eq. **2**) agreed well in the parameter regime of interest (Fig. S2). Viral load data were analyzed using Eq. **3** only until day 2, as only a single dose of daclatasvir was given. On such a short time scale, the loss rate of infected cells cannot be identified, and we fixed $\delta = 0.14\ d^{-1}$, the mean estimated in patients treated with Peg-IFN/RBV (12–14). Third, the effectiveness in enhancing the loss rate of vRNA, κ, could not be estimated separately from the intrinsic vRNA degradation rate, μ. Thus, we fixed $\mu = 1\ d^{-1}$ and, in essence, estimated the combined parameter κμ. (If we fixed $\mu = 2\ d^{-1}$, then the estimate of κ decreased by 50%, whereas if we set $\mu = 0.5\ d^{-1}$, the estimate of κ doubled.) Further, the distribution of κμ in the population could not be estimated, and hence we assumed that this parameter was similar for all patients in our study. Lastly, we fixed the rate of vRNA production per infected cell, α, to 40 vRNA d^{-1} (15). A sensitivity analysis verified that our choices for α and δ did not substantially influence our estimates of the viral clearance rate, c, or of ε_s and ε_α (Table S1).

To increase the precision of the parameter estimates, a nonlinear mixed-effects model was used to fit the data. The parameters were estimated by maximum likelihood estimation using the extended stochastic approximation expectation-maximization algorithm as implemented in the MONOLIX software (www.lixoft.com) (*SI Methods*). The model fit the individual data well (Fig. 1). The mean pharmacological delay, t_0, until treatment influences viral load was significantly shorter with daclatasvir than with IFN (0.97 h vs. 10.0 h, $P < 10^{-10}$), which was expected because daclatasvir, unlike IFN, is a direct antiviral. Consistent with the prediction of the standard model (12), the effectiveness in blocking vRNA production, ε_α, was significantly associated with the dose of IFN received, with mean values of 0.96 and 0.77 in the 10– or 15–million international unit (MIU) and 5-MIU dosing groups, respectively ($P = 0.0014$). Daclatasvir showed an even higher level of effectiveness in blocking vRNA production [mean effectiveness = 0.990, $CI_{95\%}$ (0.98, 1.0)]. Unlike IFN, daclatasvir also efficiently blocked the secretion of virus (mean ε_s in daclatasvir-treated patients = 0.998 vs. 0.39 in IFN-treated patients, $P < 10^{-10}$), with no significant difference between IFN doses. Using the multiscale model, all patients regardless of antiviral strategy could be fitted assuming a high rate of viral clearance, estimated as $c = 22.3\ d^{-1}$ [$CI_{95\%}$ (18.7, 25.7)] (Table 2). This clearance rate corresponds to a virion half-life $t_{½} = 45$ min. Lastly, the degradation rate of vRNA under treatment, κμ, was estimated as 1.46 d^{-1} [$CI_{95\%}$ (0.74, 2.18)], corresponding to a mean vRNA $t_{½} = 11.3$ h.

Using the approximate solution, Eq. **3**, the multiscale model predicts that after a delay t_0, the viral load, $V(t)$, decays in a triphasic manner (Fig. 3), given by $V(t) = V_0[Ae^{-ct} + Be^{-\lambda t} + Ce^{-\delta t}]$. These successive phases of decline represent the drug's ability to affect different stages of the viral lifecycle: (*i*) By blocking virion assembly/secretion, there is a deficit in virion production, and

Table 1. Parameter estimates obtained using the standard biphasic model (Eq. 1) to fit viral kinetic data from patients treated with daclatasvir

Patient	Daclatasvir dose (mg)	Age (y)	Sex	Race	BMI (kg/m²)	Genotype	V_0($\log_{10}$IU/mL)	t_0 (h)	c (d^{-1})	ε	δ (d^{-1})
8	100	45	F	AA	33	1b	5.64	1.42	31.3	0.996	1.89
42	10	47	F	Caucasian	25	1b	5.65	2.4	21.0	0.998	0.39
68	100	32	F	Caucasian	30	1b	7.15	1.63	20.2	0.998	1.27
69	100	44	F	AA	26	1a	6.14	0.91	22.0	0.999	0.75
83	100	44	F	AA	31	1b	5.45	2.21	21.8	0.996	1.01
Mean							6.00	1.71	23.3	0.997	1.06

Individual viral kinetic parameter estimates made assuming constant antiviral effectiveness of daclatasvir until day 2 in the five patients (Fig. 1) who did not show a viral rebound until day 3. AA, African American; BMI, body mass index; c, serum HCV RNA clearance rate; δ, loss rate of infected cells; ε, effectiveness in blocking virion production/release; F, female; t_0, pharmacological delay.

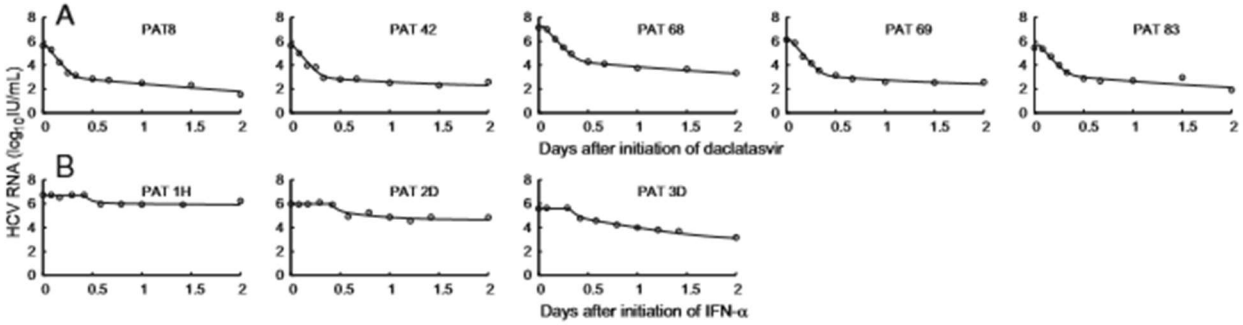

Fig. 1. Viral kinetics and model predictions. Viral load data (○) and standard and multiscale models' predictions (solid line) for (*A*) five patients receiving one dose (four received 100 mg and one, Pt42, received 10 mg) of daclatasvir (BMS-790052) and (*B*) three representative patients receiving daily IFN-α of 5 MIU (*Left*), 10 MIU (*Center*), and 15 MIU (*Right*). Although interpretations are different, the model curves of the standard model (Eq. 1) and of the multiscale model (Eq. 3) overlap and cannot be distinguished.

virions naturally eliminated with rate c are not replaced. (*ii*) By blocking its production and/or increasing its rate of loss intracellularly or by infected cell death, vRNA levels decrease with rate λ, which limits the material available for producing new virions. (*iii*) The remaining virus production ultimately declines with rate δ, reflecting the progressive elimination of infected cells over time.

In this model, A, B, and C are constants that depend on model parameters; thus, the duration of these phases depends on the drug's mode of action. For daclatasvir, A is 500-fold larger than B and we calculate that for the initial 8 h, the first term reflecting virion clearance is larger than the second term and a first phase decay with a slope reflecting the virion clearance rate c is apparent (Fig. 3*A*, black line). For IFN, A is smaller than B and the phase representing virion clearance now is too short to be observed in the clinical data, and only a single phase of HCV RNA decay with rate λ is seen during the first 2 d of therapy (Fig. 3*A*, blue line). This phase reflects the decay of vRNA and infected cells and not virion clearance as incorrectly concluded in prior work (12). At longer times, approximately day 3 with either IFN or daclatasvir (Fig. 3*B*), the last phase of decay driven by infected cell loss is predicted to be observed.

If high clearance rate estimates are indicative of drug therapies that block viral assembly/secretion, one may ask whether other direct-acting antiviral agents also have this property. Interestingly, for the protease inhibitor TVR, using the standard model, a mean $c = 12.1\ d^{-1}$ was reported for all TVR doses and $c = 16.7\ d^{-1}$ for nine patients from our recent publication (16) treated with the highest dosage of 1,250 mg twice daily (BID), values two- to threefold greater than for IFN, with no explanation. To test whether this might be the result of TVR having an effect on virion assembly/secretion, we added the nine patients treated with 1,250 mg BID TVR monotherapy as an additional group in our population analysis. All data could be well fit with the multiscale model (Fig. S3), and a high value of $c = 22.7\ d^{-1}$ was found (Table S2). TVR also was found to have an effect in blocking assembly/secretion (mean $\varepsilon_s = 0.94$); however, this effect was significantly weaker than for daclatasvir ($P < 10^{-6}$). Comparing $(1 - \varepsilon_s)$ for TVR (0.06) with that of daclatasvir (0.002) reveals that daclatasvir reduces assembly/secretion 30-fold more than TVR. Our prediction that TVR has an effect on assembly/secretion in vivo is consistent with in vitro findings (17) that the NS3 protease domain is important in late steps in the viral lifecycle that involve intracellular assembly of virus.

Whereas the multiscale model prediction that daclatasvir inhibits both HCV replication and HCV assembly/secretion in vivo is consistent with published data indicating that NS5A plays a role in both these viral processes (4–11), we confirmed these effects in cell culture HCV infection experiments in which both intracellular and extracellular viral parameters can be measured in parallel (*SI Methods*). Specifically, we found that treatment of infected cells with daclatasvir resulted in an intracellular HCV

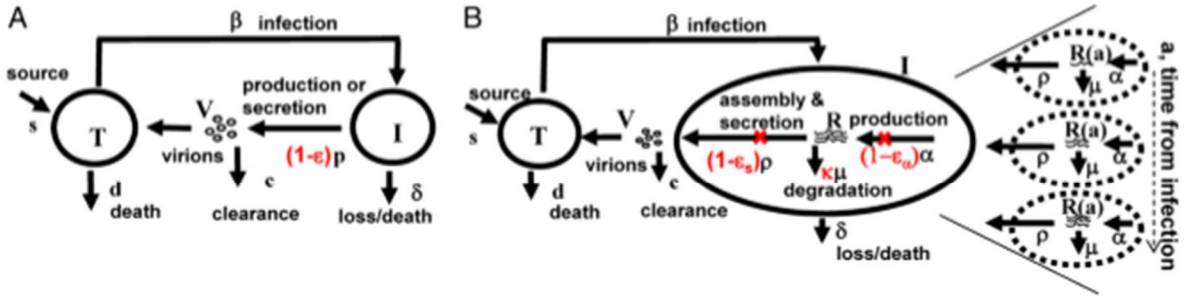

Fig. 2. Standard and multiscale models of HCV infection. (*A*) The standard model (12) considers only the level of cell infection and virus in serum. Treatment acts by reducing the average number of virions produced by infected cells from p to $p(1 - \varepsilon)$. Thus, ε represents a global measure of antiviral effectiveness that does not distinguish the stages of intracellular viral replication that are blocked by treatment. (*B*) The multiscale model was designed to account for essential features of intracellular HCV RNA (vRNA) replication, R, i.e., production, degradation, and assembly/secretion with rate parameters α, μ, and ρ, respectively. The vRNA level within an infected cell (dashed circle) is assumed to increase with time since infection and reach a steady state. Treatment (parameters in red) may block vRNA production with effectiveness ε_α and/or virion assembly/secretion with effectiveness ε_s, and/or enhance the degradation rate of vRNA by a factor κ. In both models, T and I represent target and infected cells, respectively, and V represents virus. Target cells are created and die with constant rates s and d, respectively, and are infected by virus, V, with rate constant β. Infected cells, I, are lost with rate constant δ, and virus, V, is cleared from serum with rate constant c.

Table 2. Population parameter estimates obtained using the approximate solution (Eq. 3) of the multiscale model

Parameter	Estimate	Standard Error
ε_α		
IFN		
5 MIU	0.77	0.087
10/15 MIU*	0.96	0.011
Daclatasvir	0.99	0.011
ε_s		
IFN, 5/10/15 MIU†	0.39	0.018
Daclatasvir	0.998	0.00017
t_0 (h)		
IFN, 5/10/15 MIU†	10.0	2.88
Daclatasvir	0.97	0.38
ρ (d^{-1})	8.18	1.8
c (d^{-1})	22.3	1.7
$\kappa\mu$ (d^{-1})	1.46	0.36

c, serum HCV RNA clearance rate; ε_α, drug effectiveness in blocking intracellular HCV RNA (vRNA) synthesis; ε_s, drug effectiveness in blocking virion assembly/secretion; $\kappa\mu$, degradation rate of vRNA during treatment; ρ, export rate of vRNA into virions; t_0, pharmcological delay.

*The patients treated with 10- and 15-MIU doses of IFN were analyzed together because previous analysis (12) showed no difference in effectiveness.

†t_0 and ε_s were found not to differ among the IFN dosing groups.

RNA decline comparable with that observed when infected cells were treated with the polymerase inhibitor NM107, consistent with both drugs blocking HCV replication (Fig. 4). As expected, for a replication inhibitor, extracellular virus titers in NM107-treated cultures declined in parallel with intracellular RNA levels. However, daclatasvir treatment resulted in an immediate and more rapid decrease in extracellular HCV titers that preceded the drop in intracellular HCV RNA, consistent with some aspect of HCV assembly/secretion being inhibited independently of the effects on HCV replication.

Discussion

NS5A is an HCV-encoded nonstructural protein that has become a promising target for anti-HCV therapy (3, 18). In a phase IIa study, 4 of 11 patients who received the NS5A inhibitor daclatasvir and the protease inhibitor asunaprevir for 24 wk had a sustained virologic response at 12 and 24 wk after treatment ended, establishing that HCV may be cured by an all-oral treatment regime that lacks IFN/RBV (18).

NS5A is a phosphoprotein that may exist in multiple phosphorylated states (11, 19). Possibly because of this, it appears to have multiple functions in the virus lifecycle, likely mediated by its ability to bind HCV RNA (20) and to interact with several virus and host proteins (21). Given the uncertain nature of the molecular mechanisms by which NS5A functions and the absence of direct screening assays for NS5A function, it is not surprising that the MOA of NS5A inhibitors is uncertain (22). One means of uncovering an antiviral agent's MOA is to analyze the kinetics of the response it generates.

Here, we have shown that after in vivo administration of the NS5A inhibitor daclatasvir, HCV RNA declines with extreme rapidity, falling appoximately 2 logs within the first 6 h post dosing, followed by a slower phase of decline. Using a multiscale model, we have shown that this kinetic pattern would arise if and only if daclatasvir effectively blocks both intracellular viral HCV RNA (vRNA) synthesis and virion assembly/secretion in vivo. If daclatasvir blocked only vRNA synthesis, the kinetics of viral decline would be similar to that seen with IFN and the first phase would not be as rapid as observed (Fig. S4). Alternatively, if daclatasvir blocked only virion assembly/secretion, then one would see only a rapid first phase followed by a flat second phase, differing from the second phase that was observed, and which cannot fit the data (Fig. S5). It is only when we assume that daclatasvir blocks both vRNA synthesis and virion assembly/secretion that we match the data (Fig. 1). Although this finding is consistent with a large body of data obtained in vitro showing that NS5A is essential for both viral replication (4–7) and the assembly and release of infectious particles (8–11), we confirmed the modeling predictions by assessing the effect of daclatasvir on HCV infection in vitro, where both intracellular and extracellular HCV can be measured simultaneously (Fig. 4). Although daclatasvir treatment reduced intracellular HCV RNA with the same kinetics as the HCV polymerase inhibitor NM107—suggesting that at the doses used, both drugs block HCV replication to a similar degree—a more rapid extracellular decline in HCV was observed in response to daclatasvir, consistent with an additional block in assembly/secretion of infectious viral particles. In addition, an early transient increase in intracellular HCV RNA levels was observed in multiple experiments. Although this increase was not statistically significant, it suggests that blocking assembly/secretion may result in a transient accumulation of intracellular HCV RNA.

If daclatasvir blocks virion assembly/secretion, the viral decline after dosing should provide a more precise estimate of the HCV $t_{1/2}$ than the one observed with other anti-HCV compounds. Indeed, when virus secretion is not blocked efficiently, there is a continued release of new virus particles; thus, the observed rate of decay after treatment initiation provides only a minimal estimate of the true virion half-life. We now estimate, both from fitting our model to the data and by empirically measuring the rate

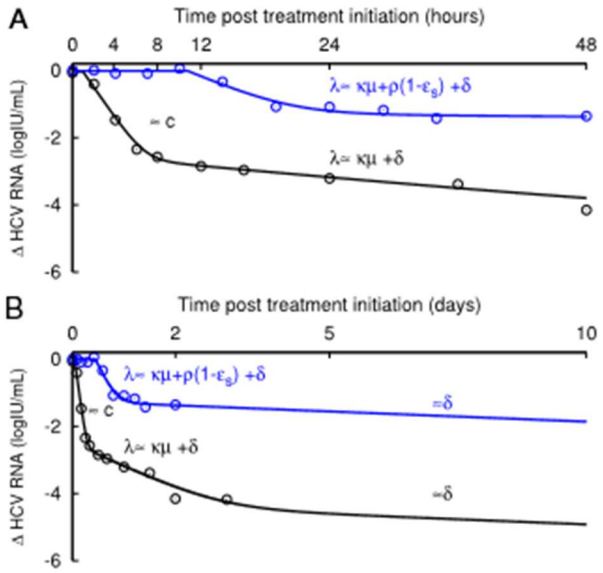

Fig. 3. Patterns of viral decline predicted by the multiscale model. Viral load decline from baseline in a patient treated with daclatasvir (Pt 8, black ○) compared with the decline seen in a patient treated with 10 MIU IFN (Pt 2C, blue ○) at early (*A*) and late (*B*) times, and the corresponding best-fit model prediction (solid lines) using the multiscale model (Eq. 3 and Table S3). When treatment efficiently blocks both vRNA production, with effectiveness ε_α, and virion assembly/secretion, with effectiveness ε_s, as estimated for daclatasvir (Table 2), the multiscale model predicts two phases of viral decline in the first 2 d of treatment (*A*, black line). The first phase is the result of HCV clearance in serum, with rate c. The second phase reflects vRNA decline with rate $\lambda = \kappa\mu + \rho(1 - \varepsilon_s) + \delta \sim \kappa\mu + \delta$, as $\varepsilon_s \sim 1$ (Table S3). When treatment does not efficiently block virion assembly/secretion, as predicted with IFN (Table 2), the first early phase is not visible and only the second early phase of viral decline is observed (*A*, blue line). After day 3, assuming that the treatment is effective in blocking vRNA production and regardless of the effectiveness in blocking secretion, the long-term viral decline is driven by the loss rate of infected cells, with rate δ (*B*).

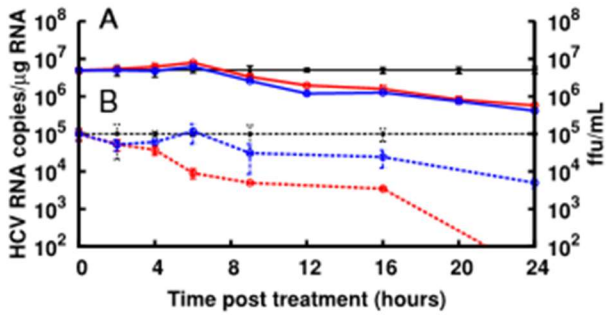

Fig. 4. Intracellular and extracellular HCV kinetics during treatment in cell culture. (*A*) RTqPCR analysis of intracellular HCV RNA levels in Huh7 cultures at the indicated times during mock treatment (black), 1 nM daclatasvir treatment (red), or treatment with 25 μM of the HCV NS5B polymerase inhibitor NM107 (blue). A delay of 6–9 h before HCV RNA declined from mock was observed with daclatasvir and NM107. Thereafter, intracellular HCV RNA declined at a similar rate with both daclatasvir and NM107. (*B*) Extracellular HCV titer (focus-forming units per milliliter) determined at the indicated times during treatment with 1 nM daclatasvir (red dashed line) or 25 μM NM107 (blue dashed line) compared with mock-treated cultures (black dashed line). Under NM107 treatment, HCV titer declined at the same rate as intracellular HCV RNA, whereas daclatasvir treatment resulted in a rapid and immediate decline in HCV titer. Data are representative of three independent experiments.

of HCV decline, that the HCV $t_{½}$ is ~45 min, i.e., around four times shorter than the previous estimate of 2.7 h. This implies that to maintain viral levels at steady state, viral production must be four times larger than previously estimated (12); hence, there is more opportunity for viral mutation than previously appreciated. Lastly, our $t_{½}$ estimate for HCV is similar to the estimated 56-min $t_{½}$ of HIV (23) and may imply that both viruses are cleared by similar mechanisms.

An off-target effect of daclatasvir in enhancing HCV clearance also might account for our estimate of the HCV half-life. However, if daclatasvir's only MOA was to enhance viral clearance by fourfold, then HCV RNA would rapidly decline fourfold, i.e., 0.6 $\log_{10}$ during therapy (Fig. S6) and not the 2–3 logs observed. To obtain the observed kinetics, daclatasvir still would also need to block virion assembly/secretion and vRNA replication. Also, a similar 45-min estimate of the virion half-life was made by Powers et al. (24), in the absence of daclatasvir, by analyzing the kinetics of viral decline in six patients during the anhepatic and early reperfusion stages after liver transplantation, when no or little new virus is being made.

Interestingly, Ramratnam et al. (23), using large-volume apheresis to artificially increase virion clearance, estimated the HCV $t_{½}$ in two HCV/HIV-coinfected patients as 1.67 h and 3 h, which suggests that if our current estimate of a 45-min $t_{½}$ is accurate, HCV clearance might be impaired in coinfected patients.

Although the viral decline observed during the first 2 d post dosing was biphasic, the second-phase viral decline with daclatasvir is not the persistent second-phase viral decline predicted by the standard biphasic model but rather represents a transient phase that mainly reflects the drug's ability to reduce vRNA levels by blocking vRNA production and/or by increasing its degradation rate by a factor κ. Although the magnitude of κ could not be estimated, the model predicts that the vRNA $t_{½}$ during daclatasvir therapy $[\ln(2)/\kappa\mu]$ in vivo is about 11 h. Recently, we showed that in replicon cells treated with NM107, the $t_{½}$ of genotype 1b subgenomic HCV RNA was 17 h (25). A similar estimate was found in replicon cells treated with 100 U/mL of IFN in one study (26) but was 12 h in another study (27). The fact that the in vitro and in vivo estimates of $t_{½}$ differ by a factor of 1.1–1.5 suggests that the effect of daclatasvir on enhancing vRNA degradation, if existent, likely is modest.

The multiscale model shows that the first phase of viral decline reflecting HCV serum clearance is visible only if a drug efficiently blocks viral secretion. We have shown for IFN that the first phase should not be apparent in clinical data, and what we previously thought was the first phase may in fact be the new intermediate phase we identified in the daclatasvir data analysis. This is the explanation for why earlier analyses of viral decay in patients treated with IFN led to inaccurate estimates of the viral clearance rate. For TVR, in which we predict the drug inhibits assembly/secretion, a similar analysis shows that a short first phase with $c = 22.7\ d^{-1}$ should be apparent before transitioning into the new immediate phase.

The multiscale model most likely is valid only for short periods after the initiation of antiviral therapy. Its use for longer periods probably will require one to include the possibility that under potent therapy, the rates of vRNA production, $\alpha(1-\varepsilon_\alpha)$, and degradation, κμ, are not constant. One can easily imagine that under potent therapy, the replication complexes, which are responsible for vRNA production, will decrease in number, effectively lowering α. Also, vRNA in different cellular compartments, e.g., cytoplasm and membranous web (28), may degrade at different rates; thus, once vRNA in one compartment is mostly depleted, the vRNA degradation rate, κμ, may change. Lastly, our model solution assumes that the drug effectivenesses, ε_α, ε_α, and κ, are all constant. Thus, Eq. **3** would need to be modified in cases in which drug effectivenesses change with time, such as for the HCV polymerase inhibitor mericitabine (29).

In summary, we have developed a multiscale model of HCV infection and treatment in vivo that includes both intracellular and serum HCV RNA dynamics. The model provides a conceptual framework to explain the observed decline of serum HCV during therapy. Because the model considers several different steps in the HCV lifecyle, it provides a promising tool for selecting agents with complementary modes of action to maximize cure rates. When applied to the HCV kinetics observed in patients during daily IFN therapy, during protease inhibitor therapy, or after a single dose of daclatasvir, several insights into the mechanisms of action of these drugs were obtained. In particular, the multiscale model confirms that IFN mainly slows intracellular HCV RNA replication/synthesis, but suggests it also may have a small effect on virion assembly/secretion. Thus, it is plausible that during the first phase of viral decline, there is continued packing and release of the vRNA that was present in the cell before IFN administration, which masks the intrinsic plasma HCV clearance rate. Further, our results suggest that both daclatasvir and TVR block virion assembly/secretion, with mean effectivenesses in vivo equal to 99.8% and 94%, respectively (Table S2), with TVR being significantly less effective ($P < 10^{-6}$). Lastly, we now estimate the mean half-life of HCV RNA in serum to be about 45 min. This estimate is around four times shorter than previous estimates made by modeling the HCV RNA decline following initiation of IFN-based therapy (12, 13) but is consistent with some estimates of viral decline rates observed during the anhepatic and early reperfusion phases in subjects who underwent liver transplantation (24, 30).

Methods

Standard model of viral dynamics. The standard model of HCV dynamics predicts that viral decline is governed by the following set of differential equations:

$$\frac{dT}{dt} = s - dT - \beta VT,\quad \frac{dI}{dt} = \beta VT - \delta I,\quad \frac{dV}{dt} = (1-\varepsilon)pI - cV, \qquad [1]$$

where T represents the density of target cells, which are created with constant rate s, die with constant rate d, and are infected by virus, V, with rate constant β. In the model, infected cells, I, are lost with rate constant δ and produce virions at constant rate p per cell (Fig. 2*A*). Virions are assumed to be cleared from serum with rate constant c. Because we focus on short-term kinetics, we assumed that the target cell level is constant throughout the study period and remains at its pretreatment steady-state value $T_0 = c\delta/p\beta$ (12). After an initial pharmacologic delay of length t_0, therapy is assumed to reduce the rate of viral production per cell from p to $p(1-\varepsilon)$, where ε is the drug effectiveness.

Multiscale model of viral dynamics. We denote by $R(a)$ the concentration of intracellular vRNA in a cell that has been infected for time a. In the absence

of treatment, $R(a)$ may be described by $dR/da = \alpha - \mu R - \rho R$, where α represents the rate of vRNA production, μ is the (intracellular) rate of vRNA degradation, and ρ is the export rate of vRNA in virions. Treatment may act by blocking intracellular viral production with effectiveness ε_α, by blocking virion assembly and/or secretion with effectiveness ε_s, and by increasing the degradation rate of vRNA by a factor κ, so that the full model combining intracellular and extracellular dynamics is

$$\frac{dT}{dt} = s - dT - \beta VT, \quad \frac{\partial I}{\partial a} + \frac{\partial I}{\partial t} = -\delta I(a,t)$$

$$\frac{\partial R}{\partial a} + \frac{\partial R}{\partial t} = (1-\varepsilon_\alpha)\alpha - \kappa\mu R - (1-\varepsilon_s)\rho R \qquad [2]$$

$$\frac{dV}{dt} = (1-\varepsilon_s)\rho \int_0^\infty R(a,t)I(a,t)da - cV$$

with boundary conditions $I(0,t) = \beta VT$, $I(a,0) = I_0(a)$, $R(0,t) = 1$, $R(a,0) = R_0(a)$, where $I_0(a)$ and $R_0(a)$ are the pretherapy steady-state distributions. We have assumed that treatment begins at time $t = 0$ and that cells, when initially infected, contain one vRNA.

Because the amount of intracellular vRNA depends on both the length of time a cell has been infected and the length of treatment, a partial differential equation is needed to describe intracellular vRNA kinetics. We previously showed that a drug blocking entry leads to very slow viral decays and when included with effects such as blocking replication that give rise to rapid declines, this effect cannot be discerned (12). Thus, we have not included a potential effect of daclatasvir on reducing β and, hence, cannot determine whether daclatasvir also has an effect on viral entry.

Fig. 2*B* gives a schematic representation of this model. If one assumes that treatment is potent enough that the number of new cell infections is negligible after treatment initiation, i.e., $I(a,t) = 0$ for $a < t$, this model can be solved using the method of characteristics, yielding

$$V(t) = V_0\left\{e^{-c(t-t_0)} + \frac{\bar{\rho}c}{N}\left[\frac{\bar{\alpha}}{\bar{\lambda}\delta(\delta-c)}\left(e^{-c(t-t_0)} - e^{-\delta(t-t_0)}\right) + \frac{1}{\bar{\lambda}+\delta-c}\left(\frac{N}{\rho} - \frac{\bar{\alpha}}{\bar{\lambda}\delta}\right)\left(e^{-c(t-t_0)} - e^{-(\bar{\lambda}+\delta)(t-t_0)}\right)\right]\right\}, \qquad [3]$$

where we have incorporated a pharmacologic delay of length t_0 before the viral load decline begins, $\bar{\alpha} = \alpha(1-\varepsilon_\alpha)$, $\bar{\rho} = \rho(1-\varepsilon_s)$, $\bar{\lambda} = \bar{\rho} + \kappa\mu$, and $N = \rho\frac{\alpha+\delta}{\delta(\rho+\mu+\delta)}$.

Data. ***IFN-α2b treatment in vivo.*** To compare the kinetics observed with daclatasvir to that observed with IFN-based therapy, we considered 24 treatment-naïve patients infected with HCV genotype 1 randomly assigned to receive daily s.c. injections of 5, 10, or 15 MIU) of IFN-α2b (12). As done in ref. 12, the four nonresponder patients were not included in this analysis.
Daclatasvir (BMS-790052) treatment in vivo. In a double-blind single ascending-dose study, three groups of six subjects were randomly assigned to receive one dose of 1, 10, or 100 mg of daclatasvir or placebo in a ratio of 5:1 (Fig. S1). As 1 mg was suboptimal, we did not include it in our study. One subject in the 10-mg group withdrew from the study 8 h after administration of the study drug and was not included in our analysis. After drug levels dropped to a low level, viral rebounds were observed (Fig. S1). To avoid bias in the parameter estimation due to these rebounds, we constrained our viral kinetic analysis to the five patients (one given 10 mg and four given 100 mg of daclatasvir) who did not show a viral rebound throughout the 3 d post dosing (Fig. S1 and Table S3).
Daclatasvir (BMS-790052) treatment in vitro. Cell culture experiments used Huh7-1 cells and cell culture–propagated HCV (HCVcc) from the JFH-1 HCV consensus clone provided by Takaji Wakita (National Institute of Infectious Diseases, Tokyo, Japan), as described in detail in *SI Methods*. For HCV infection experiments, Huh7 cultures were inoculated with HCVcc and cultured for an additional 10 d to allow HCV infection to reach steady state. Parallel cultures of steady-state HCV-infected cells were then mock treated or treated with 25 μM NM107 or 1 nM daclatasvir. At indicated times, medium was harvested from eight replicate wells for titer analysis and cellular RNA isolated lysate was harvested in 200 μL 1× nucleic acid purification lysis solution (Applied Biosystems) from four replicate wells for real-time quantitative PCR (RTqPCR) analysis for HCV RNA and cellular GAPDH mRNA, as described in detail in *SI Methods*.

ACKNOWLEDGMENTS. Portions of this work were performed under the auspices of the US Department of Energy under Contract DE-AC52-06NA25396 and supported by National Institutes of Health Grants R56/R01-AI078881-, P20-GM103452, OD011095, and AI028433; the National Science Foundation under Grants NSF PHY11-25915 and DMS 1122290; and the University of Illinois Walter Payton Liver Center Guild.

1. World Health Organization (July 2012) Hepatitis C. Fact sheet no.164. Available at http://who.int/mediacentre/factsheets/fs164/en/.
2. Armstrong GL, et al. (2006) The prevalence of hepatitis C virus infection in the United States, 1999 through 2002. *Ann Intern Med* 144(10):705–714.
3. Gao M, et al. (2010) Chemical genetics strategy identifies an HCV NS5A inhibitor with a potent clinical effect. *Nature* 465(7294):96–100.
4. Blight KJ, Kolykhalov AA, Rice CM (2000) Efficient initiation of HCV RNA replication in cell culture. *Science* 290(5498):1972–1974.
5. Lohmann V, Hoffmann S, Herian U, Penin F, Bartenschlager R (2003) Viral and cellular determinants of hepatitis C virus RNA replication in cell culture. *J Virol* 77(5): 3007–3019.
6. Lohmann V, et al. (1999) Replication of subgenomic hepatitis C virus RNAs in a hepatoma cell line. *Science* 285(5424):110–113.
7. Tellinghuisen TL, Foss KL, Treadaway JC, Rice CM (2008) Identification of residues required for RNA replication in domains II and III of the hepatitis C virus NS5A protein. *J Virol* 82(3):1073–1083.
8. Appel N, et al. (2008) Essential role of domain III of nonstructural protein 5A for hepatitis C virus infectious particle assembly. *PLoS Pathog* 4(3):e1000035.
9. Hughes M, Griffin S, Harris M (2009) Domain III of NS5A contributes to both RNA replication and assembly of hepatitis C virus particles. *J Gen Virol* 90(Pt 6):1329–1334.
10. Masaki T, et al. (2008) Interaction of hepatitis C virus nonstructural protein 5A with core protein is critical for the production of infectious virus particles. *J Virol* 82(16): 7964–7976.
11. Tellinghuisen TL, Foss KL, Treadaway J (2008) Regulation of hepatitis C virion production via phosphorylation of the NS5A protein. *PLoS Pathog* 4(3):e1000032.
12. Neumann AU, et al. (1998) Hepatitis C viral dynamics in vivo and the antiviral efficacy of interferon-alpha therapy. *Science* 282(5386):103–107.
13. Snoeck E, et al. (2010) A comprehensive hepatitis C viral kinetic model explaining cure. *Clin Pharmacol Ther* 87(6):706–713.
14. Adiwijaya BS, et al. (2009) Rapid decrease of wild-type hepatitis C virus on telaprevir treatment. *Antivir Ther* 14(4):591–595.
15. Quinkert D, Bartenschlager R, Lohmann V (2005) Quantitative analysis of the hepatitis C virus replication complex. *J Virol* 79(21):13594–13605.
16. Guedj J, Perelson AS (2011) Second-phase hepatitis C virus RNA decline during telaprevir-based therapy increases with drug effectiveness: Implications for treatment duration. *Hepatology* 53(6):1801–1808.
17. Shimakami T, et al. (2011) Protease inhibitor-resistant hepatitis C virus mutants with reduced fitness from impaired production of infectious virus. *Gastroenterology* 140(2):667–675.
18. Lok AS, et al. (2012) Preliminary study of two antiviral agents for hepatitis C genotype 1. *N Engl J Med* 366(3):216–224.
19. Huang Y, Staschke K, De Francesco R, Tan SL (2007) Phosphorylation of hepatitis C virus NS5A nonstructural protein: A new paradigm for phosphorylation-dependent viral RNA replication? *Virology* 364(1):1–9.
20. Foster TL, Belyaeva T, Stonehouse NJ, Pearson AR, Harris M (2010) All three domains of the hepatitis C virus nonstructural NS5A protein contribute to RNA binding. *J Virol* 84(18):9267–9277.
21. Macdonald A, Harris M (2004) Hepatitis C virus NS5A: Tales of a promiscuous protein. *J Gen Virol* 85(Pt 9):2485–2502.
22. Targett-Adams P, et al. (2011) Small molecules targeting hepatitis C virus-encoded NS5A cause subcellular redistribution of their target: insights into compound modes of action. *J Virol* 85(13):6353–6368.
23. Ramratnam B, et al. (1999) Rapid production and clearance of HIV-1 and hepatitis C virus assessed by large volume plasma apheresis. *Lancet* 354(9192):1782–1785.
24. Powers KA, et al. (2006) Kinetics of hepatitis C virus reinfection after liver transplantation. *Liver Transpl* 12(2):207–216.
25. Dahari H, Barretto N, Sansone N, Guedj J, Perelson AS, Uprichard SL (2011) Modeling inhibition kinetics of HCV SG1B RNA during IFN/DAAS treatment in non-growing Huh7 cells. *Hepatology* 54(Suppl S1):538A, (abstr).
26. Dahari H, Sainz B, Jr., Perelson AS, Uprichard SL (2009) Modeling subgenomic hepatitis C virus RNA kinetics during treatment with alpha interferon. *J Virol* 83(13):6383–6390.
27. Guo JT, Bichko VV, Seeger C (2001) Effect of alpha interferon on the hepatitis C virus replicon. *J Virol* 75(18):8516–8523.
28. Egger D, et al. (2002) Expression of hepatitis C virus proteins induces distinct membrane alterations including a candidate viral replication complex. *J Virol* 76(12): 5974–5984.
29. Guedj J, Dahari H, Shudo E, Smith P, Perelson AS (2012) Hepatitis C viral kinetics with the nucleoside polymerase inhibitor mericitabine (RG7128). *Hepatology* 55(4): 1030–1037.
30. Dahari H, Feliu A, Garcia-Retortillo M, Forns X, Neumann AU (2005) Second hepatitis C replication compartment indicated by viral dynamics during liver transplantation. *J Hepatol* 42(4):491–498.

APPENDIX A (CONTINUED)

Supporting Information

Guedj et al. 10.1073/pnas.1203110110

SI Methods

Data Fitting and Statistical Methods. Patient viral load data were fit using nonlinear mixed-effect models, which borrow strength from the whole sample to estimate more precisely the population parameters, such as the mean, and the interindividual variation (IIV) (1). In this approach, each parameter θ_i comprises a fixed part θ, which represents the median value of the parameter in the population, and a random part η_i chosen from a Gaussian distribution with mean 0 and SD equal to IIV that accounts for the IIV. Parameters are log-transformed to ensure positivity, and we write $\theta_i = \theta \cdot e^{\eta_i}$. We used a logistic transformation of the ε_j's ($j = s, \alpha$) to ensure that the antiviral treatment effectiveness is between 0 and 1, and we write $\varepsilon_{ji} = \frac{\varepsilon_j}{\varepsilon_j + (1-\varepsilon_j)e^{\eta_i}}$.

Data were analyzed using MONOLIX (www.lixoft.com), a software devoted to maximum likelihood estimation of parameters in nonlinear mixed-effect models (2). After the population parameters were found, the values of the parameters for individual patients were deduced using empirical Bayes estimates (3).

Cells and Virus. Huh7-1 cells were described previously (4). Cells were passaged in complete DMEM (HyClone) supplemented with 10% (vol/vol) FBS (HyClone), 100 U/mL penicillin, 100 mg/mL streptomycin, and 2 mM L-glutamine (Gibco Invitrogen). JFH-1 cell culture–propagated HCV (HCVcc) viral stocks were obtained by infection of naïve Huh7-1 cells at a multiplicity of infection (MOI) of 0.01 focus-forming units (FFU) per cell, using medium from Huh7-1 cells electroporated with in vitro–transcribed full-length infectious HCV JFH-1 RNA generated from pJFH-1 provided by Takaji Wakita (National Institute of Infectious Diseases, Tokyo, Japan) as described previously (5).

HCVcc Inhibition Experiments. Huh7 cells were seeded in 96-well BioCoat culture plates at a density of 8×10^3 cells per well in complete DMEM (cDMEM). Upon reaching 90–95% confluence, medium was replaced with 200 μL cDMEM supplemented with 1% DMSO (Sigma), and cells were cultured for an additional 20 d, replacing medium every 2 d. These cultures are referred to as DMSO-Huh7 cells and were described and characterized previously (5–7). For HCV infection experiments, DMSO-Huh7 cultures were inoculated with HCVcc JFH-1 at an MOI of 0.05 FFU per cell and cultured for an additional 10 d to allow HCV levels to reach steady state. Parallel cultures of steady-state HCV-infected cells were then either mock treated or treated with 25 μM NM107 or 1 nM daclatasvir. At indicated times, medium was harvested from eight replicate wells for titer analysis and cell lysate was harvested in 200 μL 1× Nucleic Acid Purification Lysis Solution (Applied Biosystems) from four replicate wells for isolation of RNA. Real-time quantitative PCR (RTqPCR) analysis for HCV RNA and cellular GAPDH mRNA was performed as described below.

RNA Isolation and RTqPCR Analysis. Total cellular RNA was purified using an ABI PRISM 6100 Nucleic Acid Prep Station (Applied Biosystems) according to the manufacturer's instructions. Reverse transcription and RTqPCR were performed using TaqMan reverse transcription reagents (Applied Biosystems) and FastStart Universal SYBR Green Master mix (Roche), respectively, and using the following primers: universal HCV primers (8) 5′-GCC TAG CCA TGG CGT TAG TA -3′ (sense) and 5′-CTC CCG GGG CACTCG CAA GC-3′ (antisense) and human GAPDH (9) 5′-GAA GGT GAA GGT CGG AGT C-3′ (sense) and 5′-GAA GAT GGT GAT GGG ATT TC-3′ (antisense). HCV RNA copies were determined relative to a standard curve composed of serial dilutions of a plasmid containing the JFH-1 HCV cDNA (pJFH-1).

Extracellular Infectivity Titration Assay. Cell supernatants were serially diluted 10-fold in cDMEM, and 200 μL per well was used to infect quadruplicate Huh7 cultures in 96-well plates (BD Biosciences). Because NM107- and daclatasvir-treated samples contained potentially inhibitory drugs, the same concentration of each drug was added to two of the four mock-treated samples before serial dilution. The drug-containing virus/medium sample was then removed at 8 h post inoculation, cells were washed so that the titer assay could proceed in the absence of the antiviral compounds, and monolayers were overlaid with DMEM containing 0.25% methylcellulose (wt/vol) (Fluka BioChemika). As a control to monitor for possible inhibitor effects of the compounds, representative mock samples also were titered in the absence of any drug addition. At 72 h post inoculation, medium was removed, cells were fixed with 4% paraformaldehyde (Sigma), and immunohistochemical staining for HCV E2 was performed as described previously (10). Viral infectivity titers are expressed as FFU per milliliter of supernatant, determined by the average number of E2-positive foci detected in quadruplicate samples at the highest HCV-positive dilution.

1. Guedj J, Thiébaut R, Commenges D (2007) Maximum likelihood estimation in dynamical models of HIV. *Biometrics* 63(4):1198–1206.
2. Kuhn E, Lavielle M (2005) Maximum likelihood estimation in nonlinear mixed effects models. *Comput Stat Data Anal* 49(4):1020–1038.
3. Pinheiro J, Bates D (2000) *Mixed-Effects Models in S and S-PLUS* (Springer, New York).
4. Sainz B, Jr., Barretto N, Uprichard SL (2009) Hepatitis C virus infection in phenotypically distinct Huh7 cell lines. *PLoS ONE* 4(8):e6561.
5. Yu X, Uprichard SL (2010) Cell-based hepatitis C virus infection fluorescence resonance energy transfer (FRET) assay for antiviral compound screening. *Curr Protoc Microbiol*, Chapter 17:Unit 17.15.
6. Sainz B, Jr., Chisari FV (2006) Production of infectious hepatitis C virus by well-differentiated, growth-arrested human hepatoma-derived cells. *J Virol* 80(20):10253–10257.
7. Choi S, Sainz B, Jr., Corcoran P, Uprichard SL, Jeong H (2009) Characterization of increased drug metabolism activity in dimethyl sulfoxide (DMSO)-treated Huh7 hepatoma cells. *Xenobiotica* 39(3):205–217.
8. Komurian-Pradel F, et al. (2004) Strand specific quantitative real-time PCR to study replication of hepatitis C virus genome. *J Virol Methods* 116(1):103–106.
9. Zhong J, et al. (2005) Robust hepatitis C virus infection in vitro. *Proc Natl Acad Sci USA* 102(26):9294–9299.
10. Yu X, Sainz B, Jr., Uprichard SL (2009) Development of a cell-based hepatitis C virus infection fluorescent resonance energy transfer assay for high-throughput antiviral compound screening. *Antimicrob Agents Chemother* 53(10):4311–4319.

APPENDIX A (CONTINUED)

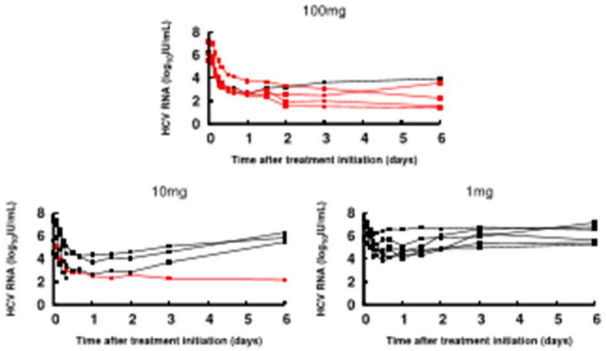

Fig. S1. Observed changes in viral load after one dose of daclatasvir, according to the dose. Patients in red are those selected for the final analysis.

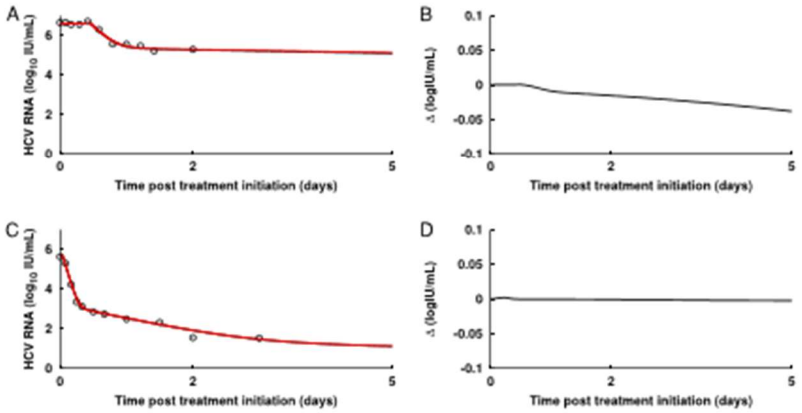

Fig. S2. The approximate solution (Eq. 3 in the main text, black line) and the numerical solution of the model (Eq. 2 in the main text, red line) for two representative patients treated with IFN (Pt 2C, *A*) or daclatasvir (Pt 8, *C*) overlap and are indistinguishable. The difference Δ between the two solutions is very small (*B*, *D*), particularly for the patient treated with daclatasvir (*D*), for whom the effectiveness was very high.

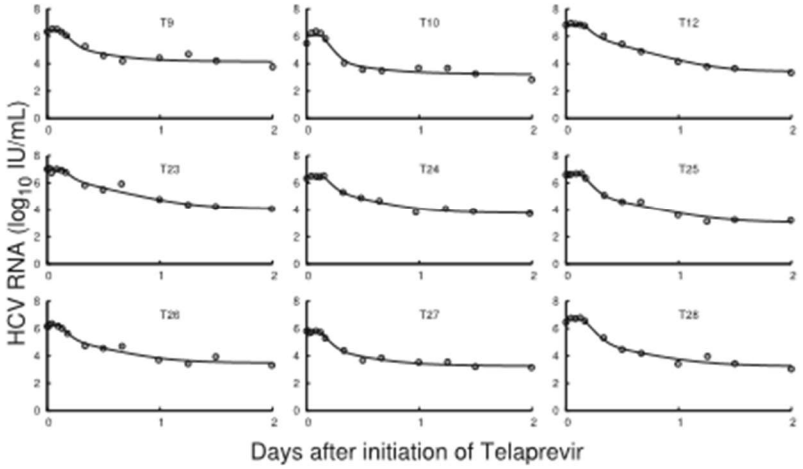

Fig. S3. Best-fit of the multiscale model (solid line) to the data (○) from the nine patients treated with telaprevir, 1,250 mg twice daily.

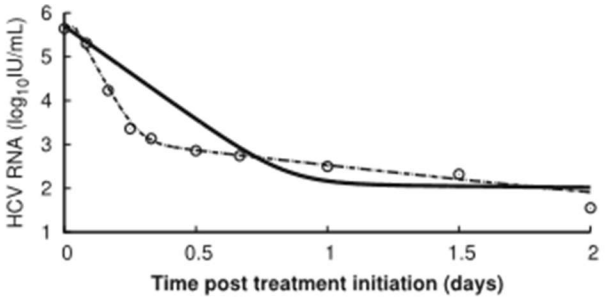

Fig. S4. Viral load decline in a patient treated with daclatasvir (Pt 8, ○) and the corresponding best-fit model prediction (solid line) using the multiscale model (Eq. 3), asssuming daclatasvir blocks only viral RNA (vRNA) replication and has no effect on virion assembly/secretion (i.e., $\varepsilon_s = 0$). Estimated parameters are $V_0 = 5.64$ $\log_{10}$ IU/mL, $t_0 = 0$, $c = 200$ d^{-1}, and $\varepsilon_\alpha = 0.99989$. Other parameters are fixed to values given in Table 2. Dashed line is the best-fit prediction assuming daclatasvir blocks both vRNA replication and assembly/secretion (parameters are given in Table S3).

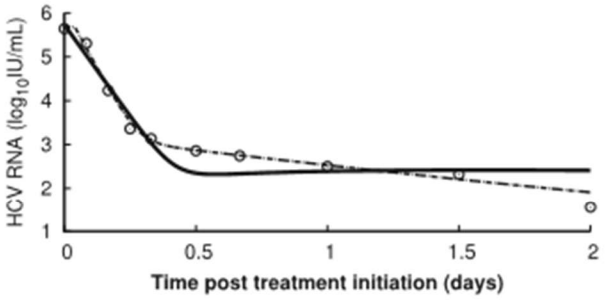

Fig. S5. Viral load decline in a patient treated with daclatasvir (Pt 8, ○) and the corresponding best-fit model prediction using the multiscale model, asssuming daclatasvir blocks only viral assembly/secretion and has no effect on vRNA replication (i.e., $\varepsilon_\alpha = 0$). Estimated parameters are $V_0 = 5.64$ $\log_{10}$ IU/mL, $t_0 = 0$, $c = 19$ d^{-1}, and $\varepsilon_s = 0.99997$. Other parameters are fixed to values given in Table 2. Dashed line is the best-fit prediction assuming daclatasvir blocks both vRNA replication and assembly/secretion (parameters are given in Table S3).

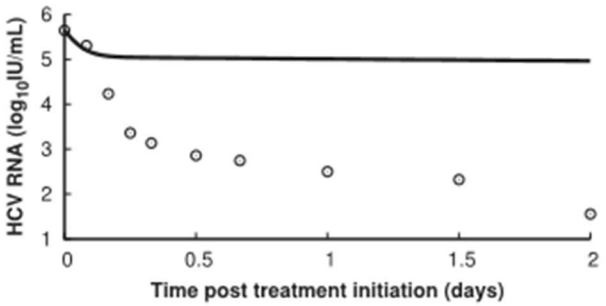

Fig. S6. Multiscale model prediction (solid line) assuming that daclatasvir increases only the virion clearance rate, c, fourfold. Parameters are as given in Table 2, except $\varepsilon_\alpha = 0$, $\varepsilon_s = 0$, and c is increased from 5.625 d^{-1} to 22.5 d^{-1}, i.e., fourfold at $t = 0$. Note that increasing the clearance rate alone does not lead to predictions consistent with patient data (Pt 8, ○).

Table S1. Population parameter estimates for patients treated with daclatasvir for different values of α and δ

	α															
	10				20				40				100			
δ	κμ	c	ε_s	ε_α	κμ	c	ε_s	ε_α	κμ	c	ε_s	ε_α	κμ	c	ε_s	ε_α
0.01	1.63	22.3	0.998	0.99	1.6	22.3	0.998	0.991	1.52	22.2	0.998	0.992	1.56	22.5	0.998	0.992
0.14	1.51	22.2	0.998	0.99	1.51	22.3	0.998	0.99	1.46	22.3	0.998	0.99	1.6	22.4	0.998	0.99
0.58	1.35	22.5	0.998	0.97	1.14	22.1	0.998	0.98	1.13	22.4	0.998	0.98	1.14	22	0.998	0.98

Default values used in the main analysis are $\alpha = 40$ d^{-1} and $\delta = 0.14$ d^{-1}.

APPENDIX A (CONTINUED)

Table S2. Population parameter estimates obtained using the approximate solution (Eq. 3) of the multiscale model including data from nine patients treated with 1,250 mg TVR twice daily

	ε_α				ε_s					$\kappa\mu$ (d^{-1})	
δ (d^{-1})	IFN, 5 MIU	IFN, 10/15 MIU	Daclatasvir	TVR	IFN, 5/10/15 MIU	Daclatasvir	TVR	ρ (d^{-1})	c (d^{-1})	IFN/daclatasvir*	TVR
0.01	0.79	0.97	0.98	0.99	0.36	0.997	0.95	6.32	22.6	1.77	3.97
0.14	0.76	0.96	0.98	0.99	0.44	0.997	0.94	7.46	22.7	1.68	3.85
0.58	0.66	0.94	0.97	0.98	0.33	0.998	0.93	8.16	23.2	1.67	4.05

MIU, milliion international units.
*We found that $\kappa\mu$ is identical under IFN and daclatasvir monotherapy.

Table S3. Empirical Bayes estimates of individual parameter in the multiscale model

Treatment	Pt	ε_α	ρ	V_0	t_0	ε_s	$\kappa\mu$	c
IFN, 5 MIU	1A	0.67	7.88	6.65	0.46	0.33	1.46	22.27
	1B	0.78	8.95	6.37	0.37	0.37	1.46	22.42
	1E	0.91	9.26	6.03	0.43	0.31	1.46	22.35
	1F	0.80	7.36	6.87	0.50	0.34	1.46	22.22
	1H	0.63	8.44	6.68	0.42	0.77	1.46	22.41
	1Q	0.78	8.95	6.37	0.37	0.37	1.46	22.42
Mean		0.76	8.47	6.49	0.43	0.41	1.46	22.35
IFN, 10/15 MIU	2A	0.80	7.67	6.78	0.47	0.34	1.46	22.26
	2B	0.97	8.63	7.17	0.47	0.32	1.46	22.29
	2C	0.94	8.76	6.64	0.45	0.32	1.46	22.32
	2D	0.90	8.95	6.00	0.40	0.79	1.46	22.97
	2E	0.995	12.65	7.55	0.39	0.23	1.46	22.33
	2F	0.93	8.14	6.93	0.35	0.40	1.46	22.42
	2G	0.88	6.95	7.37	0.36	0.52	1.46	22.35
	2H	0.99	9.43	6.39	0.38	0.28	1.46	22.27
	3A	0.99	5.46	6.81	0.48	0.56	1.46	22.26
	3B	0.93	7.75	6.59	0.40	0.81	1.46	22.85
	3C	0.97	7.80	6.67	0.81	0.28	1.46	22.08
	3D	0.99	8.29	5.59	0.30	0.82	1.46	22.90
	3E	0.93	9.36	7.24	0.34	0.35	1.46	22.48
	3F	0.88	7.06	6.05	0.56	0.32	1.46	22.16
Mean		0.94	8.35	6.70	0.44	0.45	1.46	22.42
Daclatasvir	8	0.997	7.39	5.68	0.04	0.997	1.46	25.44
	42	0.97	9.17	5.57	0.03	0.997	1.46	23.12
	68	0.99	8.02	7.24	0.05	0.998	1.46	20.10
	69	0.98	8.75	6.15	0.04	0.999	1.46	22.74
	83	0.99	8.19	5.67	0.05	0.997	1.46	20.46
Mean		0.98	8.30	6.06	0.04	0.998	1.46	22.37

APPENDIX B

Modeling HCV cure after an ultra-short duration of therapy with direct acting agents

Ashish Goyal [a, b], Yoav Lurie [c], Eric G. Meissner [d, e], Marian Major [f], Natasha Sansone [a, g], Susan L. Uprichard [a, g], Scott J. Cotler [a], Harel Dahari [a, *]

[a] The Program for Experimental and Theoretical Modeling, Division of Hepatology, Department of Medicine, Loyola University Medical Center, Maywood, IL, United States
[b] Theoretical Biology & Biophysics Group, Los Alamos National Laboratory, Los Alamos, NM, United States
[c] Liver Unit, Digestive Disease Institute, Sha'are Zedek Medical Center, Jerusalem, Israel
[d] Division of Infectious Diseases, Department of Microbiology and Immunology, Medical University of South Carolina, Charleston, SC, United States
[e] Laboratory of Immunoregulation, National Institute of Allergy and Infectious Diseases, National Institutes of Health, Bethesda, MD, United States
[f] Division of Viral Products, Center for Biologics Evaluation and Research, Food and Drug Administration, Silver Spring, MD, United States
[g] Department of Microbiology and Immunology, University of Illinois Chicago, Chicago, IL, United States

ARTICLE INFO

Article history:
Received 3 March 2017
Received in revised form
26 May 2017
Accepted 28 June 2017
Available online 30 June 2017

ABSTRACT

Background: Cases of sustained-virological response (SVR or cure) after an ultra-short duration (≤27 days) of direct-acting antiviral (DAA)-based therapy, despite HCV being detected at end of treatment (EOT), have been reported. Established HCV mathematical models that predict the treatment duration required to achieve cure do not take into account the possibility that the infectivity of virus produced during treatment might be reduced. The aim of this study was to develop a new mathematical model that considers the fundamental and critical concept that HCV RNA in serum represents both infectious virus (V_i) and non-infectious virus (V_{ni}) in order to explain the observation of cure with ultrashort DAA therapy.

Methods: Established HCV models were compared to the new mathematical model to retrospectively explain cure in 2 patients who achieved cure after 24 or 27 days of paritaprevir, ombitasvir, dasabuvir, ritonavir and ribavirin or sofosbuvir plus ribavirin, respectively.

Results: Fitting established models with measured longitudinal HCV viral loads indicated that in both cases, cure would not have been expected without an additional 3–6 weeks of therapy after the actual EOT. In contrast, the new model fits the observed outcome by considering that in addition to blocking V_i and V_{ni} production (ε~0.998), these DAA + ribavirin treatments further enhanced the ratio of V_{ni} to V_i, thus increasing the log (V_{ni}/V_i) from 1 at pretreatment to 6 by EOT, which led to <1 infectious-virus particle in the extracellular body fluid (i.e., cure) prior to EOT.

Conclusions: This new model can explain cure after short duration of DAA + ribavirin therapy by suggesting that a minimum 6-fold increase of log (V_{ni}/V_i) results from drug-induced enhancement of the V_{ni}/V_i.

1. Introduction

Treatment of chronic hepatitis C virus infection has dramatically improved with >~90% cure (or sustained virological response, SVR) rates using all-oral direct–acting-antivirals (DAAs), with shorter treatment and minimal side-effects, relative to interferon-based treatment (WHO, 2015). Theoretically, cure is achieved when there is less than one virus particle and HCV-infected cell in the body (termed cure boundary) (Dixit et al., 2004; Snoeck et al., 2010). The typical HCV decline under DAA treatment is biphasic, consisting of a 1st phase rapid virus decline (12–48 h), followed by a slower 2nd phase virus decay (Dahari et al., 2016). Mathematical modeling of HCV kinetics can reproduce this biphasic viral decline and can estimate the duration of treatment needed to clear the

* Corresponding author. The Program for Experimental & Theoretical Modeling, Division of Hepatology, Department of Medicine, Loyola University Medical Center, 2160 S. First Ave, Maywood, IL, 60153, United States.
E-mail address: hdahari@luc.edu (H. Dahari).

http://dx.doi.org/10.1016/j.antiviral.2017.06.019
0166-3542/

virus (and infected cells) to reach the cure boundary. For example, real-time modeling successfully predicted the duration of interferon-free therapy with silibinin plus ribavirin required to achieve cure (Dahari et al., 2015). Recently, the cure boundary concept was retrospectively examined using data from 58 HCV genotype-1 infected patients treated for 12 weeks with three different approved sofosbuvir (SOF)-based regimens (Dahari et al., 2016). Modeling predicted that the majority of patients would reach cure with ≤8 weeks of therapy, which is in agreement with clinical studies showing high cure rates with 8 weeks of treatment in non-cirrhotic HCV genotype-1 patients (Buggisch et al., 2016; Kowdley et al., 2014; O'Brien et al., 2016). Moreover, 43% of patients treated with SOF-based regimens were predicted to reach cure within 6 weeks.

We previously observed cure in two patients treated with DAAs for less than 4 weeks, despite having detectable HCV RNA close to end of treatment (EOT) (Hasin et al., 2016; Meissner et al., 2014). HCV RNA detected at EOT in patients who subsequently develop SVR might be due in part to the presence of non-infectious RNA or virus (V_{ni}), which has been identified in-vivo in HCV-infected chimpanzees and in-vitro (Feinstone et al., 1981; Major et al., 2002; Sansone et al., 2014). Further, in vitro inhibition experiments utilizing HCV DAAs directed again NS5A (such as ombitasvir prescribed to patient 1 in this study) have documented a reduction in the infectivity of the virus produced during treatment resulting in an increase in the relative amount of noninfectious particles (V_{ni}) to infectious particles (V_i) (Sansone et al., 2014). In the current study we show that established mathematical models cannot explain cure in these two patients and suggest a new model in which the cure boundary is related not to the total viral load in blood, but to the number of infectious viral particles.

2. Methods

2.1. Patients

Viral kinetics were measured from two patients treated in clinical practice who achieved cure after 24 days of paritaprevir, ombitasvir, dasabuvir, ritonavir (PODr) and ribavirin (RBV) (Hasin et al., 2016) (patient 1) or 27 days of SOF + RBV (Meissner et al., 2014) (patient 2).

2.2. Mathematical model

Since the standard biphasic (Dahari et al., 2016) and the multiscale (Guedj et al., 2013) models (termed established models) would have predicted treatment failure in these cases (Eqs. S1 and S2, Supplementary text), we developed a new extended biphasic model (Fig. 1), reminiscent of an extended multiscale model presented by Nguyen et al. (2015), that incorporated assumptions about infectious and non-infectious virus, as shown here:

$$\begin{aligned}\frac{dI}{dt} &= \beta T_0 V_i - \delta I \\ \frac{dV_i}{dt} &= (1-\varepsilon)p_i \exp(-gt) I - cV_i \\ \frac{dV_{ni}}{dt} &= (1-\varepsilon)p_i(1-\exp(-gt))I + (1-\varepsilon)p_{ni} I - cV_{ni}\end{aligned} \quad (1)$$

where V_i *and* V_{ni} represent infectious and non-infectious HCV, respectively. V_i infects target cells, T_0, with constant rate β, generating infected cells, I, which produce new infectious and non-infectious virions at rate p_i *and* p_{ni} per infected cell, respectively. Both V_i and V_{ni} are assumed to be cleared at rate c per virion. DAA-containing regimens such as PODr inhibit HCV replication which effects both V_i and V_{ni} production with a constant effectiveness, ε. However, the ability of DAAs (such as NS5A inhibitors (Sansone et al., 2014)) and RBV (Dahari et al., 2007; Dixit et al., 2004) to alter the infectivity of secreted virus would result in a gradual increase in the ratio of non-infectious to infectious virus, which is modelled by $exp(-gt)$, where g is a constant and t is time post treatment initiation.

2.3. Parameter estimation

We assume the target cell (i.e., hepatocyte) level per ml is constant at 1×10^7 cells (Dahari et al., 2007). Thus, target cell number was kept constant and initial infected cell number is given by $I_0 = \beta V_{i0} T_0/\delta$, where V_{i0} represents pre-treatment level of infectious virus. Reverse titration studies in chimpanzees have provided quantification of HCV RNA copy number and infectious titers within HCV-positive samples (Engle et al., 2008; Major et al., 2002), suggesting a pretreatment ratio of V_i and V_{ni} of 1:11 (i.e., $p_i/p_{ni} = 1/11$). Thus, we have $V_{i0} = V_{tot0}/12$ where V_{tot0} is the measured pre-treatment HCV level. Employing initial steady state conditions also yields $p_i = cV_{i0}/I_0$ and $p_{ni} = 11p_i$. Parameter β was set to 7×10^{-8} mL/virion/day to target a low fraction of HCV-infected hepatocytes (~4%), consistent with a previously estimated range (Liang et al., 2009). Due to lack of frequent sampling in patient 1, especially during the first 2 days of therapy, the effectiveness of PODr + RBV in blocking HCV production was set to $\varepsilon = 0.998$ as recently estimated (Gambato et al., 2016) and HCV clearance rate was set to $c = 6$/day (Dahari et al., 2016). In the SOF + RBV treated patient (patient 2), the availability of frequent HCV measurements allowed for the estimation of both ε and c parameters.

2.4. Cure boundary

The time to eradication of the last infected cell is more speculative due to the lack of experimental data on the infected cell number (Dahari et al., 2016). Therefore we focused on the viral cure boundary, i.e., <1 virus particle in the extracellular body fluid (approximately 13.5 L) which corresponds to one virion/13,500 mL = 7×10^{-5} (Dahari et al., 2016).

2.5. Fitting and sensitivity analysis

The available 2 patient datasets were used to estimate unknown parameters of the three models (Eqs. S1 and S2, and Eq. (1)) using fitting procedure lsqnonlin in MATLAB R2016a. The estimation procedure also yields Jacobian matrix and covariates which were then used to determine 95% CI of the estimated parameters using 'nlparci' in MATLAB R2016a (Bates and Watts, 1988). It should also be noted that the estimated value of parameter g represents a minimum estimate due to the inability to measure Vi. A robustness analysis of the estimated model parameters is further described in the Supplementary text.

3. Results

Established HCV mathematical models fail to explain cure. The standard model (Eq. S(1)) predicts a time-to-cure for the two cases of 8–10 weeks with an estimated loss of infected cells (δ) of 0.278/day [95% confidence intervals, 95%CI:0.229–0.337] for patient 1 (Fig. S1; Table S1). For patient 2, δ, c and ε were estimated at 0.042/day [95%CI:0.001, 2.177], 4.87/day [95%CI:3.797–6.254] and 0.999 [95%CI:0.997–0.999], respectively, with time-to-cure being greater than 52 weeks (Fig. S1; Table S1). The multiscale model (Eq. S2) predicts time-to-cure to be greater than 8 and 18 weeks for

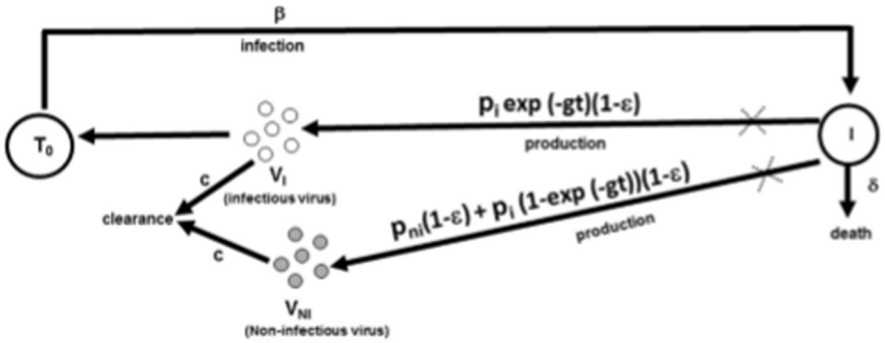

Fig. 1. Schematic representation of the extended model (Eq. (1)). In the figure, infected cells (I) produce both infectious virions (V_i) and non-infectious virions (V_{ni}). Only V_i infects target cells, T_0, with constant rate β, generating infected cells, I, which produce new infectious and non-infectious virions at rate p_i and p_{ni} per infected cell, respectively. Both V_i and V_{ni} are assumed to be cleared at rate c per virion. DAA-containing regimens such as PODr inhibit HCV replication which effects both V_i and V_{ni} production with a constant effectiveness ε but under the effect of some DAAs ± RBV, which alter progeny virion infectivity, there is a time-dependent reduction in secretion of infectious virions relative to non-infectious virions which is modelled through the term $exp(-g^*t)$.

patients 1 (δ=0.246/day [95%CI:0.218–0.278]) and patient 2 (δ=0.080/day [95%CI:0.016–0.388] and ε_a = 0.995 [95% CI:0.962–0.999]) respectively (Fig. S2; Table S2). Thus, both established models suggested a time-to-cure of at least 4 additional weeks of therapy than what both patients actually received.

A model that accounts for infectious and non-infectious virus can explain cure. The new extended biphasic model (Fig. 1; Eq. (1)) fits well with measured viral load and predicts cure with ultra-short therapy (Fig. 2). The new model predicts that DAAs plus RBV not only block HCV production but in addition reduce the infectivity of the virus produced, which is modelled through parameter g. For patient 1, the estimated infected cell loss, δ, and g were 0.281/day [95%CI:0.229–0.343] and 0.366/day [95%CI:0.305-0.440], respectively. For patient 2, δ = 0.042 [95%CI:0.005–0.374], g = 0.404 [95%CI:0.330–0.496], c = 4.875/day [95%CI:3.801-6.251], and ε = 0.999 [95%CI:0.997-0.999](Table 1). Despite the reduced production of infectious virions, the mean loss of infected cells was estimated to be similar as in the standard model (0.278/day vs 0.281/day for patient 1; 0.042/day vs 0.042/day for patient 2) (Table 1; Table S1). The new model can explain a time-to-cure

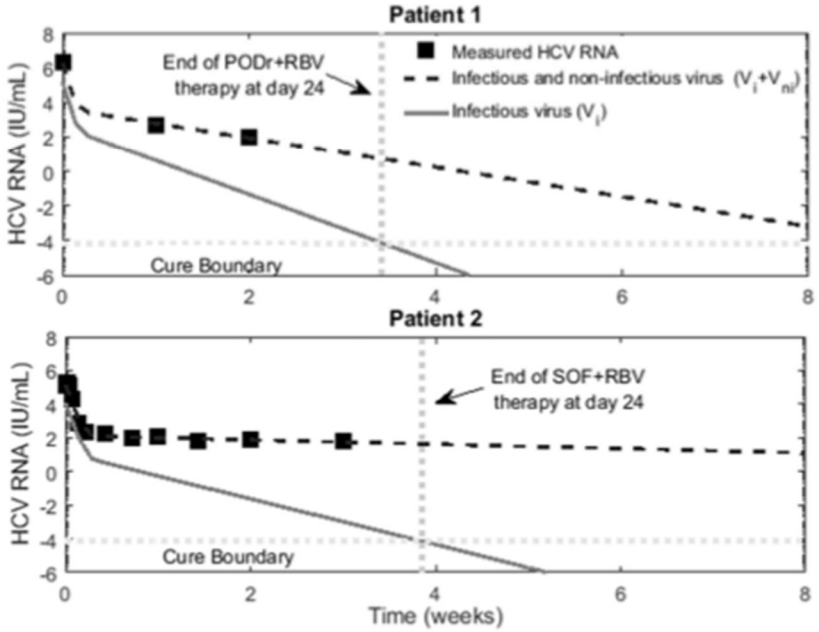

Fig. 2. Extended biphasic model curve fits with measured viral kinetic data and predicted time-to-cure. Total viral load (Dashed line) was fit to the measured HCV RNA (Squares) with mean estimated infected cell loss/death rate of δ = 0.281/d and δ = 0.042/d for patients 1 and 2, who were treated with PODr + RBV and SOF + RBV, respectively. To bring the predicted infectious viral load (Solid line) to cross the cure boundary (7×10^{-5} IU/mL represented by horizontal dotted line) before PODr + RBV was stopped at day 24 and 27 for P1 and P2 respectively (vertical dotted line), minimum values of parameter g were estimated as 0.366/d and 0.404/d for patient 1 and patient 2 respectively. Pretreatment total viral load, V_{tot0} was at 2,000,000 IU/mL and 147,910 IU/mL for patient 1 and 2 respectively, as measured before either PODr + RBV and SOF + RBV therapy was initiated. Pretreatment infectious virus level V_{tot0}/12 was assumed in both patients based on empirically measured HCV specific infectivity in chronically infected chimpanzees as explained in Methods. Parameters c = 6/d and ε = 0.998 were kept fixed in patient 1 as explained in Methods while they were estimated at 4.875/d and 0.999 in patient 2.

APPENDIX B (CONTINUED)

Table 1
Estimated parameters of the extended model.

Parameter	Patient 1 (PODr + RBV) estimate [95% CI]	Patient 2 (SOF + RBV) estimate [95% CI]
δ	0.281 [0.229 0.343]	0.042 [0.005 0.374]
[a] g	0.366 [0.305 0.440]	0.404 [0.330 0.496]
c	6.0[b]	4.875 [3.801 6.251]
ε	0.998[b]	0.999 [0.997 0.999]

δ, HCV-infected cell death/loss rate [1/d]; c, HCV clearance rate in blood [1/d]; ε, drug efficacy in blocking HCV production; g, drug-induced increase rate in the ratio of non-infectious to infectious virus [1/d]; PODr, paritaprevir, ombitasvir, dasabuvir, ritonavir; RBV, ribavirin; SOF, sofosbuvir; CI, confidence interval.

[a] Minimal estimate.

[b] Due to lack of measured viral kinetic data sampling c and ε were fixed as noted in Methods.

within 24 days of treatment for patient 1 and 27 days of treatment for patient 2.

4. Discussion

Established HCV mathematical models were used to predict on treatment (real time) treatment duration needed to achieve cure with silibinin + RBV (Dahari et al., 2015), and retrospectively under approved DAAs (Dahari et al., 2016; Gambato et al., 2016). However, in the current study we showed that these models cannot explain two cases of cure after ultrashort (<4 weeks) DAA therapy. A rapid viral decline was observed in the two cases presented here (HCV RNA levels were <500 IU/mL by day 2 and 7, in patient 2 and 1, respectively). Similarly, a phase 2a study documented cure after 3 weeks of DAA (without ribavirin) therapy in all patients with HCV RNA levels<500 IU/mL by day 2 and suggested that established models failed to predict time-to-cure (Lau et al., 2016). We developed a new model to explain two ultra-short successful therapy cases that includes infectious (V_i) and non-infectious (V_{ni}) virions. The new model assumes that in addition to blocking V_i and V_{ni} production (ε–0.998), treatment further reduced the infectivity of secreted virus (parameter $g \leq 0.372$/d) thus increasing the log (V_{ni}/V_i) ratio from 1 at baseline to 6 by EOT. A conceptual implication of the new model is that while HCV RNA (i.e., $V_i + V_{ni}$) was detected close to EOT (termed EOT+), V_i reached the cure boundary before EOT.

The main limitation to validating the hypothesized relative change in V_i and V_{ni} during DAA therapy (via parameter g in the model) is the inability to measure HCV infectivity (i.e. V_i) in patient samples. However, a reduction in secreted HCV infectivity under NS5A inhibitor treatment has been shown in vitro (Sansone et al., 2014) and proposed for RBV (Dahari et al., 2007; Dixit et al., 2004; Hofmann et al., 2007; Lutchman et al., 2007). In fact, parameter g in the model would be relevant not only to ribavirin and NS5A inhibitors, but to other drugs or endogenous immune responses that might directly or indirectly alter virion infectivity. For example, restoration of the host immune response (e.g. improved neutralizing antibody response), due to a significant decline in viral burden within 2 days after initiation of DAA treatment, might contribute to the predicted increase in V_{ni}/V_i ratio. As suggested for HIV (Conway and Perelson, 2015), prevention or reversal of T cell exhaustion might result from HCV viral decline under DAA therapy, contributing to viral suppression. Moreover, the host immune response could potentially also increase death/loss of HCV-infected cells (parameter δ in the model), although an increase in death/loss of HCV-infected cells would not increase V_{ni}/V_i ratio and thus could not explain cure in the 2 cases presented here. This scenario of enhanced death might lead to complete HCV clearance after treatment was stopped (Meissner et al., 2014; Veerapu et al., 2011) but this is difficult to model due to a lack of supporting data.

In conclusion, we developed a new mathematical model that addresses the fundamental relationship between infectious and non-infectious virions during DAA therapy and explains two cases of HCV cure after an ultra-short treatment (Hasin et al., 2016; Meissner et al., 2014). The new model has the potential to explain cases of DAA therapy in which established models have failed to predict cure (Lau et al., 2016; Nguyen et al., 2015). Further studies are needed to confirm whether the new model with a cure boundary based on the eradication of infectious virus (rather than total virus) will be accurate in predicting the duration of DAA therapy needed to achieve cure and the outcomes of ultra-short treatment regimens.

Conflict of interest

The authors who have taken part in this study declared that they do not have anything to disclose regarding funding or conflict of interest with respect to this manuscript.

Acknowledgments

The research was supported in part by the U.S. National Institute of Health (NIH) grant R01-AI078881 and by the Intramural Research Program of the National Institutes of Health, National Institute of Allergy and Infectious Diseases.

Appendix A. Supplementary data

Supplementary data related to this article can be found at http://dx.doi.org/10.1016/j.antiviral.2017.06.019.

References

Bates, D.M., Watts, D.G., 1988. Nonlinear Regression Analysis and its Applications. John Wiley & Sons, NY.

Buggisch, P., Boker, K., Gunter, R., Teuber, G., Klinker, H., Pathil, A., Christensen, S., Pfeiffer-Vornkahl, H., Simon, K., Niederau, C., Wedemeyer, H., Zeuzem, S., 2016. 8 weeks treatment under real life conditions with Ledipasvir/Sofosbuvir in HIV co-infected treatment-naïve HCV genotype 1 patients demonstrates similar results to mono infected HCV patients: data from the German Hepatitis C-Registry (DHC-R). Hepatology 64 (1), 439–440A.

Conway, J.M., Perelson, A.S., 2015. Post-treatment control of HIV infection. Proc. Natl. Acad. Sci. 112, 5467–5472.

Dahari, H., Canini, L., Graw, F., Uprichard, S.L., Araujo, E.S., Penaranda, G., Coquet, E., Chiche, L., Riso, A., Renou, C., Bourliere, M., Cotler, S.J., Halfon, P., 2016. HCV kinetic and modeling analyses indicate similar time to cure among sofosbuvir combination regimens with daclatasvir, simeprevir or ledipasvir. J. Hepatol. 64, 1232–1239.

Dahari, H., Ribeiro, R.M., Perelson, A.S., 2007. Triphasic decline of hepatitis C virus RNA during antiviral therapy. Hepatology 46, 16–21.

Dahari, H., Shteingart, S., Gafanovich, I., Cotler, S.J., D'Amato, M., Pohl, R.T., Weiss, G., Ashkenazi, Y.J., Tichler, T., Goldin, E., Lurie, Y., 2015. Sustained virological response with intravenous silibinin: individualized IFN-free therapy via real-time modelling of HCV kinetics. Liver Int. Off. J. Int. Assoc. Study Liver 35, 289–294.

Dixit, N.M., Layden-Almer, J.E., Layden, T.J., Perelson, A.S., 2004. Modelling how ribavirin improves interferon response rates in hepatitis C virus infection.

APPENDIX B (CONTINUED)

Nature 432, 922–924.
Engle, R.E., Russell, R.S., Purcell, R.H., Bukh, J., 2008. Development of a TaqMan assay for the six major genotypes of hepatitis C virus: comparison with commercial assays. J. Med. Virol. 80, 72–79.
Feinstone, S.M., Alter, H.J., Dienes, H.P., Shimizu, Y., Popper, H., Blackmore, D., Sly, D., London, W.T., Purcell, R.H., 1981. Non-A, non-B hepatitis in chimpanzees and marmosets. J. Infect. Dis. 144, 588–598.
Gambato, M., Canini, L., Lens, S., Graw, F., Londono, M.C., Uprichard, S.L., Marino, Z., Reverter, E., Bartres, C., Gonzalez, P., Cotler, S.J., Forns, X., Dahari, H., 2016. Modeling early HCV kinetics to individualize DAA treatment duration in patients with advanced cirrhosis. J. Hepatol. 64 (Suppl. 1 (2)), S795.
Guedj, J., Dahari, H., Rong, L., Sansone, N.D., Nettles, R.E., Cotler, S.J., Layden, T.J., Uprichard, S.L., Perelson, A.S., 2013. Modeling shows that the NS5A inhibitor daclatasvir has two modes of action and yields a shorter estimate of the hepatitis C virus half-life. Proc. Natl. Acad. Sci. U. S. A 110, 3991–3996.
Hasin, Y., Shteingart, S., Dahari, H., Gafanovich, I., Floru, S., Braun, M., Shlomai, A., Verstandig, A., Dery, I., Uprichard, S.L., Cotler, S.J., Lurie, Y., 2016. Hepatitis C virus cures after direct acting antiviral-related drug-induced liver injury: case report. World J. Hepatol. 8, 858–862.
Hofmann, W.P., Polta, A., Herrmann, E., Mihm, U., Kronenberger, B., Sonntag, T., Lohmann, V., Schonberger, B., Zeuzem, S., Sarrazin, C., 2007. Mutagenic effect of ribavirin on hepatitis C nonstructural 5B quasispecies in vitro and during antiviral therapy. Gastroenterology 132, 921–930.
Kowdley, K.V., Gordon, S.C., Reddy, K.R., Rossaro, L., Bernstein, D.E., Lawitz, E., Shiffman, M.L., Schiff, E., Ghalib, R., Ryan, M., Rustgi, V., Chojkier, M., Herring, R., Di Bisceglie, A.M., Pockros, P.J., Subramanian, G.M., An, D., Svarovskaia, E., Hyland, R.H., Pang, P.S., Symonds, W.T., McHutchison, J.G., Muir, A.J., Pound, D., Fried, M.W., Investigators, I.O.N., 2014. Ledipasvir and sofosbuvir for 8 or 12 weeks for chronic HCV without cirrhosis. N. Engl. J. Med. 370, 1879–1888.
Lau, G., Benhamou, Y., Chen, G., Li, J., Shao, Q., Ji, D., Li, F., Li, B., Liu, J., Hou, J., Sun, J., Wang, C., Chen, J., Wu, V., Wong, A., Wong, C.L., Tsang, S.T., Wang, Y., Bassit, L., Tao, S., Jiang, Y., Hsiao, H.M., Ke, R., Perelson, A.S., Schinazi, R.F., 2016. Efficacy and safety of 3-week response-guided triple direct-acting antiviral therapy for chronic hepatitis C infection: a phase 2, open-label, proof-of-concept study. Lancet Gastroenterol. Hepatol. 1, 97–104.
Liang, Y., Shilagard, T., Xiao, S.Y., Snyder, N., Lau, D., Cicalese, L., Weiss, H., Vargas, G., Lemon, S.M., 2009. Visualizing hepatitis C virus infections in human liver by two-photon microscopy. Gastroenterology 137, 1448–1458.
Lutchman, G., Danehower, S., Song, B.C., Liang, T.J., Hoofnagle, J.H., Thomson, M., Ghany, M.G., 2007. Mutation rate of the hepatitis C virus NS5B in patients undergoing treatment with ribavirin monotherapy. Gastroenterology 132, 1757–1766.
Major, M.E., Mihalik, K., Puig, M., Rehermann, B., Nascimbeni, M., Rice, C.M., Feinstone, S.M., 2002. Previously infected and recovered chimpanzees exhibit rapid responses that control hepatitis C virus replication upon rechallenge. J. Virol. 76, 6586–6595.
Meissner, E.G., Nelson, A., Marti, M., Masur, H., Osinusi, A., Kottilil, S., 2014. Sustained virologic response for chronic hepatitis C infection after 27 Days of treatment with sofosbuvir and ribavirin. Open Forum Infect. Dis. 1, 013.
Nguyen, T.H., Guedj, J., Canini, L., Osinusi, A., Pang, P.S., McHutchison, J., Masur, H., Kohli, A., Kottilil, S., Perelson, A.S., 2015. The Paradox of Highly Effective Sofosbuvir Combo Therapy Despite Slow Viral Decline CROI, Seattle, Washington, USA, pp. 169–170.
O'Brien, T.R., Feld, J.J., Kottilil, S., Pfeiffer, R.M., 2016. No scientific basis to restrict 8 weeks of treatment with ledipasvir/sofosbuvir to patients with hepatitis C virus RNA <6,000,000 IU/mL. Hepatology 63, 28–30.
Sansone, N., Dahari, H., Subramanya, G., Perelson, A.S., Uprichard, S.L., 2014. Modeling HCVcc infection reveals new insights into the dynamics that maintain the in vitro HCV steady state and the mechanisms of action of the NS5A inhibitor daclatasvir. Hepatology 60 (4), 1165A.
Snoeck, E., Chanu, P., Lavielle, M., Jacqmin, P., Jonsson, E.N., Jorga, K., Goggin, T., Grippo, J., Jumbe, N.L., Frey, N., 2010. A comprehensive hepatitis C viral kinetic model explaining cure. Clin. Pharmacol. Ther. 87, 706–713.
Veerapu, N.S., Raghuraman, S., Liang, T.J., Heller, T., Rehermann, B., 2011. Sporadic reappearance of minute amounts of hepatitis C virus RNA after successful therapy stimulates cellular immune responses. Gastroenterology 140, 676–685 e671.
WHO, 2015. World Health Organization. Guidelines for the Screening, Care and Treatment of Persons with Hepatitis C Infection. Geneva, Switzerland. http://www.who.int/hiv/pub/hepatitis/hepatitis-c-guidelines/en/.

VITA

NAME: Natasha Danielle Sansone

EDUCATION: B.A., Biological Sciences, University of Chicago, Chicago Illinois, 2010

Ph.D., Microbiology and Immunology, University of Illinois at the Medical Center, Chicago, Illinois, 2017

LEGAL ADMISSION: USPTO Patent Agent Registration #75,160 (2016)

TEACHING: Department of Mathematics, University of Chicago, Chicago, Illinois (TITLE: Calculus Teaching Assistant), 2007

ABSTRACTS: Dahari H, Barretto N, Sansone ND, Guedj J, Perelson AS, Uprichard SL. Modeling inhibition kinetics of HCV sg1b RNA during IFN/DAAs treatment in non-growing Huh7 cells. 62nd Annual Meeting of the American Association for the study of Liver Diseases 54(Suppl): 538A (Hepatology, 2011).

Sansone ND, Dahari H, Subramanya G, Perelson AS, Uprichard SL. Characterization of intracellular and extracellular HCV inhibition kinetics during in vitro treatment with DAAs. 20th International Symposium on HCV and related Viruses. Melbourne, Australia, Oct 7-10, 2013

Sansone ND, Dahari H, Subramanya G, Perelson AS, Uprichard SL. Modeling HCVcc infection reveals new insights into the dynamics that maintain in vitro HCV steady state and the mechanisms of action of the NS5A inhibitor daclatasvir. 21st International Symposium on HCV and related Viruses. Banff, Canada, Sep 7-11, 2014.

PUBLICATIONS: Guedj J, Dahari H, Rong L, Sansone ND, Nettles RE, Cotler SJ, Layden TJ, Uprichard SL, Perelson AS. (2013). Modeling shows that the NS5A inhibitor daclatasvir has two modes of action and yields a shorter estimate of the hepatitis C virus half-life. Proc Natl Acad Sci USA, 110(10), 3991–3996.

Goyal A, Lurie Y, Meissner EG, Major M, Sansone ND, Uprichard SL, Cotler SJ, Dahari H. (2017). Modeling HCV cure after an ultra-short duration of therapy with direct acting agents. Antiviral Res. 2017 Jun 30 [Epub ahead of print]

Nomme J, Murphy JM, Su Y, Sansone ND, Armijo AL, Olson ST, Radu C, Lavie A. (2014). Structural characterization of new deoxycytidine kinase inhibitors rationalizes the affinity-determining moieties of the molecules. Acta Crystallogr D Biol Crystallogr, 70(Pt 1), 68-78.

DRAFTED: T.L. Chung, G. Crespo, N.D. Sansone, L. Mensa, S. Pérez-del-Pulgar, M. Navasa, A.S. Perelson, S. J. Cotler, S.L. Uprichard, X. Forns, H. Dahari. Modeling hepatitis C virus kinetics during liver transplantation indicates that the liver plays a role in virus clearance.

N.D. Sansone, A.S. Perelson, S.L. Uprichard, H. Dahari. Novel cell culture hepatitis C virus mathematical model predicts that NS5A inhibitor changes virus specific infectivity.